ERDC/EL TR-13-13

Environmental Laboratory

US Army Corps of Engineers®
Engineer Research and Development Center

ERDC
INNOVATIVE SOLUTIONS for a safer, better world

Civil Works Basic Research Program

Phytoplankton as Particles – A New Approach to Modeling Algal Blooms

Carl F. Cerco and Mark R. Noel

July 2013

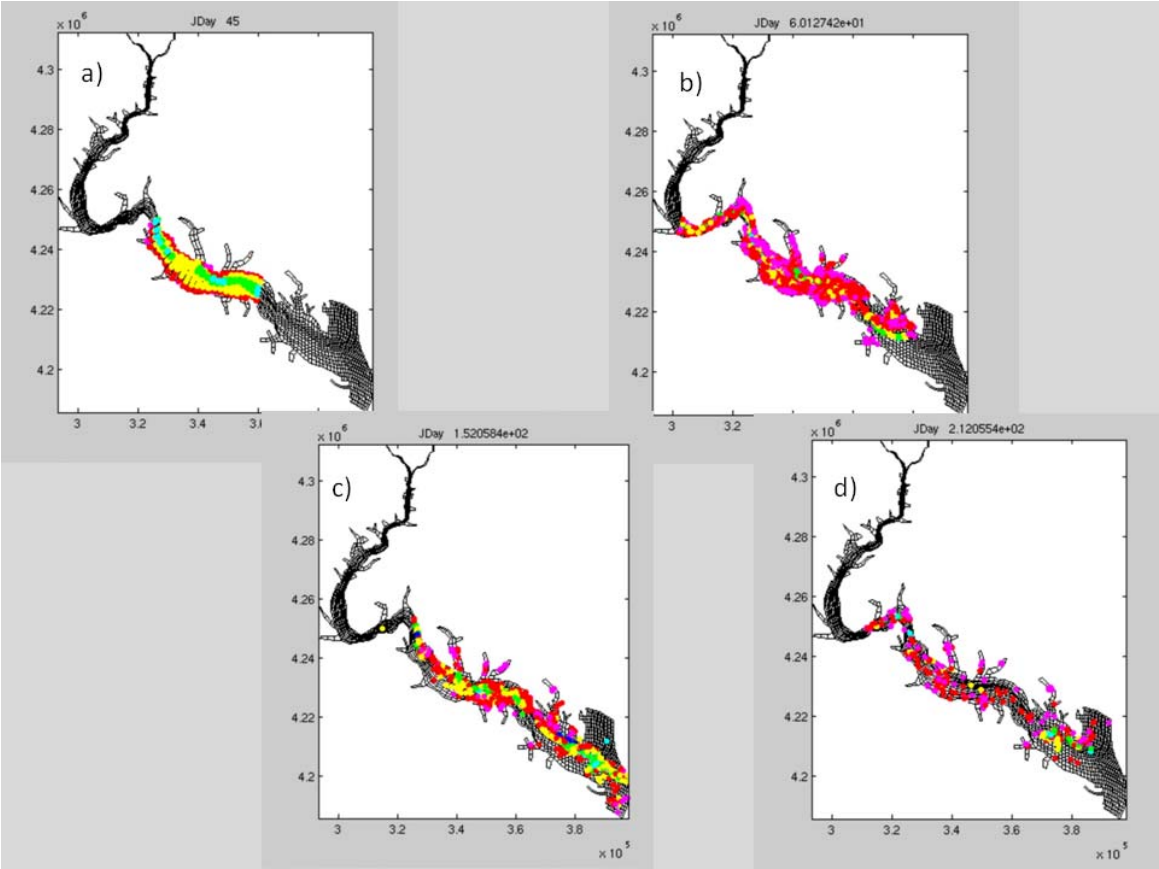

Approved for public release; distribution is unlimited.

The US Army Engineer Research and Development Center (ERDC) solves the nation's toughest engineering and environmental challenges. ERDC develops innovative solutions in civil and military engineering, geospatial sciences, water resources, and environmental sciences for the Army, the Department of Defense, civilian agencies, and our nation's public good. Find out more at www.erdc.usace.army.mil.

To search for other technical reports published by ERDC, visit the ERDC online library at http://acwc.sdp.sirsi.net/client/default.

Civil Works Basic Research Program

ERDC/EL TR-13-13
July 2013

Phytoplankton as Particles – A New Approach to Modeling Algal Blooms

Carl F. Cerco and Mark R. Noel

Environmental Laboratory
U.S. Army Engineer Research and Development Center
3909 Halls Ferry Road
Vicksburg, MS 39180

Final report

Approved for public release; distribution is unlimited.

Prepared for U.S. Army Corps of Engineers
Washington, DC 20314-1000

Abstract

The authors investigate the hypothesis that phytoplankton blooms can be modeled by treating phytoplankton as discrete particles capable of self-induced transport via buoyancy regulation or other behaviors. A particle-tracking model is inserted into the CE-QUAL-ICM eutrophication model. Phytoplankton are quantified as carbonaceous biomass attached to the particles. Kinetics are adapted from CE-QUAL-ICM. The new model is operated along with existing hydrodynamic and watershed models of the Potomac River estuary. Initial application is to the winter-spring 1994 period. The new model is compared to observations and to a conventional model of the spring diatom bloom. The particle-based model successfully computes a subsurface chlorophyll maximum. The model characteristically displays heterogeneous spatial distribution of chlorophyll with high-amplitude oscillations at the semi-diurnal period. The characteristics and applicability of the particle approach are now established. The model requires optimization of parameter values to improve representation of the observed bloom in the Potomac.

DISCLAIMER: The contents of this report are not to be used for advertising, publication, or promotional purposes. Citation of trade names does not constitute an official endorsement or approval of the use of such commercial products. All product names and trademarks cited are the property of their respective owners. The findings of this report are not to be construed as an official Department of the Army position unless so designated by other authorized documents.

DESTROY THIS REPORT WHEN NO LONGER NEEDED. DO NOT RETURN IT TO THE ORIGINATOR.

Contents

Abstract ii

Figures and Tables v

Preface ix

1 Introduction 1

2 ICM Particle Tracking 5

Introduction 5
Theory and Implementation 5
Diffusion and Dispersion 9
Caveats 9

3 Phytoplankton Kinetics 12

Basic Equation 12
From Particles to the Continuum 13
Kinetics Rules for Particles 14

4 The Potomac River Estuary 16

The Chesapeake Bay Environmental Model Package (CBEMP) 16
Water Quality Database 20
Phytoplankton Data Base 21
Phytoplankton Biomass and Species 21
Chlorophyll Observations 24

5 Potomac River Salinity and Circulation 29

Introduction 29
Longitudinal Salinity Distribution 29
Salinity Time Series 30
Potomac River Residual Currents 37

6 Basic Particle Simulation 39

Introduction 39
Presentation Formats 40
Elevation Plots 40
Plan Views 40
Tracker Statistics 41
Comparison to Dissolved Substance 42
Sensitivity to Number of Particles Released 45
Sensitivity to Rules 46
Base Run for Phytoplankton Simulation 47

7 Algae as Particles – Spatial and Temporal Distribution 50

Introduction 50
Plan and Elevation Views 51
Comparison with Conventional Model 52

8 Algae as Particles – Comparisons with Observations 56
Introduction 56
Time Series Comparisons 57
Seasonal Spatial Distributions 57
Cumulative Distribution Plots 62
Time Series Analysis 64
Continuous Monitoring Data 65
Harmonic Analysis 69
Power Spectra 69
Summary 73

9 Algae as Particles – Sensitivity Analyses 74
Sensitivity to Particle Behavior 74
Particle residence time and location 74
Chlorophyll Concentration 77
Chlorophyll Distribution Plot 79
Sensitivity to Hydrology 81

10 Summary and Conclusions 86
Introduction 86
ICM Particle Tracking 86
Phytoplankton Kinetics 86
The Potomac River Estuary 87
Basic Particle Simulation 88
Algae as Particles – Spatial and Temporal Distribution 89
Algae as Particles – Comparisons with Observations 90
Algae as Particles – Sensitivity Analyses 90
Conclusions 92

References 93

Report Documentation Page

Figures and Tables

Figures

Figure 1. Elevation view of chlorophyll along the Potomac River Estuary, April 1999. Distance is indicated from the mouth, at left, to the head of tide, at right. 3

Figure 2. Aerial view of chlorophyll concentration in the Chesapeake Bay system, April 1986. 3

Figure 3. Proposed mechanism to explain the Potomac River spring phytoplankton bloom. 3

Figure 4. Initial position of a single particle in an unstructured grid cell. 6

Figure 5. Particle paths along x and y axis. 6

Figure 6. Orthogonal box for bounding particle movement. 7

Figure 7. Grid cells in a tributary indicating flow in the positive x-direction. 10

Figure 8. The Potomac River Estuary showing CBP sample stations. 17

Figure 9. The Potomac River portion of the Chesapeake Bay computational grid. 18

Figure 10. The surface plane of the independent Potomac River computational grid showing CBP sample stations. 19

Figure 11. Elevation view of the Potomac River computational grid from the mouth (km 0) to the head of tide (km 190). 20

Figure 12. Median monthly biomass for the sum of three diatoms at three stations, 1991 – 2000.. 22

Figure 13. Median monthly biomass for each of three diatom species at Station RET2.2, 1991 – 2000. 23

Figure 14. Median monthly biomass for each of three diatom species at Station LE2.2, 1991 – 2000. 23

Figure 15. Median monthly biomass for each of three diatom species at Station CB5.2, 1991 – 2000. 24

Figure 16. Chlorophyll concentrations (ug L^{-1}) in December of seasons of average, wet, and dry hydrology. 25

Figure 17. Chlorophyll concentrations (ug L^{-1}) in January of seasons of average, wet, and dry hydrology. 26

Figure 18. Chlorophyll concentrations (ug L^{-1}) in February of seasons of average, wet, and dry hydrology. 26

Figure 19. Chlorophyll concentrations (ug L^{-1}) in late March of seasons of average, wet, and dry hydrology. 27

Figure 20. Chlorophyll concentrations (ug L^{-1}) in early April of seasons of average, wet, and dry hydrology. 27

Figure 21. Chlorophyll concentrations (ug L^{-1}) in late May of seasons of average, wet, and dry hydrology. 28

Figure 22. Computed and observed surface salinity in the Potomac River for spring (March – May) 1994. 30

Figure 23. Computed and observed bottom salinity in the Potomac River for spring (March – May) 1994. 31

Figure 24. Computed and observed surface salinity in the Potomac River for spring (March – May) 1996. 31

Figure 25. Computed and observed bottom salinity in the Potomac River for spring (March – May) 1996. 32

Figure 26. Computed and observed surface salinity in the Potomac River for spring (March – May) 1999. 32

Figure 27. Computed and observed bottom salinity in the Potomac River for spring (March – May) 1999. 33

Figure 28. Time series of observed (blue circles) and computed (red line) surface salinity at RET2.2. 33

Figure 29. Time series of observed (blue circles) and computed (red line) bottom salinity at RET2.2. 34

Figure 30. Time series of observed (blue circles) and computed (red line) surface salinity at RET2.4.. 34

Figure 31. Time series of observed (blue circles) and computed (red line) bottom salinity at RET2.4. 35

Figure 32. Time series of observed (blue circles) and computed (red line) surface salinity at LE2.2. 35

Figure 33. Time series of observed (blue circles) and computed (red line) mid-depth salinity at LE2.2.. 36

Figure 34. Time series of observed (blue circles) and computed (red line) bottom salinity at RET2.4.. 36

Figure 35. Model residual currents in the Potomac River corresponding to Elliott's (1978) measurements. 38

Figure 36. Fall-line flow in the Potomac River November 1, 1993, to May 31, 1994. 39

Figure 37. Elevation view of particle distribution at four time intervals: a) Day 45 (particle release); b) Day 60; c) Day 152; d) Day 212 (end of simulation). 40

Figure 38. Plan view of particle distribution at four time intervals: a) Day 45 (particle release); b) Day 60; c) Day 152; d) Day 212 (end of simulation). 41

Figure 39. Tracker statistics at four time intervals: a) Day 45 (particle release); b) Day 60; c) Day 150; d) Day 210 (end of simulation). The plots indicate the number of particles at 10-km intervals and three depth levels. 42

Figure 40. The fraction of initial mass remaining following simultaneous releases of particles and dissolved substance. 43

Figure 41. Elevation view of dissolved substance concentration at four time intervals: a) Day 45 (release); b) Day 80; c) Day 115; d) Day 150. 43

Figure 42. Surface view of dissolved substance concentration at four time intervals: a) Day 45 (release); b) Day 80; c) Day 115; d) Day 150. 44

Figure 43. Elevation view of particle concentration at four time intervals: a) Day 45 (release); b) Day 80; c) Day 115; d) Day 150. 44

Figure 44. Surface view of particle concentration at four time intervals: a) Day 45 (release); b) Day 80; c) Day 115; d) Day 150. 45

Figure 45. Sensitivity to number of particles released. Tracker statistics are shown at the end of the simulation for release of: a) 10,000 particles; b) 20,000 particles; c) 40,000 particles. 46

Figure 46. Sensitivity to Kinetics Rules for Particles (Elevation views). 47

Figure 47. Sensitivity to Kinetics Rules for Particles (Tracker Statistics). 48

Figure 48. Elevation view of particle distribution for base phytoplankton run. 49
Figure 49. Tracker statistics for base phytoplankton run. 49
Figure 50. Surface view of particle distribution and attached algal biomass for base phytoplankton run. 52
Figure 51. Elevation view of chlorophyll concentration derived from the model of algae as particles. 54
Figure 52. Elevation view of chlorophyll concentration computed by the conventional algal model. 54
Figure 53. Surface view of chlorophyll concentration derived from the model of algae as particles. 55
Figure 54. Surface view of chlorophyll concentration computed by the conventional model. 55
Figure 55. Observed and computed chlorophyll concentrations at station LE2.3. 58
Figure 56. Observed and computed chlorophyll concentrations at station LE2.2. 59
Figure 57. Observed and computed chlorophyll concentrations at station RET2.4. 60
Figure 58. Observed and computed chlorophyll concentrations at station RET2.2. 60
Figure 59. Observed and computed chlorophyll concentrations for the winter season (December – February). Km zero is at the mouth of the estuary. 61
Figure 60. Observed and computed chlorophyll concentrations for the spring season (March - May). Km zero is at the mouth of the estuary. 62
Figure 61. Cumulative distribution plot of observed and modeled surface chlorophyll concentration. 63
Figure 62. Cumulative distribution plot of observed and modeled bottom chlorophyll concentration. 63
Figure 63. Cumulative distribution plot of observed and modeled chlorophyll concentration at all depths. 64
Figure 64. Location of Nomini Bay and St. George's Island continuous monitoring stations. 66
Figure 65. Observed chlorophyll at Nomini Bay, April – May 2008. 67
Figure 66. Observed chlorophyll at St. George's Island, April – May 2012. 67
Figure 67. Surface chlorophyll computed at Station LE2.2 using a conventional model of algae as a dissolved substance. 68
Figure 68. Surface chlorophyll computed at Station LE2.2 using a model of algae as particles. 68
Figure 69. Amplitudes of lunar semi-diurnal and diurnal harmonics of observed and computed chlorophyll time series. 70
Figure 70. Power spectrum of chlorophyll observations at Nomini Bay. 70
Figure 71. Power spectrum of chlorophyll observations at St. George's Island. 71
Figure 72. Power spectrum of surface chlorophyll computed at Station LE2.2 using a conventional model of algae as a dissolved substance. 72
Figure 73. Power spectrum of surface chlorophyll computed at Station LE2.2 using the model of algae as particles. 72
Figure 74. Initial particle distribution (Day 45) for four model runs: a) base case; b) particles rise at 1 m d^{-1}; c) particles sink at 1 m d^{-1}; and d) particles rise in RET and sink in LE. 75
Figure 75. Particle distribution at Day 60 for four model runs: a) base case; b) particles rise at 1 m d^{-1}; c) particles sink at 1 m d^{-1}; and d) particles rise in RET and sink in LE. 75

Figure 76. Particle distribution at Day 150 for four model runs: a) base case; b) particles rise at 1 m d^{-1}; c) particles sink at 1 m d^{-1}; and d) particles rise in RET and sink in LE. 76

Figure 77. Particle distribution at run completion (Day 210) for four model runs: a) base case; b) particles rise at 1 m d^{-1}; c) particles sink at 1 m d^{-1}; and d) particles rise in RET and sink in LE. 77

Figure 78. Observed and computed winter, bottom, chlorophyll concentrations for four model runs: a) base case; b) particles rise at 1 m d^{-1}; c) particles sink at 1 m d^{-1}; and d) particles rise in RET and sink in LE. 78

Figure 79. Observed and computed winter, surface, chlorophyll concentrations for four model runs: a) base case; b) particles rise at 1 m d^{-1}; c) particles sink at 1 m d^{-1}; and d) particles rise in RET and sink in LE. 78

Figure 80. Observed and computed spring, bottom, chlorophyll concentrations for four model runs: a) base case; b) particles rise at 1 m d^{-1}; c) particles sink at 1 m d^{-1}; and d) particles rise in RET and sink in LE. 79

Figure 81. Observed and computed spring, surface, chlorophyll concentrations for four model runs: a) base case; b) particles rise at 1 m d^{-1}; c) particles sink at 1 m d^{-1}; and d) particles rise in RET and sink in LE. 80

Figure 82. Cumulative distribution plot of observed and computed chlorophyll concentration at all depths and stations. Computed results from four model runs: base case; particles rise at 1 m d^{-1}; particles sink at 1 m d^{-1}; and particles rise in RET and sink in LE. 80

Figure 83. Fall-line flow in the Potomac River for dry (1999) versus wet (1994) hydrologic conditions. 81

Figure 84. Particle distribution computed for dry hydrology (1999) versus base (1994) conditions. Base conditions are in the left column (panels a - d). 82

Figure 85. Observed and computed chlorophyll at LE2.2 for three depths (surface, mid-depth, bottom) and two hydrologic conditions: 1994, wet (panels a - c) and 1999, dry (panels d - f). 83

Figure 86. Observed and computed spring chlorophyll concentrations for two hydrologic conditions: 1994, wet (panels a, b) and 1999, dry (panels c, d). 84

Figure 87. Cumulative distribution plot of observed and computed chlorophyll concentration at all depths and stations for 1999. 85

Tables

Table 1. Physical characteristics of Potomac River Estuary segments. These are derived from corresponding properties of the model computational grid. 17

Table 2. Algal Kinetics Parameters 50

Preface

Funding for the preparation of this report was provided by the Ecosystem Management & Restoration Research Program.; Glenn Rhett is Program Manager. This report was prepared by Dr. Carl F. Cerco and Mark R. Noel of the Water Quality Modeling Branch (WQMB), Environmental Laboratory (EL), US Army Engineer Research and Development Center (ERDC).

The report was prepared under the direct supervision of Dr. Dorothy Tillman, Branch Chief, WQMB; under the general supervision of Dr. Warren Lorentz, Division Chief, Environmental Processes and Engineering Division (EPED); and Dr. Beth Fleming, Director, EL, ERDC.

At the time of publication, COL Kevin Wilson was ERDC Commander. Dr. Jeffery Holland was ERDC Director.

1 Introduction

Reliable prediction of phytoplankton transport and production is central to the understanding and remediation of a host of environmental problems, including eutrophication and the occurrence of harmful algal blooms. Quantitative phytoplankton models have existed for decades (Riley 1946), yet virtually all examples are based on the original framework wherein phytoplankton are a dissolved substance transported passively and exclusively by hydrodynamic processes. The authors will test the hypothesis that phytoplankton dynamics (particularly the occurrence of blooms) can be more accurately predicted by treating phytoplankton as discrete particles capable of self-induced transport via buoyancy regulation or other behaviors.

One of the earliest quantitative phytoplankton models was presented by Riley (1946). Riley's model described the seasonal trends in phytoplankton biomass as the sum of three processes: photosynthesis, respiration, and grazing. These processes were expressed as functions of fundamental variables, including: irradiance, light attenuation, temperature, mixed-layer depth, herbivore abundance, and nutrient availability. Later models (DiToro et al. 1971; Steele 1974) significantly expanded on Riley's formulations while retaining the basic processes. These landmark studies all described time variability in phytoplankton biomass that was at a single location.

Spatial variability was added to phytoplankton models through division of large systems into well-mixed boxes (Kremer and Nixon 1978; Thomann and Fitzpatrick 1982). The basic process relationships were applied within each box and exchange of material between the boxes was quantified by means of long-term flows and/or exchange coefficients. The final step in the development of modern phytoplankton models was the coupling of phytoplankton dynamics to physics-based multi-dimensional hydrodynamic models (e.g., Cerco and Cole 1993; Fennel and Neuman 1996; Moll and Radach 2003). These state-of-the-art models fundamentally assume that 1) phytoplankton are well-mixed throughout model cells, as defined by the computational grid; and 2) phytoplankton move passively with prevailing currents and turbulence. At present, computer codes for coupled hydrodynamic/phytoplankton simulations are widely distributed

(http://www.myroms.org; http://www.epa.gov/athens/wwqtsc/html/efdc.html) and large-scale, multi-dimensional simulations are commonplace. Despite the spread of technology and increase in computational complexity, however, the basics of phytoplankton models remain largely as expressed by Riley more than 60 years ago.

The current, advanced models still fail to describe all observed phytoplankton processes. For example, the Potomac River Estuary, a tributary of the Chesapeake Bay system, regularly exhibits a spring diatom bloom not captured by conventional models due to a fundamental departure from current assumptions of phytoplankton dynamics. Most significantly, maximum algal concentrations commonly occur at the bottom of the estuary, in the total absence of light (Figure 1). A conventional phytoplankton model predicts the maximum biomass should occur in the photic zone, at or near the surface. A second quandary is that maximum surface concentration occurs mid-estuary, distant from the oceanic source of the diatoms and from the watershed nutrient load (Figure 2). The proposed conceptual model is that the observed properties of the bloom represent a propagation mechanism (Figure 3). Oceanic diatoms travel upstream with prevailing currents near the bottom. When they reach the head of the salt intrusion, they are advected upwards into the light, forming a surface bloom. As they are subsequently carried downstream with prevailing surface currents, they sink towards the bottom (potentially as a result of internal buoyancy control), forming a subsurface concentration maximum. Near the bottom, they are carried upstream again, propagating the bloom. A similar mechanism was proposed by Tyler and Seliger (1978) to explain the occurrence of dinoflagellate blooms in upper Chesapeake Bay.

Several model innovations are necessary to test the proposed model. First, phytoplankton must be treated as particles with the potential to behave, in order to maintain themselves in favorable currents; this will be achieved by building upon existing particle-tracking technology. Second, the number of individual cells must be reduced to some feasible number, done by employing super-individuals that represent a population of individual cells, thus limiting the number of particles to approximately 100,000. Last, the particles must dynamically interact with the model environment; phytoplankton must be able to respond to potential cues from light, temperature, salinity, and other factors. The authors will install the newly-developed algorithms into an existing comprehensive eutrophication model which will provide transport and ambient conditions to the modeled particles.

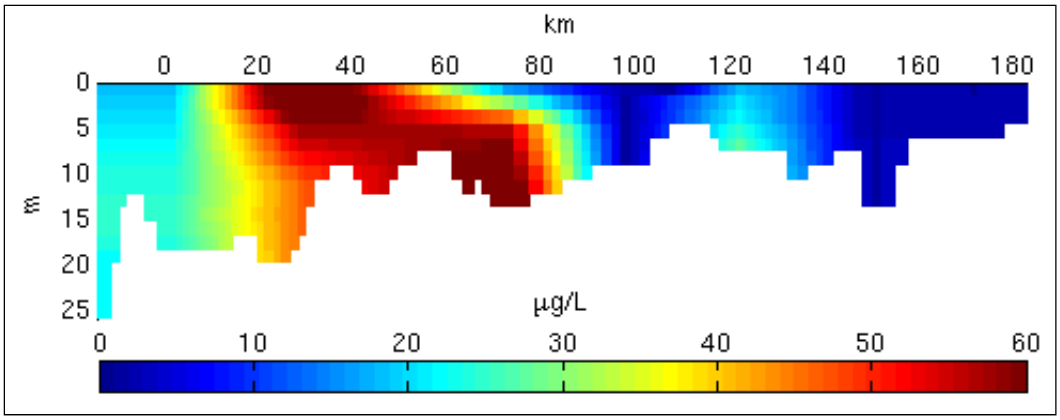

Figure 1. Elevation view of chlorophyll along the Potomac River Estuary, April 1999. Distance is indicated from the mouth, at left, to the head of tide, at right. Note that chlorophyll concentrations in excess of 60 µg L^{-1} occur at depths greater than 10 m from km 60 to 80 and that subsurface concentration exceeds surface concentration in that region. Note also the suggestion that chlorophyll is borne by gravitational circulation, from mouth to head near the bottom and from head to mouth at the surface.

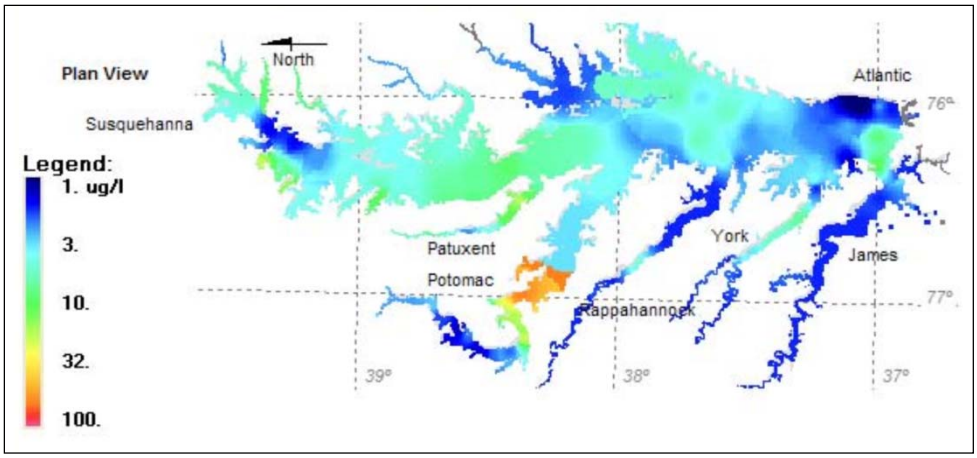

Figure 2. Aerial view of chlorophyll concentration in the Chesapeake Bay system, April 1986. The Potomac River Estuary is in the lower, central portion of the figure. Note that the highest chlorophyll concentrations in the entire system occur at an upwelling region, located at the head of the salt intrusion in the Potomac River.

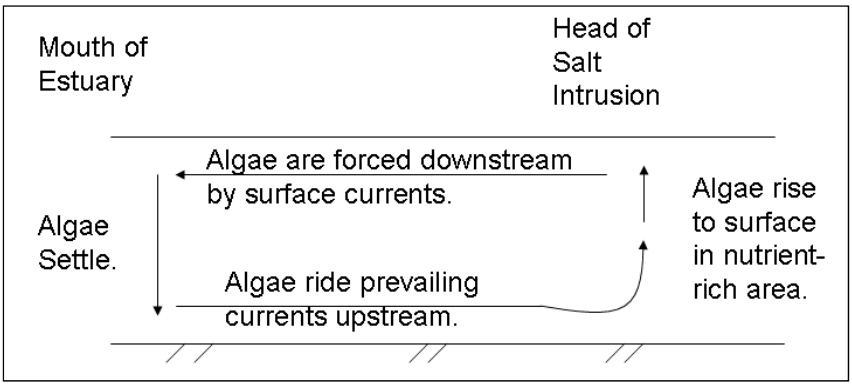

Figure 3. Proposed mechanism to explain the Potomac River spring phytoplankton bloom (elevation view).

Exploratory steps in modeling phytoplankton as particles provide a research framework on which to build. One approach examined the occurrence of harmful algal blooms by treating plankton as passive particles (Lanerolle et al. 2006). This approach validated the concept of treating plankton as particles, but omitted plankton behavior and interactions with the environment. An "agent-based model" (ABM), in which phytoplankton are treated as motile particles, has been used to describe vertical migration and cyst formation as mechanisms behind cyanobacteria blooms (Hellweger et al. 2008). A complete "Eulerian-Lagrangian model," which represents motile plankton particles in an environmental continuum has been described (Woods 2005) and at least one application to a prototype environment has been conducted (Grieco et al. 2005). These studies indicate that modeling phytoplankton as particles, passive or active, is conceptually possible and that the technique has promise. A tremendous amount of research, however, remains in developing the requisite algorithms to capture phytoplankton dynamics, coupling with spatially and temporally resolved water quality models, and investigating the applicability of these approaches to various systems where the current advanced models do not sufficiently predict phytoplankton distribution.

2 ICM Particle Tracking[1]

Introduction

Particle tracking methods can generally be divided into two categories depending upon the way in which they treat the model grid. One approach is to perform the calculations on the physical plane of the grid, while the other is to perform the calculations on a transformed numerical grid. The particle tracking application by Chapman et al. (1994) used a transformed grid to perform all calculations. The calculations on the transformed grid may appear simpler initially; however, the drawbacks with this approach are the numerical complexity, the need to transform the grid both before and after calculations, and the complication of the code. For the ICM implementation, the calculations are performed within the physical plane through the use and application of general algebra, geometry, and physics equations.

Theory and Implementation

Although the ICM grid is unstructured, the orthogonal box approach can still be used with some slight modifications. Consider a particle at position P in the box shown in Figure 4. This figure is shown in only the x-y plane for simplicity.

Although none of the cell faces are orthogonal, an orthogonal box can be created using the points at which the particle would exit the cell if moving along the x and y axes. This is illustrated in Figure 5.

The dashed lines, A-B and C-D, show the paths that the particle would take if it moved strictly along either the x or y axis. The points at which the particle would exit the grid cell along these paths are then used to construct an orthogonal box as shown in Figure 6.

Since the box shown in Figure 6 is perfectly orthogonal and the movement of the particle along each axis is performed separately, the velocities at points A, B, C, and D can be used along with the formulas from Zheng and Bennett (2006a, 2006b) to determine the particle's final location through

[1] Portions of this chapter are adapted from material provided by Mr. Scott Fant, formerly of SpecPro Inc.

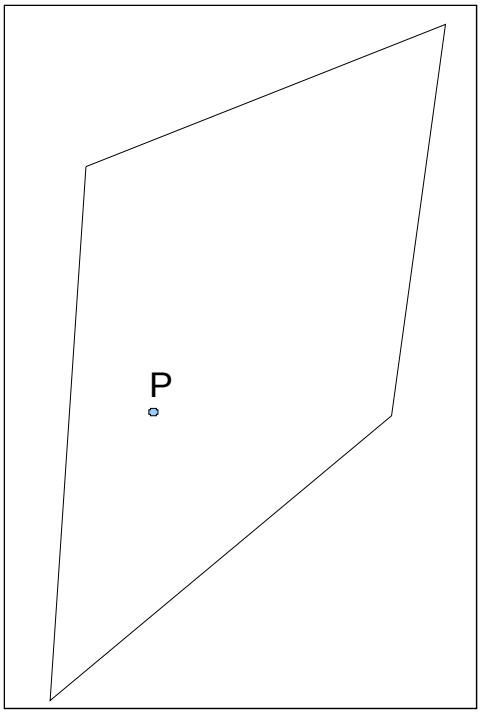

Figure 4. Initial position of a single particle in an unstructured grid cell.

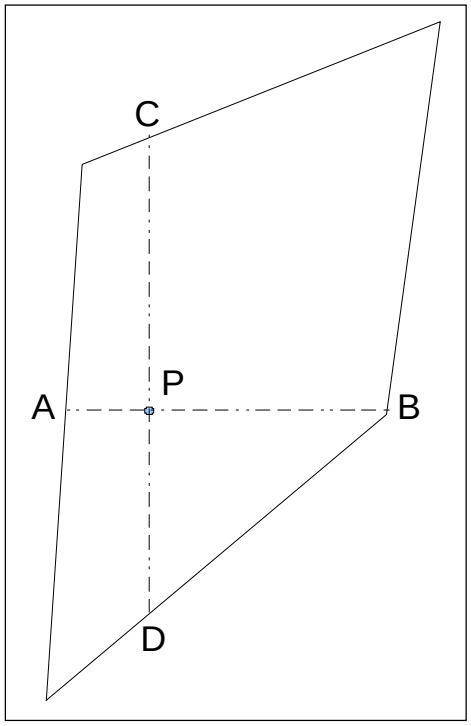

Figure 5. Particle paths along x and y axis.

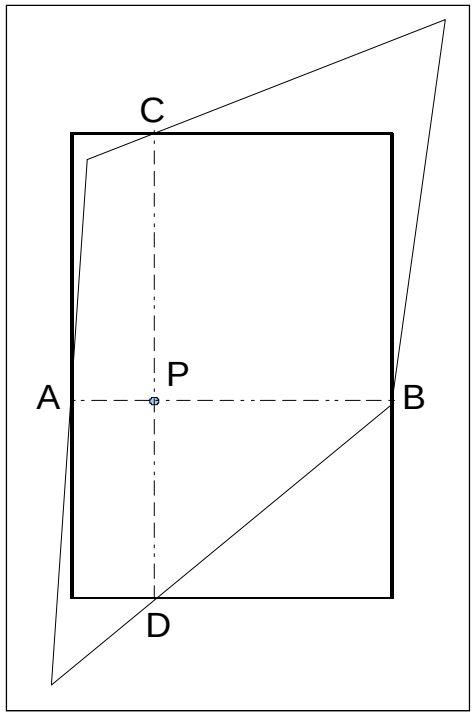

Figure 6. Orthogonal box for bounding particle movement.

integration. Although the lectures from Zheng and Bennett (2006a, 2006b) show the use of these methods for tracking particles in groundwater flow, the same equations should apply to movement in surface water.

The velocities at points A, B, C, and D are determined by finding the vector components of the velocities through the faces. Since the flows are given perpendicular to the flow faces, the angle of each face relative to its appropriate axis is required to determine the components of the vector along the x and y axes. The points at the cell corners are used to determine the equations of the facial lines in the x-y plane. This gives the slope, y-intercept, and facial angle for each flow face. The equations for the facial lines are also used to determine whether a particle has passed through one of the flow faces.

Once the velocities are known, the following equation from Zheng and Bennett (2006a, 2006b) is used to determine the amount of time required for the particle to cross the cell boundary in the x-direction. Similar equations are used for the y and z axes:

$$\Delta t_x = \frac{1}{A_x} \ln\left(\frac{v_{x2}}{v_{x1}}\right) \tag{1}$$

in which:

v_{xp} = Particle velocity in the x-direction at current location
v_{x1} = Particle velocity in the x-direction at point A of the bounding box
v_{x2} = Particle velocity in the x-direction at point B of the bounding box
A_x = $\frac{(v_{x2} - v_{x1})}{\Delta x}$
Δx = Distance between points A and B of the bounding box

This assumes that the flow will be in the positive x-direction. If the flow is in the negative x-direction, all occurrences of v_{x1} in Equation 1 should be replaced with v_{x2}, and vice-versa.

The time that is calculated in Equation 1 is used to determine the maximum time step. If the times calculated for flow along all axes are more than the current model time step, the model time step is used in the calculations. If one or more of the calculated values is less than the model time step, the lowest value is used in the calculations. After movement of the particle, a loop is performed and calculations are made for the remainder of the model time step.

The equation used to determine the particle's final location is given below.

$$x(t_2) = x_1 + \frac{1}{A}\left[v_{xp}(t_1)\exp(A_x \Delta t) - v_{x1}\right] \tag{2}$$

in which:

$x(t_2)$ = Particle location at the end of the time step
x_1 = Particle location at the beginning of the time step
Δt = Particle tracking time step

After performing this calculation for movement along each axis, the particle's final location at the end of the time step will be determined. However, due to the irregular shape of the grid cells, it is possible for a particle to cross a grid cell boundary without crossing any of the bounding box faces. The equations for the facial lines are used to determine whether a particle is outside of the grid cell. If the particle crosses a solid boundary,

the particle position is reset to the edge of the boundary. If the particle crosses into a new grid cell, the containing cell information is updated. If the particle moves out of the grid through a bounding flow face, the containing cell is set to "0" and calculations for the particle will no longer be performed.

Diffusion and Dispersion

The effects of turbulent diffusion and dispersion are translated into random displacement in the particle model. The random displacement is added to the deterministic location derived from advection. For spatially-uniform diffusion, the displacement is (Hellweger and Bucci 2009):

$$\Delta x = R\sqrt{2K\Delta t} \tag{3}$$

in which:

Δx = Particle displacement
R = Random number from a standard normal distribution
K = Diffusion or dispersion
Δt = Particle tracking time step

Axial and transverse dispersion are modeled with a constant value, 12 $m^2 s^{-1}$, and application of Equation 3 is straightforward. Vertical turbulent diffusion is spatially varying and influenced by turbulent shear, mixing length, and density stratification. More sophisticated formulae for addressing spatially varying diffusion are available (Ross and Sharples 2004) although their implementation can be complex on the unstructured ICM computational grid. As a first approximation, the formula for spatially uniform diffusion is employed using a characteristic value K = 10^{-5} $m^2 s^{-1}$. Investigation of the effects of spatially varying diffusion is left for additional investigation following completion of the initial stage of this investigation.

Caveats

Although the basic implementation may appear simple in nature, there are several issues that must be considered and dealt with as appropriate. When a particle is near the edge of a cell, the bounding box may be rather small. This could cause the particle to approach the boundary asymptotically, in which case the particle-tracking module may appear to loop endlessly. In order to prevent this, the bounding box is generally extended by a distance

of two meters in each direction to allow for movement of the particle across the cell boundary. Flow toward a solid boundary can also cause the same type of problem since a particle that passes a solid boundary is reset to the edge of the boundary. To avoid this situation, the velocity in the direction of a solid boundary is set to a value of "0" if the particle is within one meter of the boundary.

Another issue that can cause problems is the orientation of the grid cells. Due to the unstructured nature of the grid, positive flow in the x-direction is not always along the x-axis. This is especially true in tributaries that may curve dramatically. This is illustrated below in Figure 7.

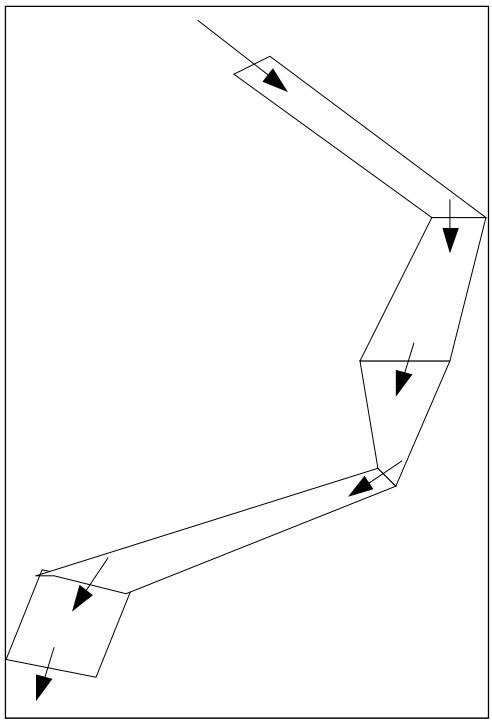

Figure 7. Grid cells in a tributary indicating flow in the positive x-direction.

As seen in this figure, all of the grid cells are linked end-to-end. However, the direction of flow through these faces changes due to the irregularities of the cell shapes. This does not impact transport of contaminants between cells, but requires a routine to reorient the faces and facial flows of the cell in order to perform the calculations accurately for spatially aware particles. This routine requires that the grid cell coordinates be specified in a clockwise manner in the input file. Although it's possible to write a routine to work with grid points specified in the opposite direction, it is much easier to simply specify the data in the required manner.

As mentioned previously, a check is performed on the particle location after each time step to determine if the particle has passed through a cell face. However, if the particle passes through the corner of the cell, the new containing cell can be difficult to determine. For this reason, another check of the particles location is performed at the beginning of the calculations. If the particle is found to be outside of the current cell, the containing cell is updated, and the test is performed again. Although this works reasonably well, there are certain cases for which this may cause an endless loop. This issue does not occur frequently and has yet to be resolved. It appears that the calculations are not accurate enough to detect the containing cell of a particle that is very close to a facial boundary. This only seems to occur with very small grid cells.

3 Phytoplankton Kinetics

A primary goal of this investigation is to transport algae as particles, rather than by analogy to a dissolved substance. Aside from potential differences in net transport, this approach allows for incorporation of algal behavior, such as rising and falling via buoyancy regulation. Algae are quantified as biomass (carbon) per particle. The number of particles in the system is constant. Changes in algal biomass are represented by altering the biomass attached to a particle rather than by changing the number of particles. The particle-based kinetics are incorporated into the framework provided by the CH3D hydrodynamic model (Johnson et al. 1993; Kim 2012) and the ICM eutrophication model (Cerco and Cole 1993; Cerco and Noel 2012)

Basic Equation

The basic equation for algal biomass is:

$$\frac{dB}{dt} = (G - Pr) \bullet B \tag{4}$$

in which:

B = Algal biomass per particle (g C)
G = Net growth rate (d^{-1})
Pr = Net predation rate (d^{-1})

The computer code employs discrete arithmetic so that the solution to Equation 3 is:

$$B^{t+\Delta t} = B^{t} \bullet \left(1 + (G - Pr) \bullet \Delta t\right) \tag{5}$$

in which:

$B^{t+\Delta t}$ = Algal biomass per particle at time t+Δt (g C)
B^{t} = Algal biomass per particle at time t (g C)
Δt = Discrete model time step (d)

The net growth rate is derived from photosynthesis minus respiratory losses:

$$G = \frac{P^B}{CChl} \bullet (1 - PRSP) - BM \tag{6}$$

in which:

P^B = Photosynthetic rate (g C g^{-1} Chl d^{-1})
CChl = Carbon-to-chlorophyll ratio (g C g^{-1} chlorophyll a)
PRSP = Active respiration ($0 \leq PRSP \leq 1$)
BM = Basal metabolism

The photosynthetic rate is influenced by ambient light, temperature, and nutrient concentration as described by Cerco (2000), Cerco and Noel (2004) and Cerco at al. (2010). These references also describe the formulations for metabolism, predation, and other influences on algal biomass.

From Particles to the Continuum

The rate of change in biomass attached to a particle is determined by the environment surrounding the particle; e.g., light and temperature. The rate of change also influences the environment; e.g., ambient nutrient concentration. A means is necessary to translate from the particle-based system to the continuum. The approach employed here takes advantage of the discrete computational grid employed by the hydrodynamic model and by the ICM eutrophication model. ICM kinetics are based on ambient conditions and on concentrations computed in individual computational cells. The cell-based conditions and concentrations provide the environment for the particles. The particles are arrayed in a computational structure which labels each particle with its current grid cell. The structure and labeling allow the computer code to loop over all particles or over all cells. The code can query particles: “What cell am I in?” Or it can query cells: “What particles do I contain?” The revised ICM code with particle-based kinetics employs the algal subroutine from the conventional ICM code to provide the particle environment, compute growth and loss rates, and provide interactions with quantities computed in the continuum such as nutrient concentration. The algal concentration is computed as:

$$Conc_i = \frac{\sum_{P=1}^{n} B_{i,P}}{V_i} \tag{7}$$

in which:

$Conc_i$ = Algal concentration in grid cell i (g C m^{-3})
n = Number of particles in grid cell i
$B_{i,P}$ = Algal biomass attached to particle P in grid cell i (g C)
V = Volume of grid cell i

Particle-based photosynthetic rate is computed:

$$P_i^B = P^B m \bullet f(I)_{CID} \bullet f(N)_{CID} \bullet f(T)_{CID} \tag{8}$$

in which:

P_i^B = Photosynthetic rate associated with particle i (g C g^{-1} Chl d^{-1})
$P^B m$ = Maximum photosynthetic rate under ideal conditions (g C g^{-1} Chl d^{-1})
$f(I)_{CID}$ = Effect of light on photosynthetic rate in cell CID, containing particle i ($0 < f(I) < 1$)
$f(N)_{CID}$ = Effect of nutrients on photosynthetic rate in cell CID, containing particle i ($0 < f(N) < 1$)
$f(T)_{CID}$ = Effect of temperature on photosynthetic rate in cell CID, containing particle i ($0 < f(T) < 1$)

Environmental effects on particle-based metabolism and similar parameters are computed by analogy to Equation 8.

Kinetics Rules for Particles

Particle-tracking models conventionally incorporate rules for particle behavior. Particle position is influenced by rules as well as by hydrodynamics. Rules are especially common for determining particle behavior when the trajectory takes a particle outside the model domain. The rules associated with the present particle-tracking algorithms are described in Chapter 2. Physical rules for particle behavior potentially affect the attached algal biomass. Behavioral rules can also be formulated based on influences from the attached biomass, instead of physical principles. Three rules are enforced which influence particle behavior and associated algal biomass. These rules are intended to keep the number of particles in the system constant and to ensure that each particle is associated with viable algal biomass:

1. When a particle leaves the system through an open boundary, the particle with the largest attached algal biomass is split in two. Half the algal biomass is assigned to each particle.
2. When a particle adheres to a solid boundary, the particle is removed from the system. The particle with the largest attached algal biomass is split in two. Half the algal biomass is assigned to each particle.
3. If algal biomass associated with a particle declines to less than 1% of the initial value, the particle is removed from the system. The particle with the largest attached algal biomass is split in two. Half the algal biomass is assigned to each particle.

4 The Potomac River Estuary

The Potomac River Estuary (Figure 8) is a major sub-estuary of the larger Chesapeake Bay system. The estuary extends 190 km from the junction with Chesapeake Bay to the head of tide at Washington DC. Mean tide range near the mouth is 0.38 m and is 0.84 m at Washington DC. The estuary is a drowned river valley and the saline portion is weakly-stratified by Pritchard's classification (Pritchard 1955). The primary freshwater source is from the 29,940 km^2 upland watershed and enters at the head of tide. Lesser volumes enter the estuary from the adjacent watershed below the head of tide. Long-term mean runoff at Washington DC is 339 $m^3 s^{-1}$. This long-term mean is subject to regular seasonal fluctuations as well as extremes due to flood and drought.

Salinity intrudes roughly 140 km from the mouth to the vicinity of Station TF2.4 (Figure 8). The EPA Chesapeake Bay Program (CBP) divides the estuary into three segments based on characteristic salinity, geometry, and other features. The tidal fresh segment corresponds to the region occupied by the stations designated "TF" in Figure 8. The oligohaline segment is occupied by the stations designated "RET." The mesohaline segment comprises the remainder of the estuary. The spring algal bloom that is the subject of this investigation is confined to the oligohaline and mesohaline regions. Physical characteristics of these regions are summarized in Table 1.

The Chesapeake Bay Environmental Model Package (CBEMP)

The particle-tracking model is inserted into the existing CBEMP. The CBEMP consists of three independent models: a watershed model (WSM), a hydrodynamic model (HM) and a eutrophication model (WQM). The WSM (Shenk and Linker 2012) provides distributed flows to the HM and nutrient and solids loads to the WQM. The HM (Johnson et al. 1993; Kim 2012) computes three-dimensional intra-tidal transport and supplies transport parameters to the WQM on an hourly basis. The WQM (Cerco et al. 2010) computes algal biomass, nutrient cycling, and dissolved oxygen, as well as numerous additional constituents and processes.

Both the HM and WQM operate on a three-dimensional grid that encompasses the entire Chesapeake Bay system. For this study, the Potomac River portion of the grid (Figure 9) was extracted along with the

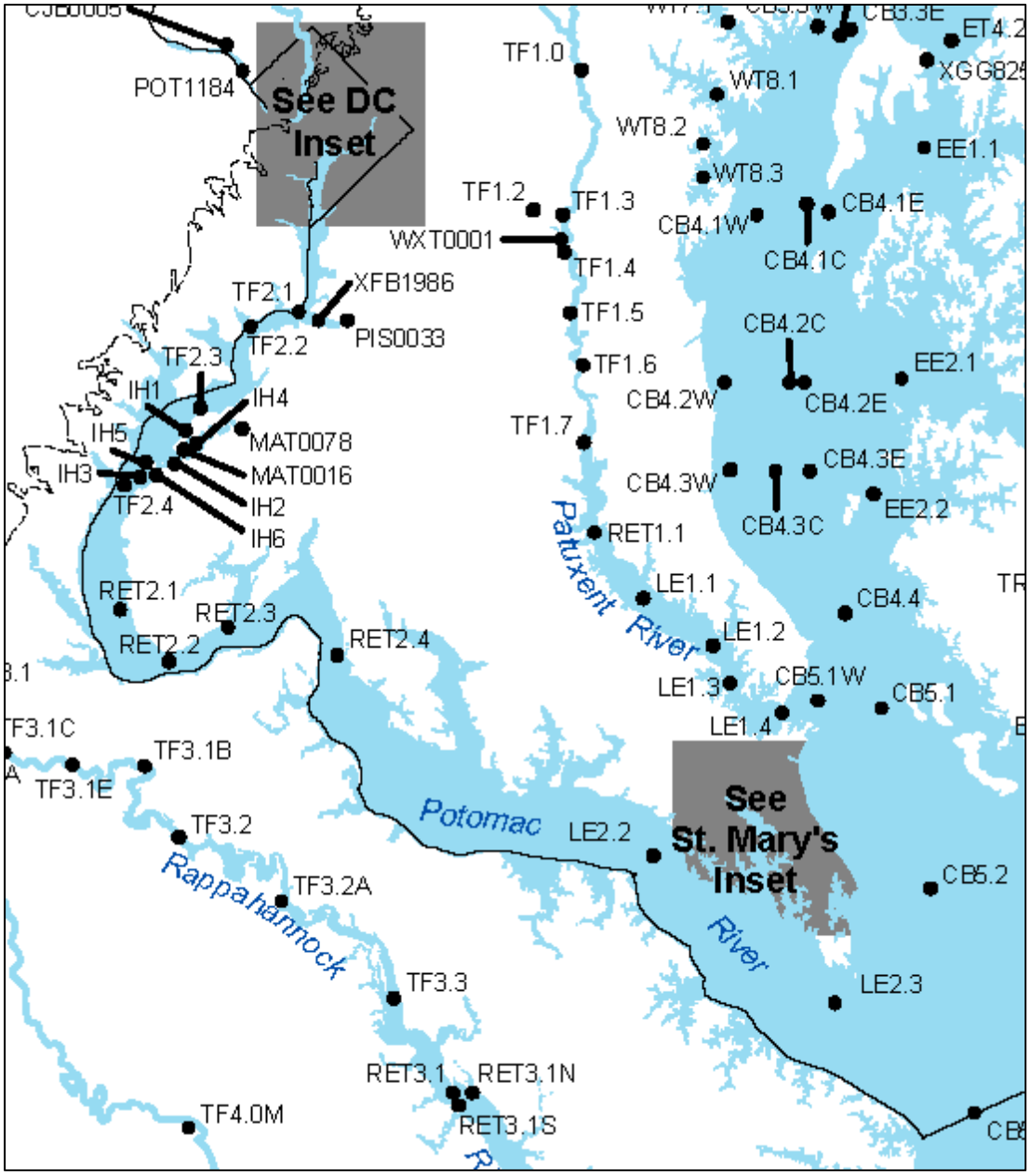

Figure 8. The Potomac River Estuary showing CBP sample stations.

Table 1. Physical characteristics of Potomac River Estuary segments. These are derived from corresponding properties of the model computational grid.

	Tidal Fresh (TF)	Oligohaline (RET)	Mesohaline (MH)
Length (km)	61.4	44.0	77.6
Surface Area (km^2)	144	207	837
Volume (10^6 m^3)	700	1089	6542
Maximum Depth (m)	14.4	12.8	20.5

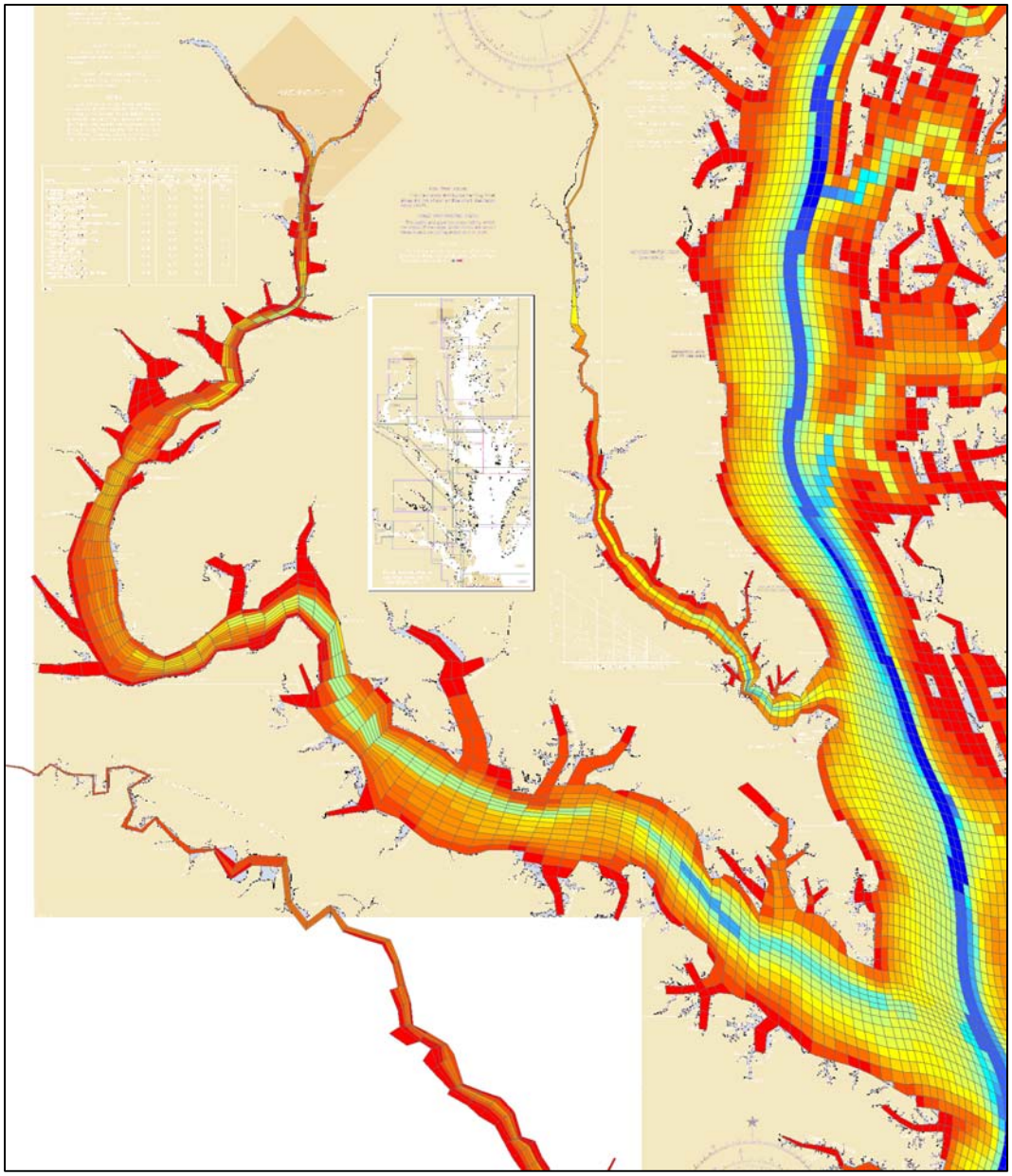

Figure 9. The Potomac River portion of the Chesapeake Bay computational grid. Depths are shown from shallow (red) to deep (blue).

associated hydrodynamics. An adjacent portion of Chesapeake Bay was included so that downstream boundary conditions could be specified at a distance sufficient to minimize influence on the upstream portions of the system. The resulting grid extended the 190 km length of the Potomac River estuary (Figures 10, 11) and incorporated numerous embayments and tributaries. The grid consisted of 1739 surface elements (650 m x 1,300 m x 1.5 m) and 8,965 total elements. A seven-year period, 1994-2000, was simulated continuously using hydrodynamic time steps of 30 seconds and water quality time steps of 200 seconds.

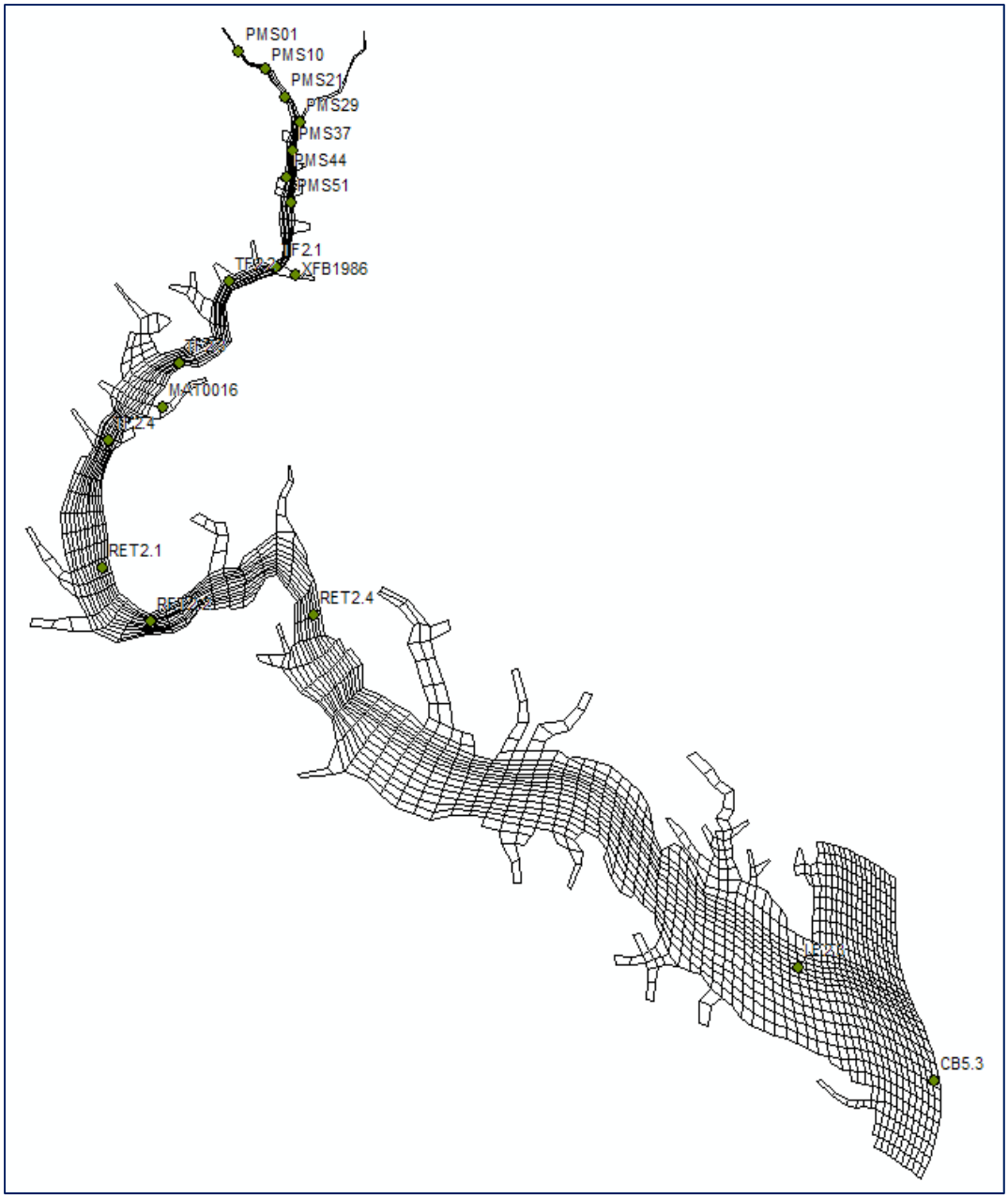

Figure 10. The surface plane of the independent Potomac River computational grid showing CBP sample stations.

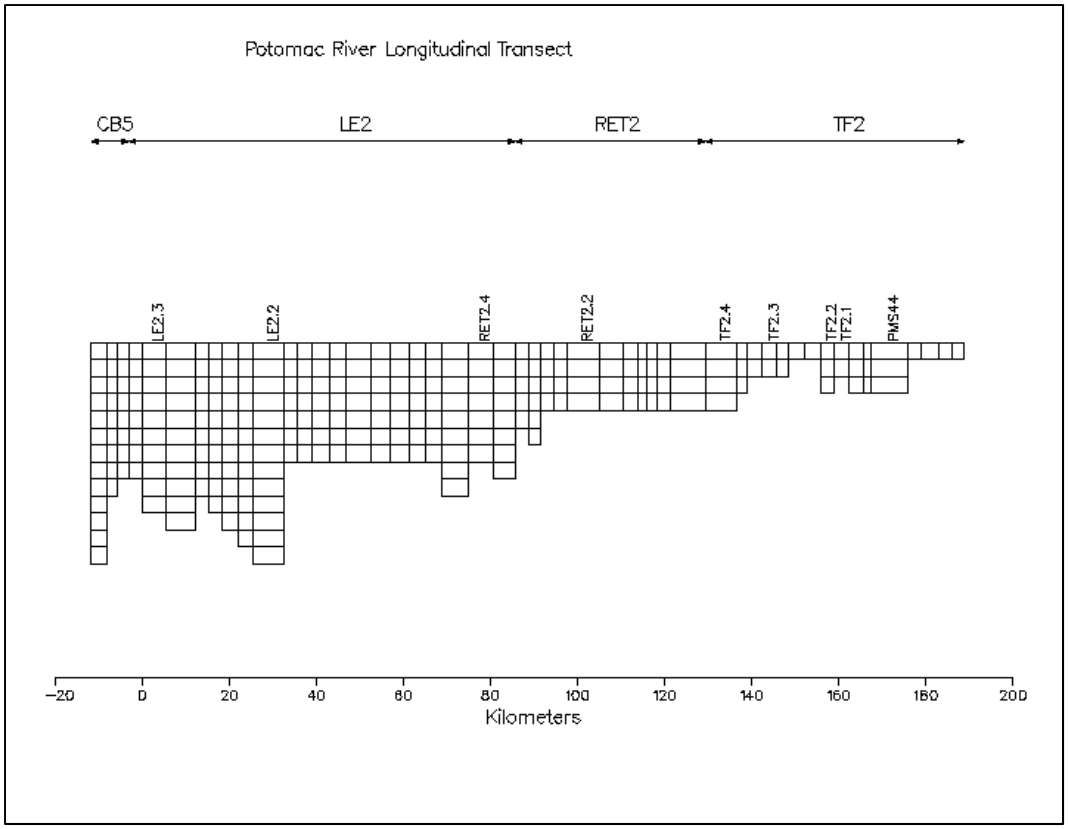

Figure 11. Elevation view of the Potomac River computational grid from the mouth (km 0) to the head of tide (km 190).

The extracted model was checked against the original model and against data to ensure that the extraction was performed correctly. This model version was used as a starting point for the particle-tracking algorithms and associated algal kinetics. The formulation and validation of the WQM have been described elsewhere (Cerco et al. 2010; Cerco and Noel 2012) and will not be repeated. The authors concentrate here on new developments associated with treatment of algae as particles.

Water Quality Database

The CBP conducts a monitoring program throughout Chesapeake Bay and tributaries (Chesapeake Bay Program 2012a). Stations are monitored at monthly intervals with measures conducted in-situ (temperature, salinity, dissolved oxygen, light attenuation) and samples collected at various depths for later analysis (chlorophyll, multiple forms of organic carbon, organic and inorganic nitrogen, organic and inorganic phosphorus, and suspended solids). Observations at the stations designated “TF,” “RET,” and “LE” (Figure 8) for the modeling period were retrieved from an on-

line database and subjected to various summary procedures for comparison with the model.

Phytoplankton Database

The CBP also conducts a Living Resources Monitoring Program which includes a phytoplankton component (Chesapeake Bay Program 2012b). The phytoplankton monitoring program is designed to detect and monitor changes in phytoplankton abundance and taxonomic composition in relation to water quality conditions in Chesapeake Bay. Sampling is conducted at roughly monthly intervals, although sampling intervals and protocols have varied over the course of the program. Relevant phytoplankton stations in the Potomac River are at RET2.2 and LE2.2 (Figure 8). Station CB5.2, in the mainstem of the bay, provides information on the region encompassing the junction of the Potomac River with the bay. Samples were collected above and below pycnocline at RET2.2 until 1989, after which a single whole-water column sample was collected. Samples were collected above and below pycnocline at LE2.2 and CB5.2 until 1995 when only a surface composite sample was analyzed.

Phytoplankton Biomass and Species

Phytoplankton counts, by species, comprised the original data contained in the Phytoplankton Database. These were converted to biomass as carbon, through multiplication by conversion factors (pg C $cell^{-1}$) associated with the database. The three diatom species with the greatest biomass during the spring months at the three relevant stations were identified as Cerataulina Pelagica (CP), Chaetoceros Subtilis (CS), and Pseudo-Nitzschia Pungens (PP). CP and PP were largely restricted to the spring months, roughly February – May, while CS was present year-round. The biomass of the three species in each observation was summed to give a total diatom biomass for the spring bloom species. The total was summarized by station, month, and level, where appropriate, for the years 1991 – 2000. The summary (Figure 12) indicated the bloom occurred primarily from February – May. While the bloom was not prominent, in an average sense, in January, an observation of CP was sufficient to skew the median and indicated that biomass of bloom magnitude was possible in that month. The observations also indicated that the bloom occurred primarily downstream of RET2.2, although the upstream limit of the bloom could not be determined due to lack of observations between RET2.2 and LE2.2. Diatoms were abundant below the pycnocline with biomass exceeding that above the pycnocline in

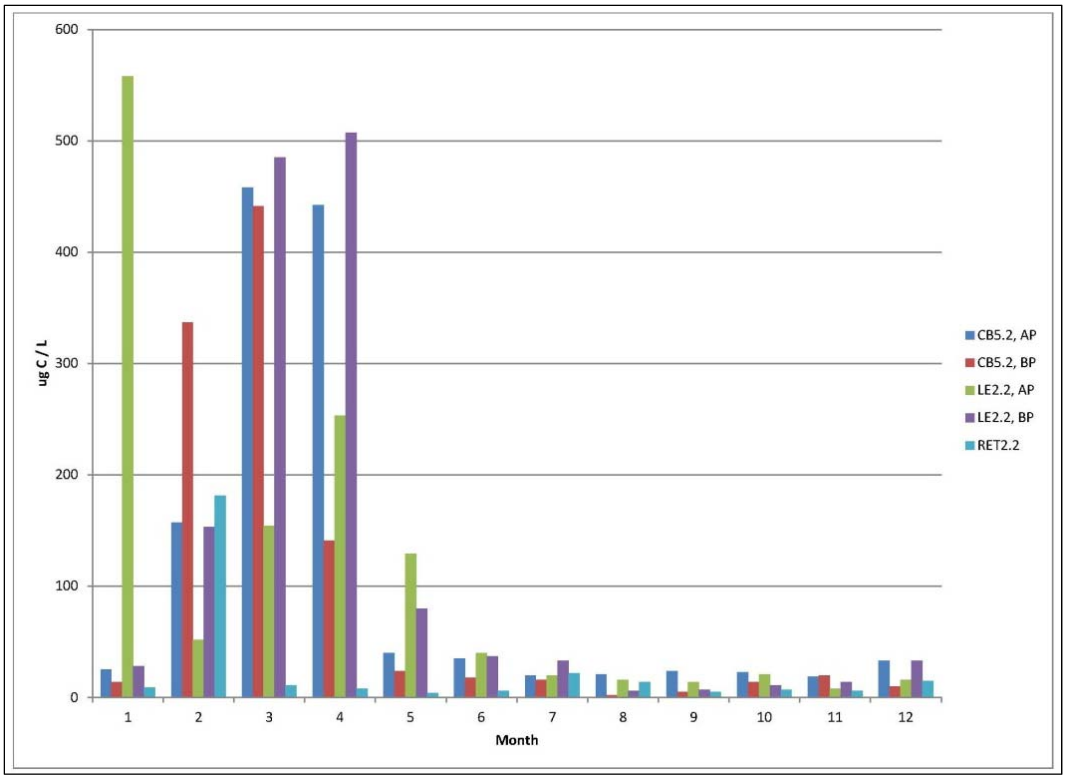

Figure 12. Median monthly biomass for the sum of three diatoms at three stations, 1991 – 2000. (AP = above pycnocline, BP = below pycnocline, RET2.2 is whole-water sample).

some months. The degree to which below-pycnocline biomass exceeds above-pycnocline may be confounded, however, by the cessation of sub-pycnocline sampling in 1995.

Biomass for individual species was subjected to similar analyses. At RET2.2, the highest bloom biomass occurred during the month of February and consisted almost exclusively of CP and PP (Figure 13). At LE2.2, the predominant bloom species was CP, which occurred primarily from February to May, although the first appearance was in December and one instance of enormous biomass was observed in January (Figure 14). Median below-pycnocline biomass of CP commonly exceeded the above-pycnocline biomass. The bloom of PP commenced a month earlier than CP, in December, and likewise ended a month earlier, in April. The timing of the bloom at CB5.2 was similar to LE2.2, although at this station PP biomass rivaled CP from December through March (Figure 15). Median below-pycnocline biomass of both CP and PP frequently exceeded the above pycnocline biomass.

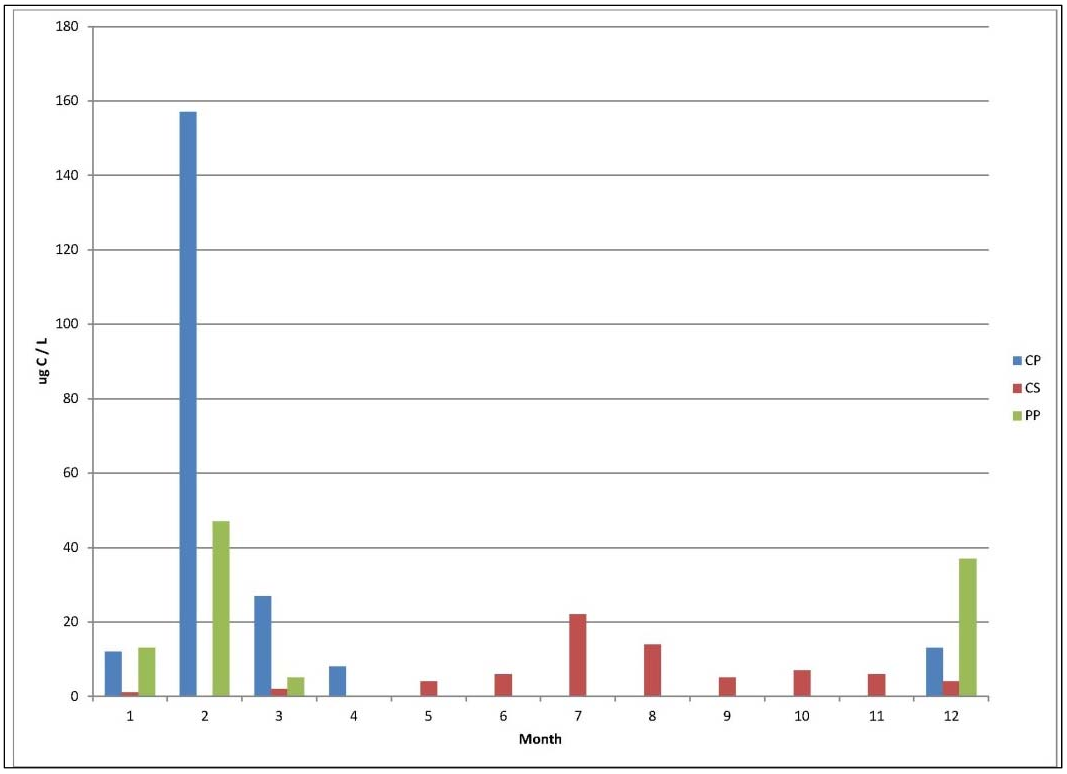

Figure 13. Median monthly biomass for each of three diatom species at Station RET2.2, 1991 – 2000. (CP = Cerataulina Pelagica, CS = Chaetoceros Subtilis, PP = Pseudo-Nitzschia Pungens)

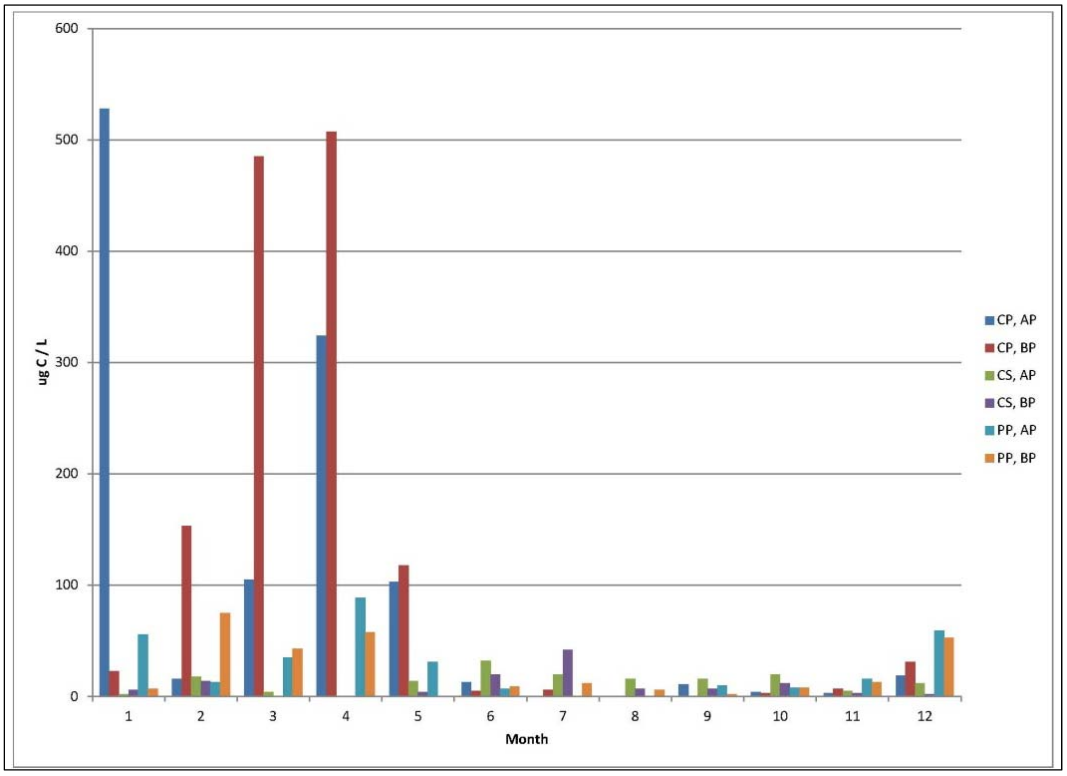

Figure 14. Median monthly biomass for each of three diatom species at Station LE2.2, 1991 – 2000.

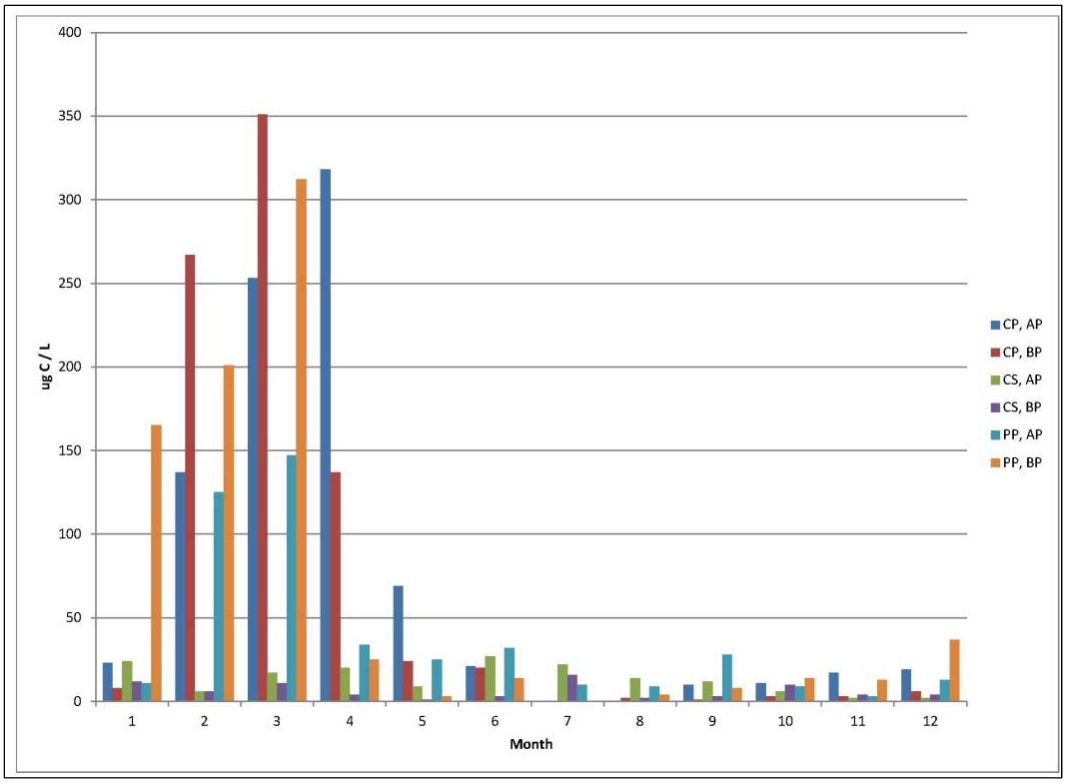

Figure 15. Median monthly biomass for each of three diatom species at Station CB5.2, 1991 – 2000.

Chlorophyll Observations

Chlorophyll observations were plotted for each survey from November through May for the years 1991 – 2000. Figures were produced as elevations, or profiles, along the Potomac axis from RET2.2 to CB5.1 and were superimposed on the model grid to provide bathymetry and spatial perspective. Results are presented for three years, 1997 (December 1996 – May 1997), 1998 (December 1997 – May 1998), and 1999 (December 1998 – May 1999). These years were selected because they represent, respectively, the average, highest, and lowest November – May flows in the ten-year series.

Peak chlorophyll concentrations in December (Figure 16) are in the range 15 – 20 μg L^{-1} and are concentrated in the region from RET2.4 to LE2.3. By January, concentrations increase to ≈ 30 μg L^{-1} and indicate the development of a subsurface chlorophyll maximum (Figure 17). By February (Figure 18), the maximum chlorophyll concentration approached 100 μg L^{-1} in 1997, the subsurface chlorophyll maximum was readily apparent, and the bloom extended from RET2.4 to LE2.3. By March of the years with low to average flow, the highest chlorophyll concentrations extend upstream to RET2.2 and RET2.3, although these concentrations, 5 to 18 μg L^{-1}, are lower

than in other months (Figure 19). In the high-flow year, chlorophyll concentrations are of greater magnitude ≈ 45 µg L^{-1}, occur between LE2.2 and CB5.1, and continue to show a subsurface maximum. By April, peak chlorophyll concentrations have recovered to 40 to 50 µg L^{-1}, and are in the lower estuary from LE2.2 to CB5.1 (Figure 20). By late May, maximum chlorophyll concentrations are 13 to 30 µg L^{-1}, and spatial patterns are difficult to detect (Figure 21). The biomass plots suggest these chlorophyll concentrations represent the last significant presence of the CP and PP bloom for the season (Figure 14, 15).

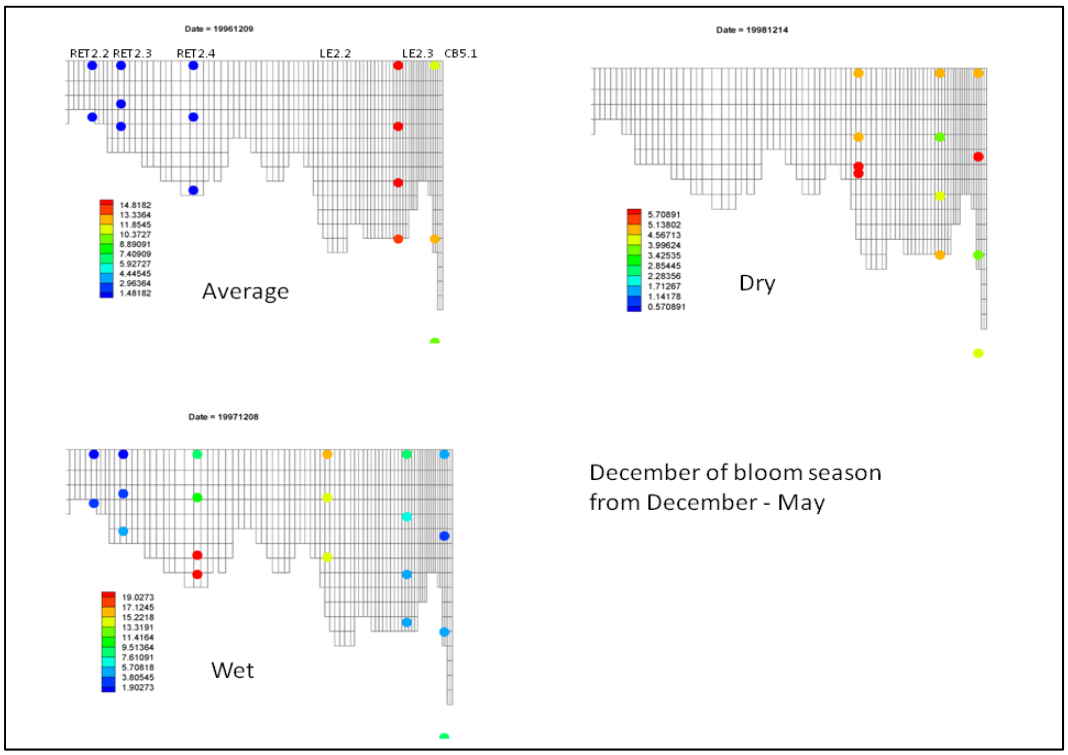

Figure 16. Chlorophyll concentrations (ug L^{-1}) in December of seasons of average, wet, and dry hydrology. Samples are superimposed on an elevation view of the computational grid. Station names are shown above the upper left panel.

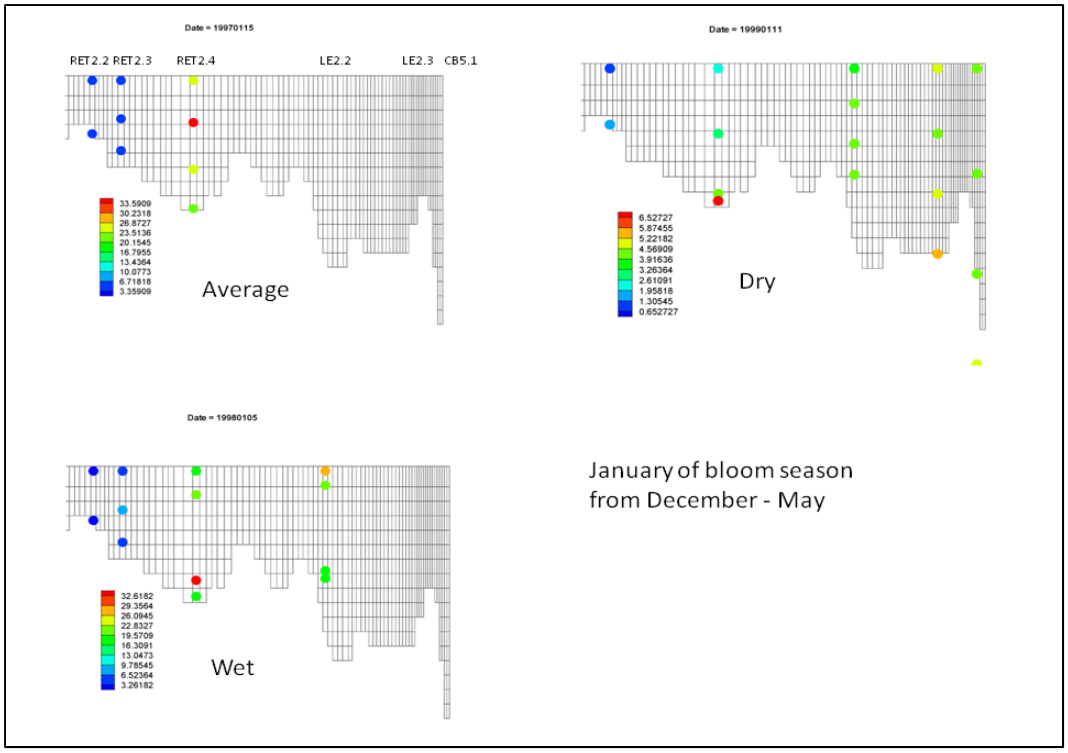

Figure 17. Chlorophyll concentrations (ug L^{-1}) in January of seasons of average, wet, and dry hydrology. Samples are superimposed on an elevation view of the computational grid. Station names are shown above the upper left panel.

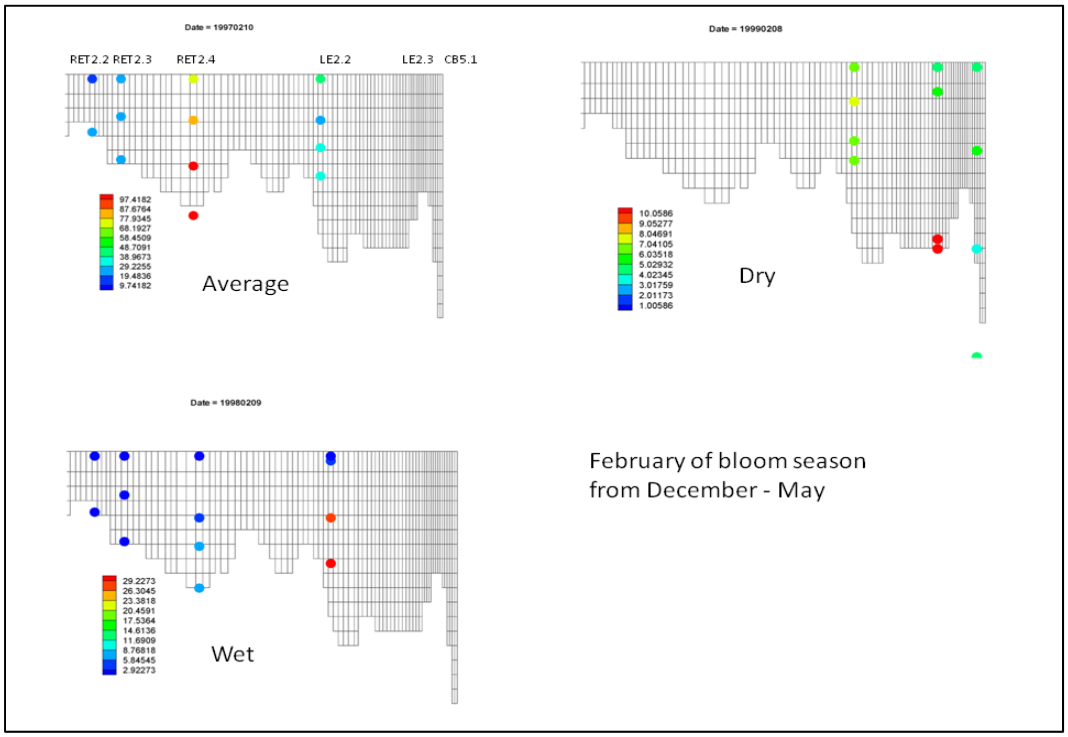

Figure 18. Chlorophyll concentrations (ug L^{-1}) in February of seasons of average, wet, and dry hydrology. Samples are superimposed on an elevation view of the computational grid. Station names are shown above the upper left panel.

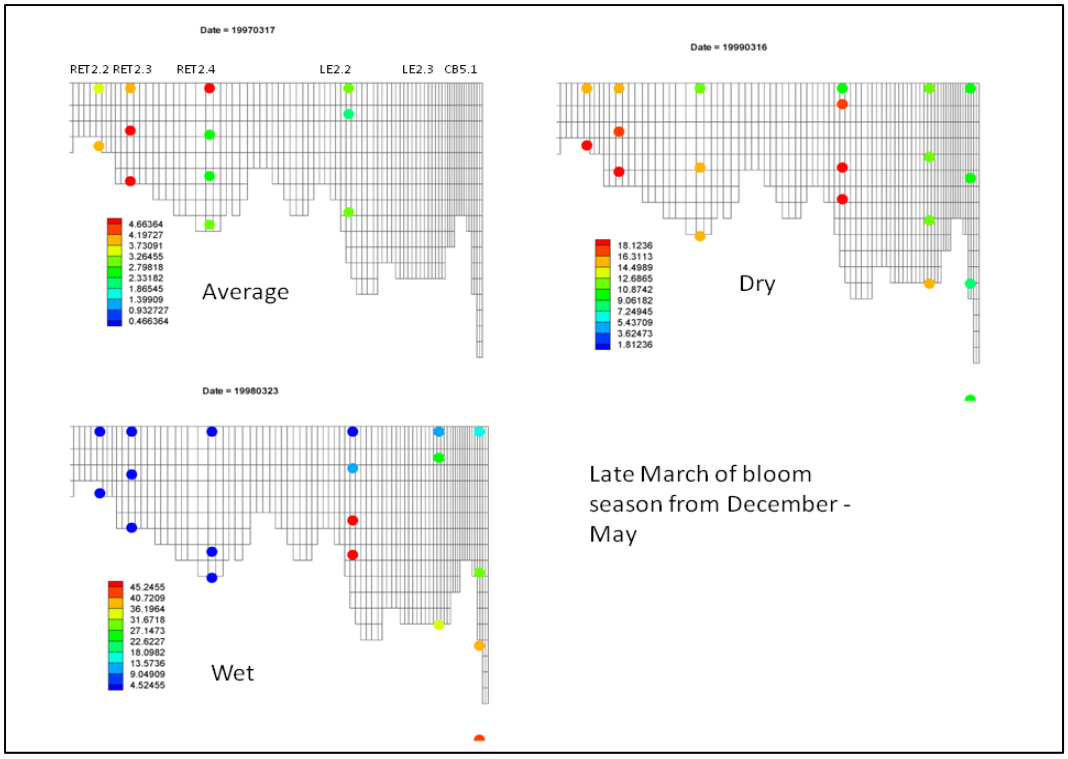

Figure 19. Chlorophyll concentrations (ug L^{-1}) in late March of seasons of average, wet, and dry hydrology. Samples are superimposed on an elevation view of the computational grid. Station names are shown above the upper left panel.

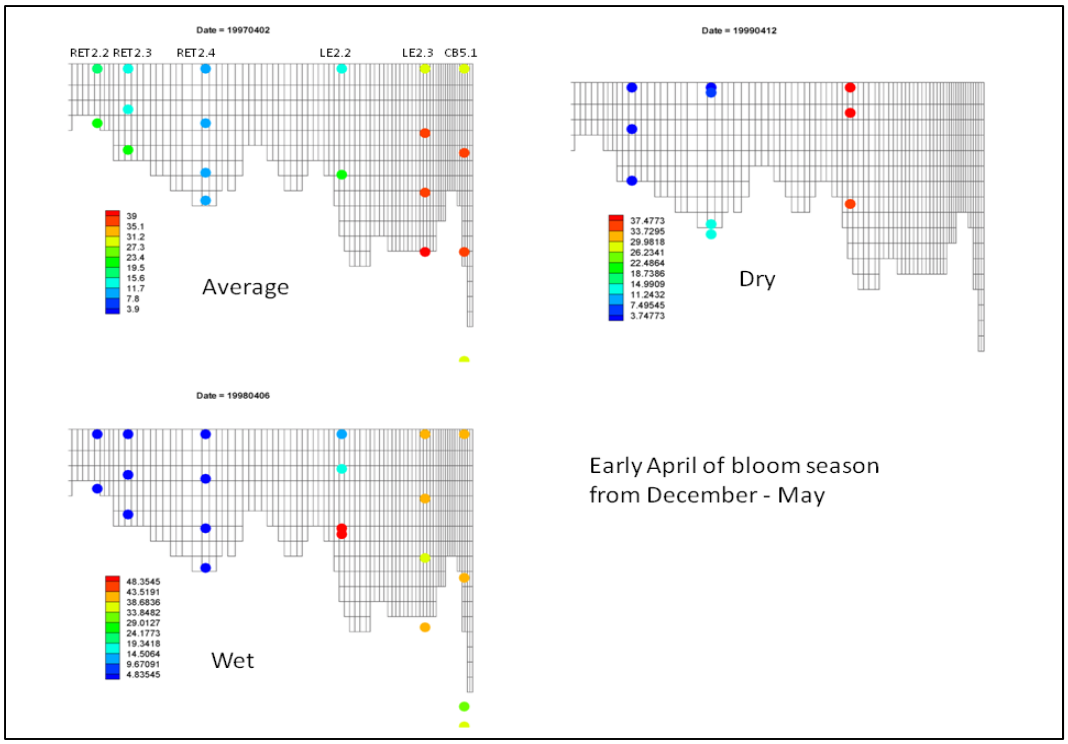

Figure 20. Chlorophyll concentrations (ug L^{-1}) in early April of seasons of average, wet, and dry hydrology. Samples are superimposed on an elevation view of the computational grid. Station names are shown above the upper left panel.

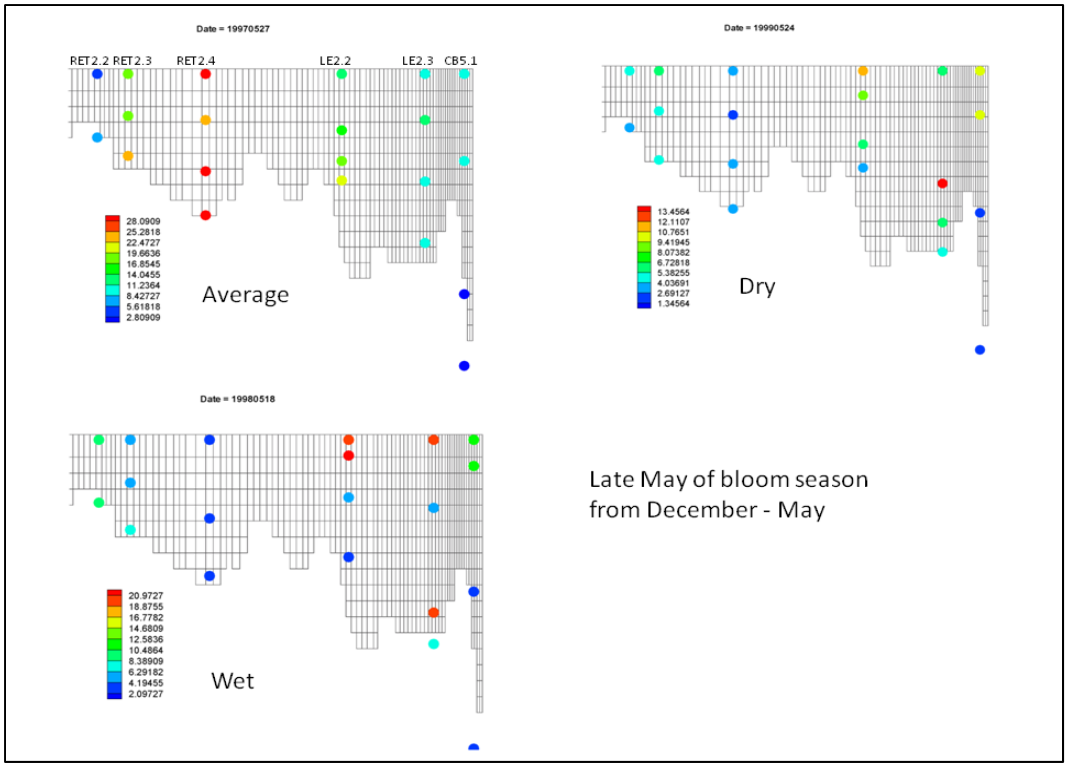

Figure 21. Chlorophyll concentrations (ug L^{-1}) in late May of seasons of average, wet, and dry hydrology. Samples are superimposed on an elevation view of the computational grid. Station names are shown above the upper left panel.

5 Potomac River Salinity and Circulation

Introduction

The Potomac River computational grid and hydrodynamics were extracted from a complete Chesapeake Bay grid as described in Chapter 4. The performance of the Potomac River portion of the complete model was examined and documented by Cerco et al. (2010). Comparisons were made of computed and observed salinity, of computed and observed tidal and current harmonics, and of computed and observed net circulation. Here, the authors present a review of the salinity and net circulation as computed on the extracted grid. Computed salinity provides an integrated view of hydrodynamics, since it depends on freshwater runoff, tidal flows, wind-driven circulation, vertical turbulence, and additional processes. Net circulation is a principal factor in the hypothesis regarding bloom maintenance presented in Chapter 1. The presentations are intended to validate the hydrodynamics, as computed on the extracted grid, and to illustrate performance in regions and periods of interest in the present application.

Longitudinal Salinity Distribution

The Chesapeake Bay Program conducts bay-wide sampling surveys at monthly intervals. For comparison with the model along the longitudinal axis, surface and bottom samples at each station (Figure 8) are averaged into seasons for each year. The seasons relevant to the spring phytoplankton bloom are winter (December – February) and spring (March – May). Results are presented here for the spring season in three years: 1994, 1996, and 1999. These years are emphasized in the complete bay simulation as representative of average, wet, and dry conditions, respectively. In the Potomac, the December – May average runoff, as measured at the fall line, exceeds the long term average, 503 $m^3 s^{-1}$, in both 1994 (886 $m^3 s^{-1}$) and 1996 (805 $m^3 s^{-1}$). The year 1999 remains characterized as dry (236 $m^3 s^{-1}$).

The longitudinal comparisons present a broad summary of the model's ability to represent axial circulation and vertical stratification. In both of the high-flow years, 1994 (Figures 22, 23) and 1996 (Figures 24, 25), computed and observed salinity penetrates 100 km up the estuary to the location of Station RET2.2 (Figure 8). Although the winter-spring flows in the

two years differ by only 10%, observed and computed salinity in the lower 50 km of the estuary is depressed by ≈ 2 ppt in 1994 compared to 1996. Observations at RET2.2 show measureable salinity in 1999 (Figures 26, 27) and the location of the salinity intrusion, observed and computed, is 10 to 20 km upstream of the location in the high-flow years. Observed salinities in the lower 75 km of the estuary are perhaps 5 ppt higher than in the high-flow years. The model provides good representation of the observed surface salinities in this low-flow year, although the computed bottom salinities near the mouth are low, indicating the computed stratification is less than observed.

Salinity Time Series

Salinity time series are presented for three stations (Figure 8), one at the head of salt intrusion (RET2.2, Figures 28, 29), a second station in the transition region (RET2.4, Figures 30, 31) and one in the lower estuary (Figures 32 – 34). Computed and observed salinities at the nominal head of salt intrusion vary from zero to 8 – 10 ppt over the course of the simulation. This station was essentially freshwater during the winter-spring seasons of 1994 and 1996 but showed salinity up to ≈ 2 ppt during spring 1999. The two downstream stations show a progression of computed salinity from

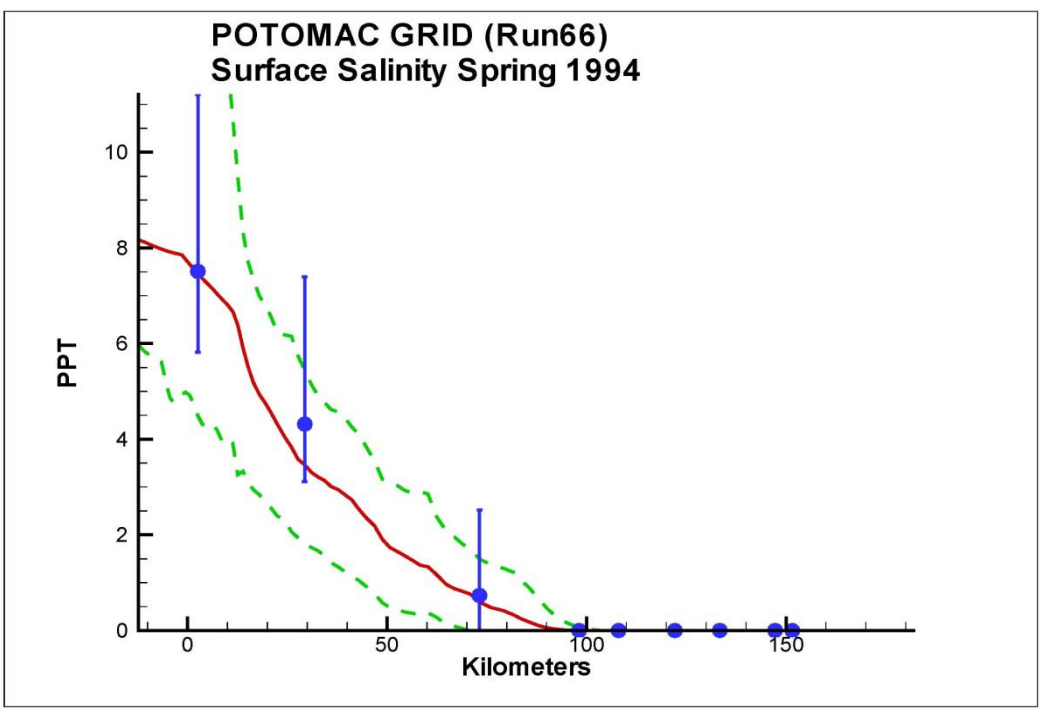

Figure 22. Computed and observed surface salinity in the Potomac River for spring (March – May) 1994. Average observations are shown as blue circles with range as a vertical line. Computed average is a red line with range shown as green dashed lines.

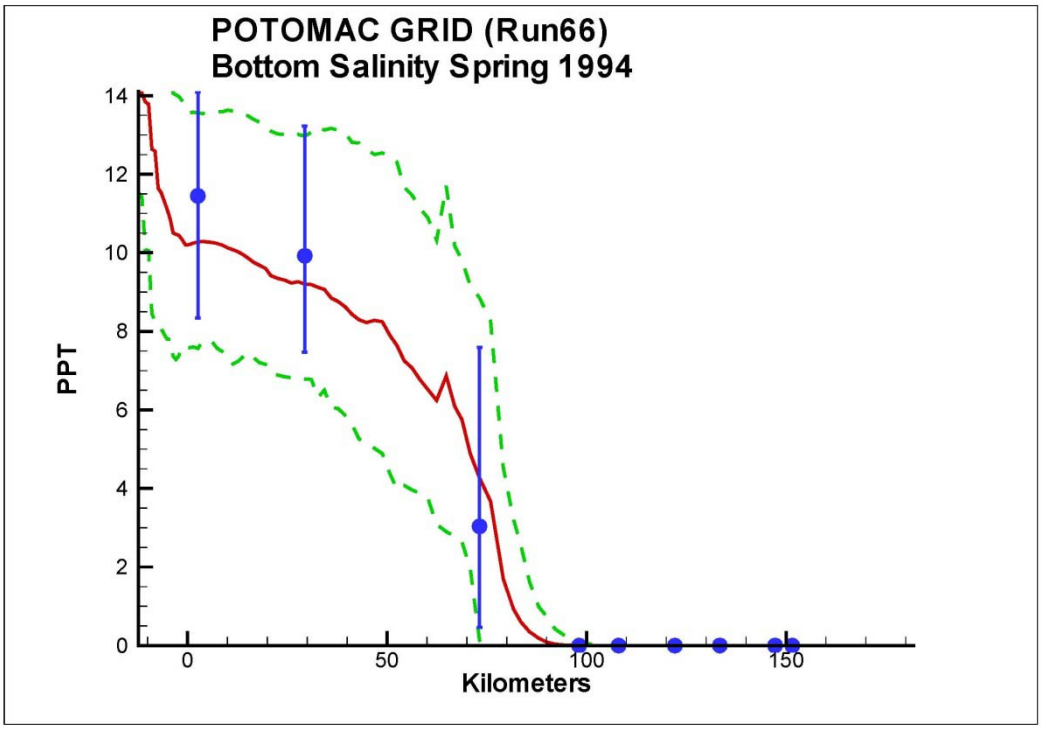

Figure 23. Computed and observed bottom salinity in the Potomac River for spring (March – May) 1994.

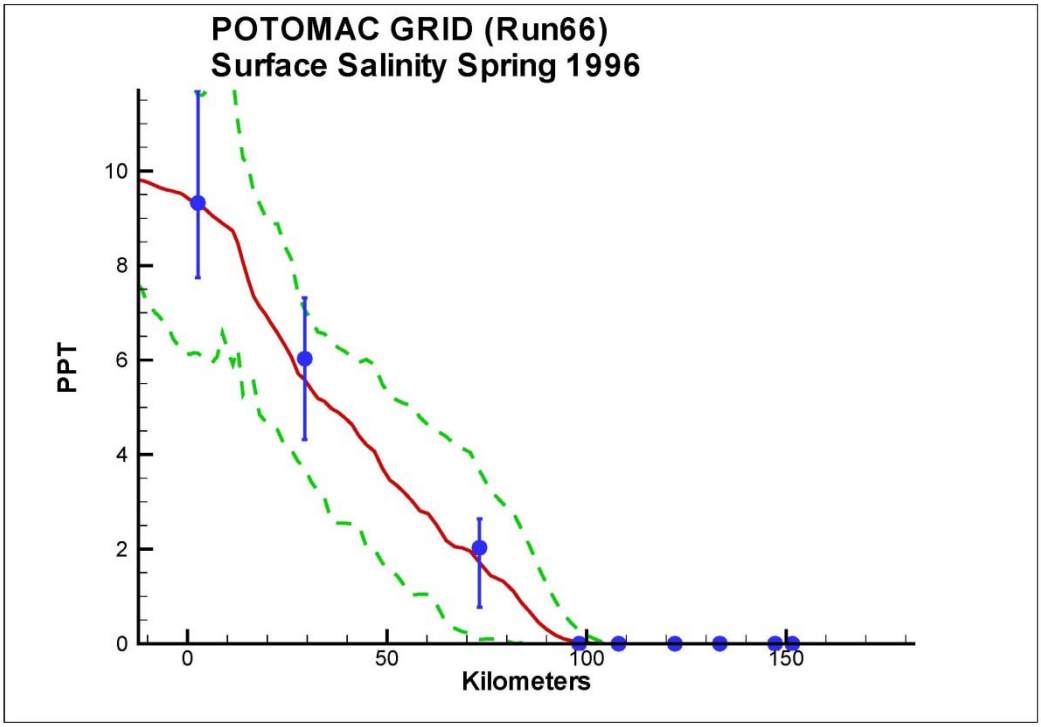

Figure 24. Computed and observed surface salinity in the Potomac River for spring (March – May) 1996.

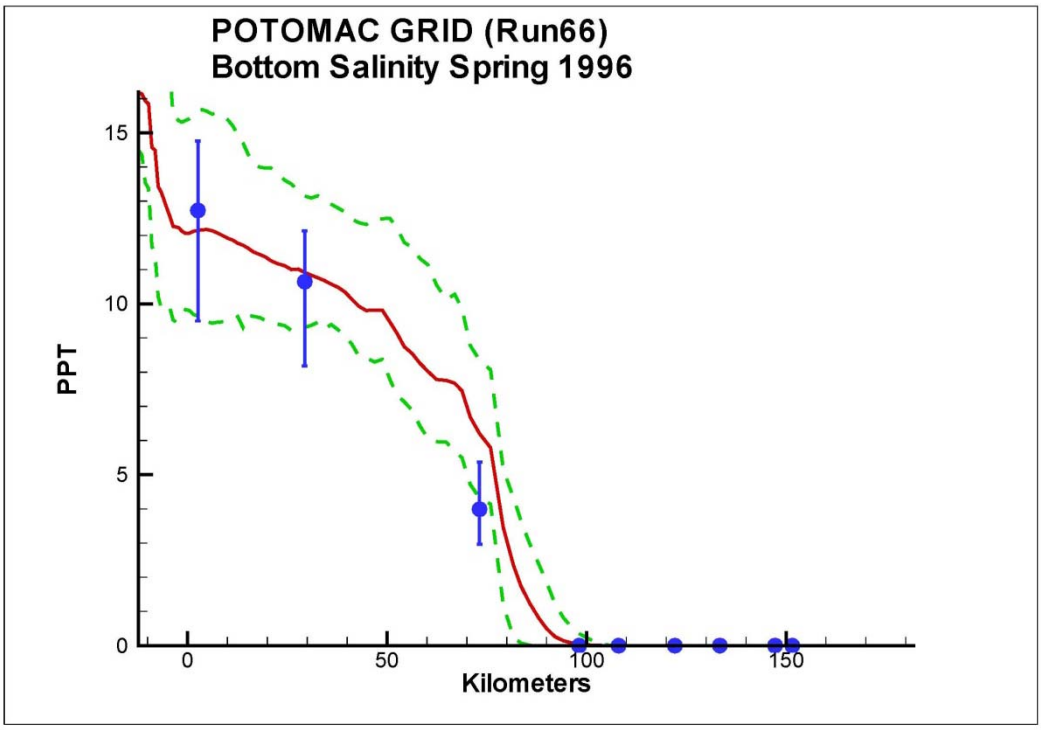

Figure 25. Computed and observed bottom salinity in the Potomac River for spring (March – May) 1996.

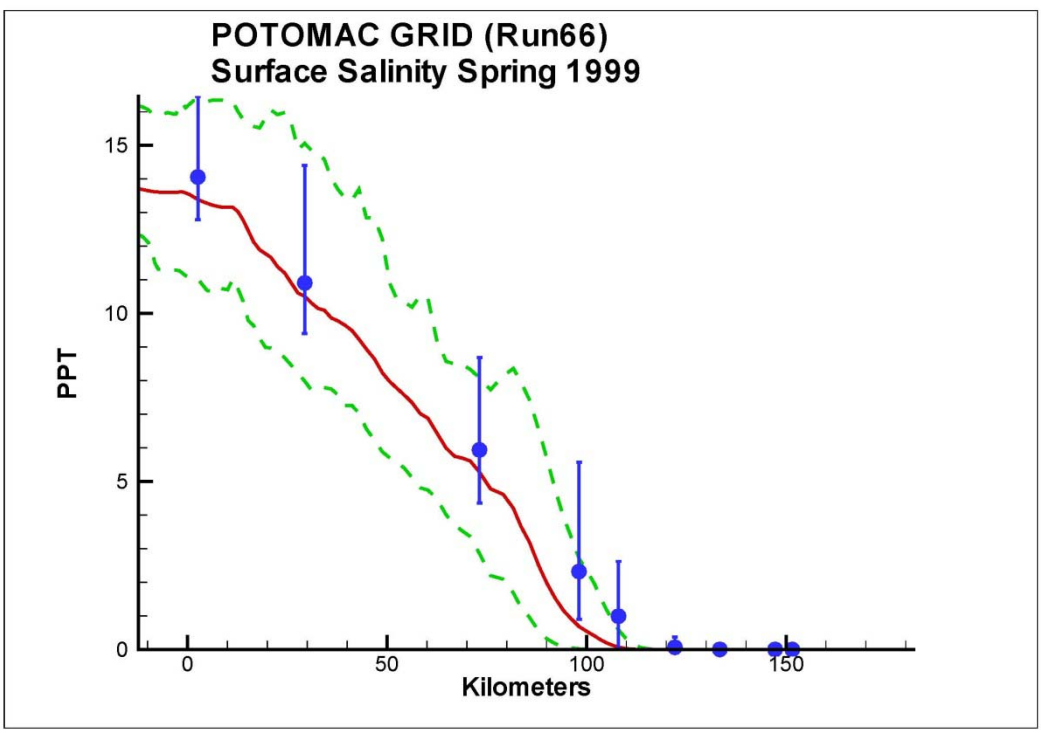

Figure 26. Computed and observed surface salinity in the Potomac River for spring (March – May) 1999.

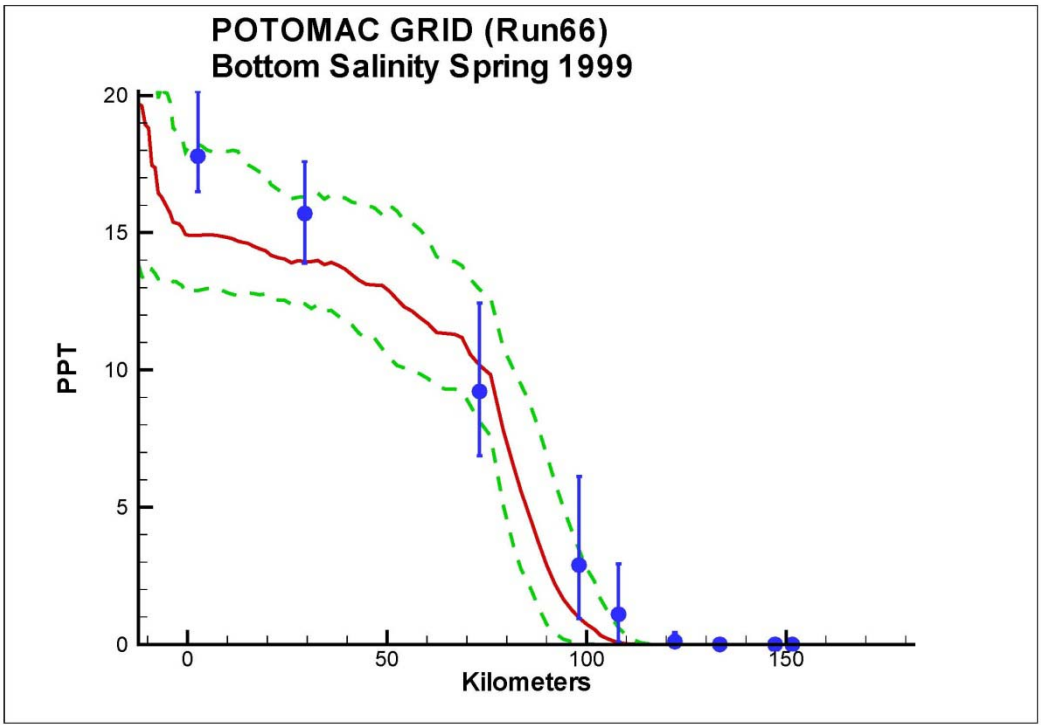

Figure 27. Computed and observed bottom salinity in the Potomac River for spring (March – May) 1999.

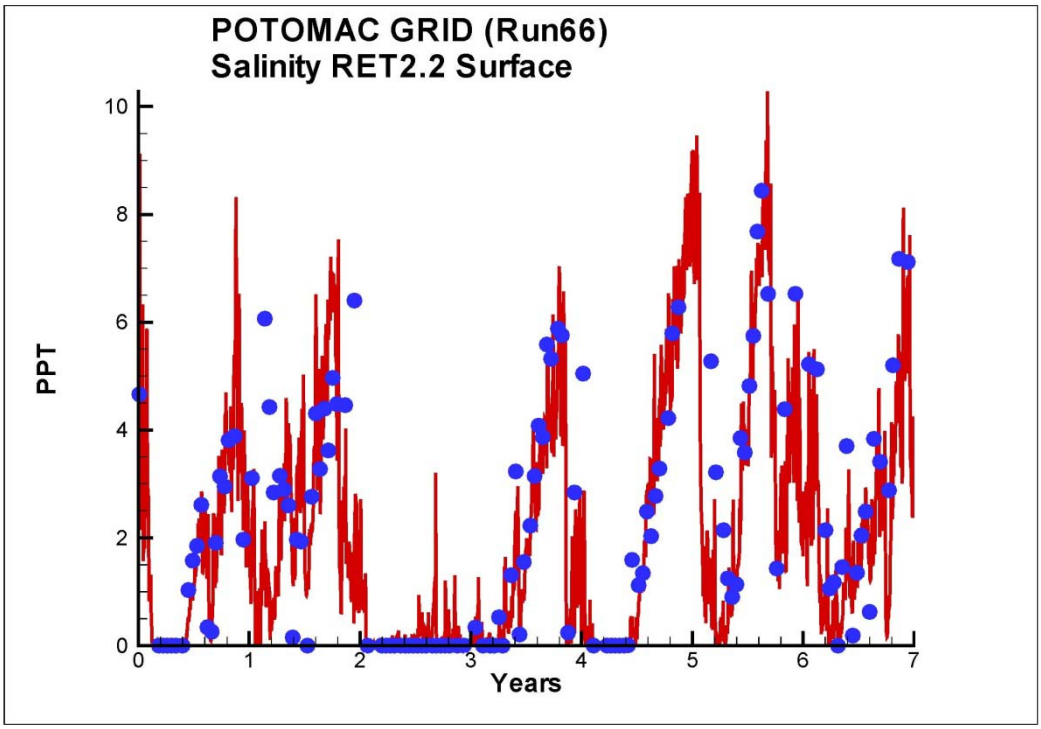

Figure 28. Time series of observed (blue circles) and computed (red line) surface salinity at RET2.2. The simulation runs from 1994 (year 0) to 2000 (year 7).

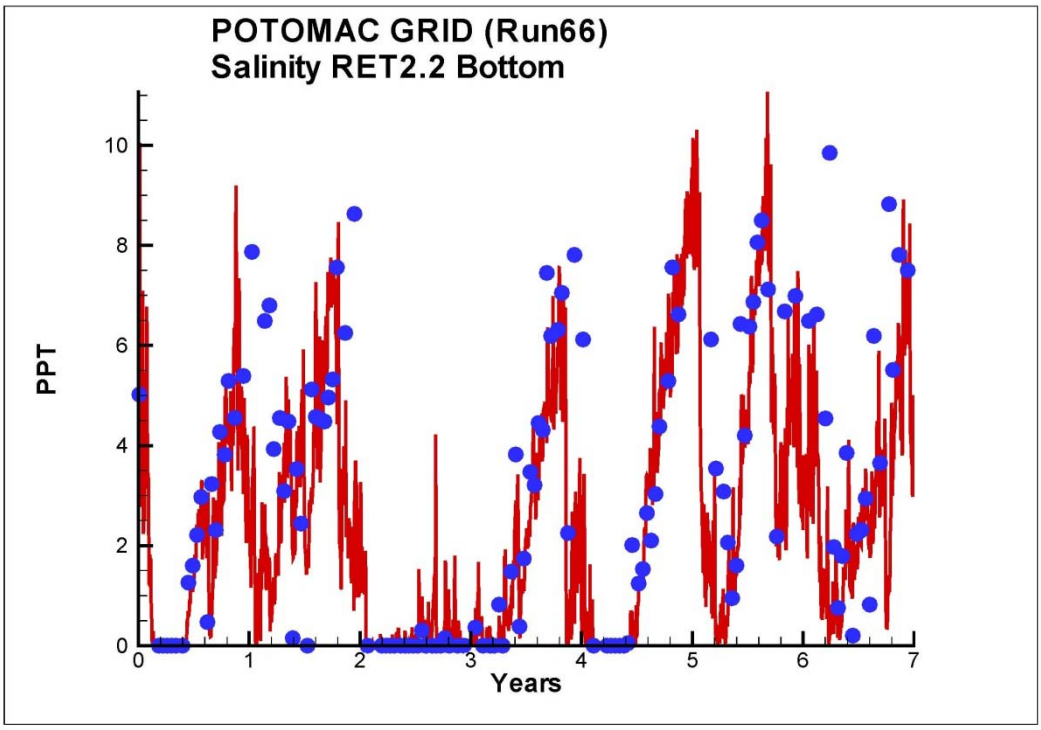

Figure 29. Time series of observed (blue circles) and computed (red line) bottom salinity at RET2.2. The simulation runs from 1994 (year 0) to 2000 (year 7).

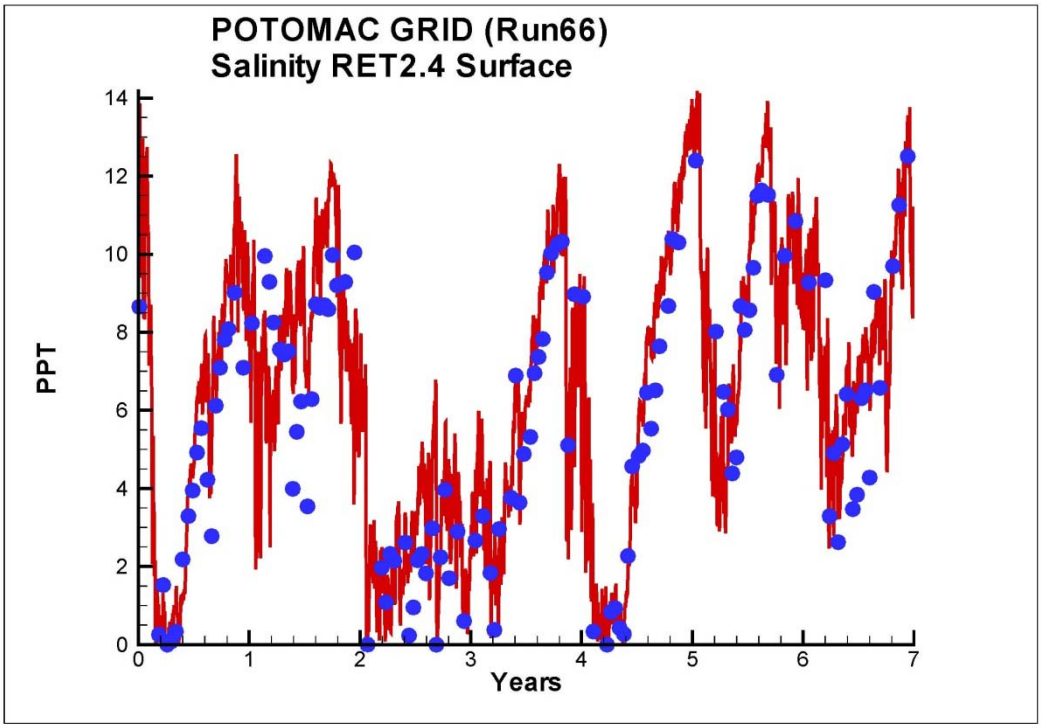

Figure 30. Time series of observed (blue circles) and computed (red line) surface salinity at RET2.4. The simulation runs from 1994 (year 0) to 2000 (year 7).

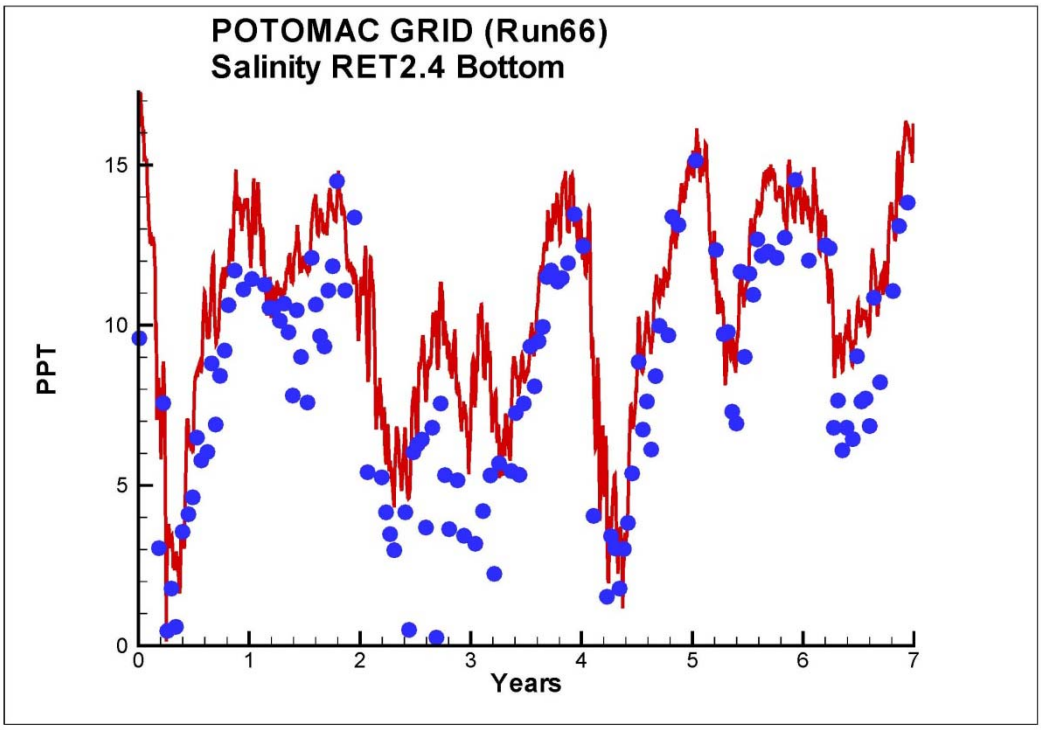

Figure 31. Time series of observed (blue circles) and computed (red line) bottom salinity at RET2.4. The simulation runs from 1994 (year 0) to 2000 (year 7).

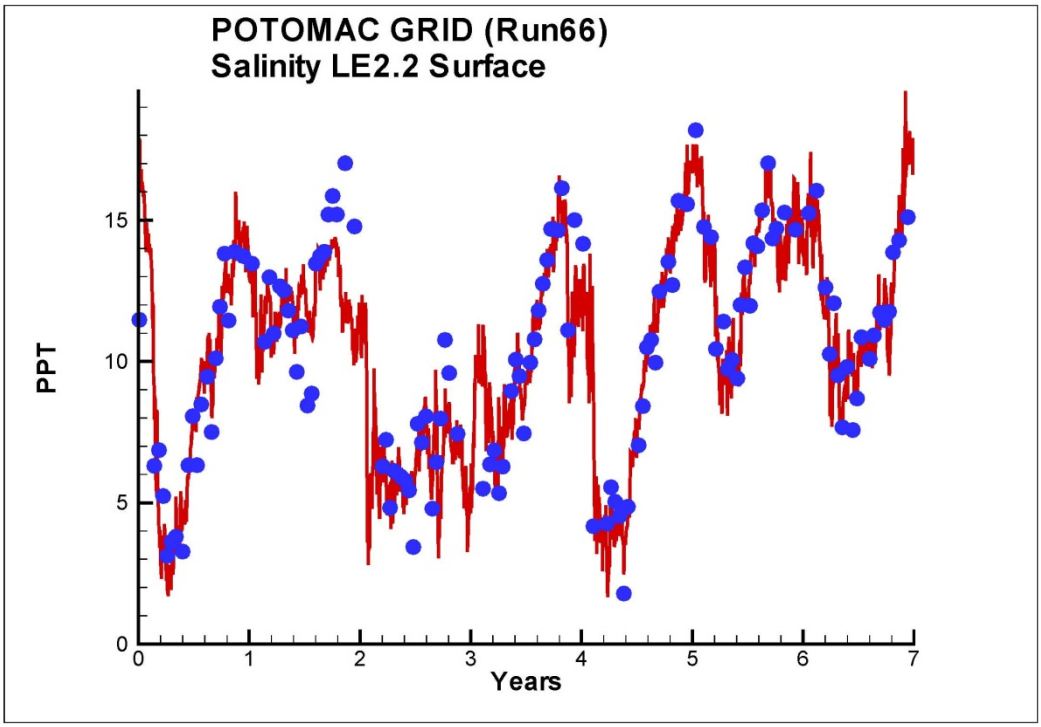

Figure 32. Time series of observed (blue circles) and computed (red line) surface salinity at LE2.2. The simulation runs from 1994 (year 0) to 2000 (year 7).

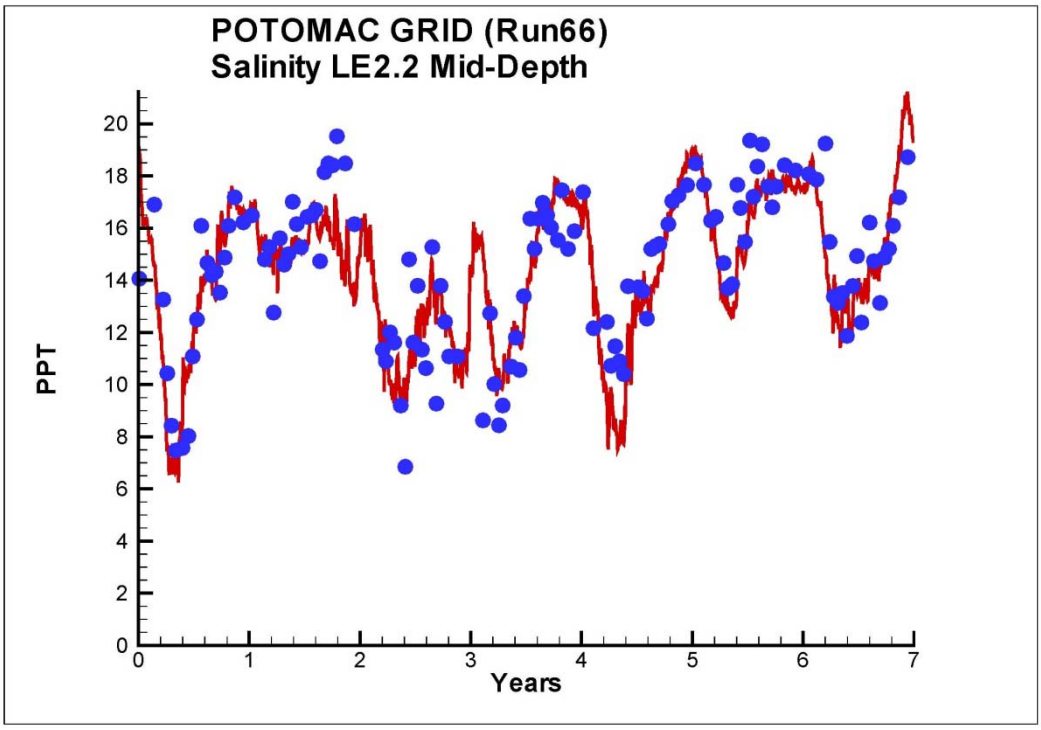

Figure 33. Time series of observed (blue circles) and computed (red line) mid-depth salinity at LE2.2. The simulation runs from 1994 (year 0) to 2000 (year 7).

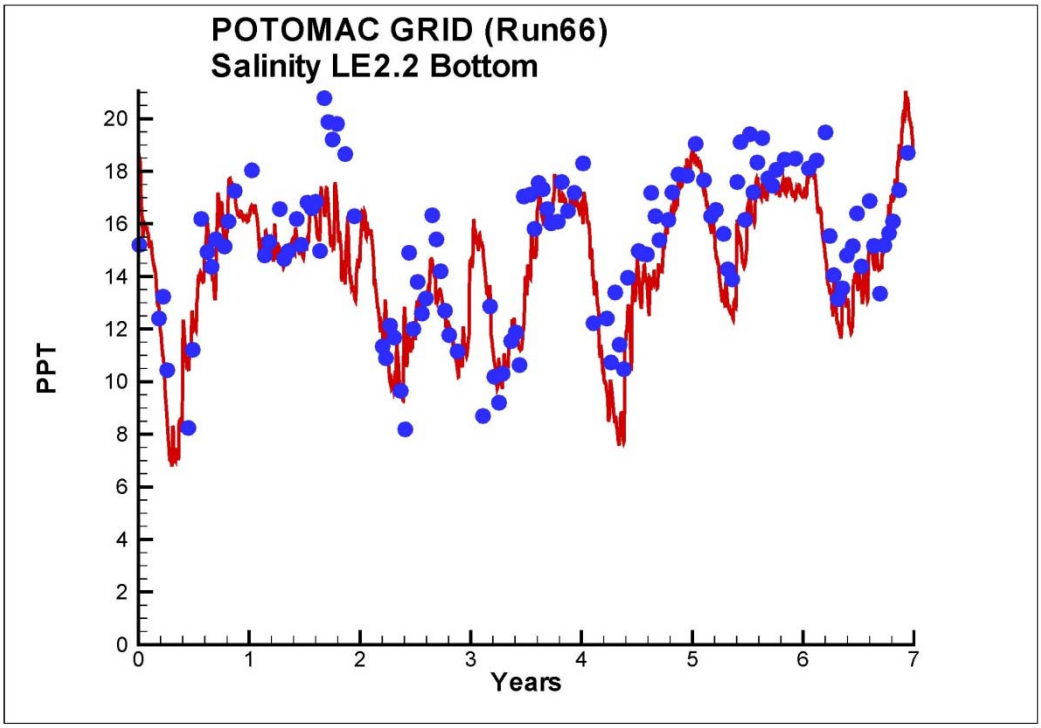

Figure 34. Time series of observed (blue circles) and computed (red line) bottom salinity at RET2.4. The simulation runs from 1994 (year 0) to 2000 (year 7).

least in winter-spring 1994 through 1996, to highest in winter-spring 1999, although the model exaggerates the higher salinity in 1996 in comparison to 1994 at Station RET2.4. This station is located ≈ 75 km from the river mouth, in a region of sharp longitudinal salinity gradient. A relatively small spatial difference in computed and observed salinity translates into an apparently large difference when results are plotted at a fixed location.

Potomac River Residual Currents

A one-year current meter mooring, nearly coincident with the present station LE2.2 (Figure 8), was maintained and analyzed by Elliott (1978). He reported that the mean flow at a 3-meter depth was seaward, while the mean flows at 7.6 m and 12.2 m were landward. Throughout the year, the daily-average flow at 3 meters reversed direction at intervals of four or five days. Daily-average flows at deeper depths were almost exclusively landward, although occasional reversals occurred. Amplitude of the current fluctuations was ≈ 20 cm s^{-1}. Model residual currents for one year were obtained at the location and depths of Elliott's measures. Residuals were determined as the 25-hour moving average of the computed velocities. Results (Figure 35) compare well with Elliott's findings. Non-tidal currents near the surface reverse directions frequently, while currents at greater depths are primarily landward but demonstrate occasional flow reversals. Currents at all depths fluctuate at periods of five to six days. The magnitude of the fluctuations is 10 to 20 cm s^{-1}.

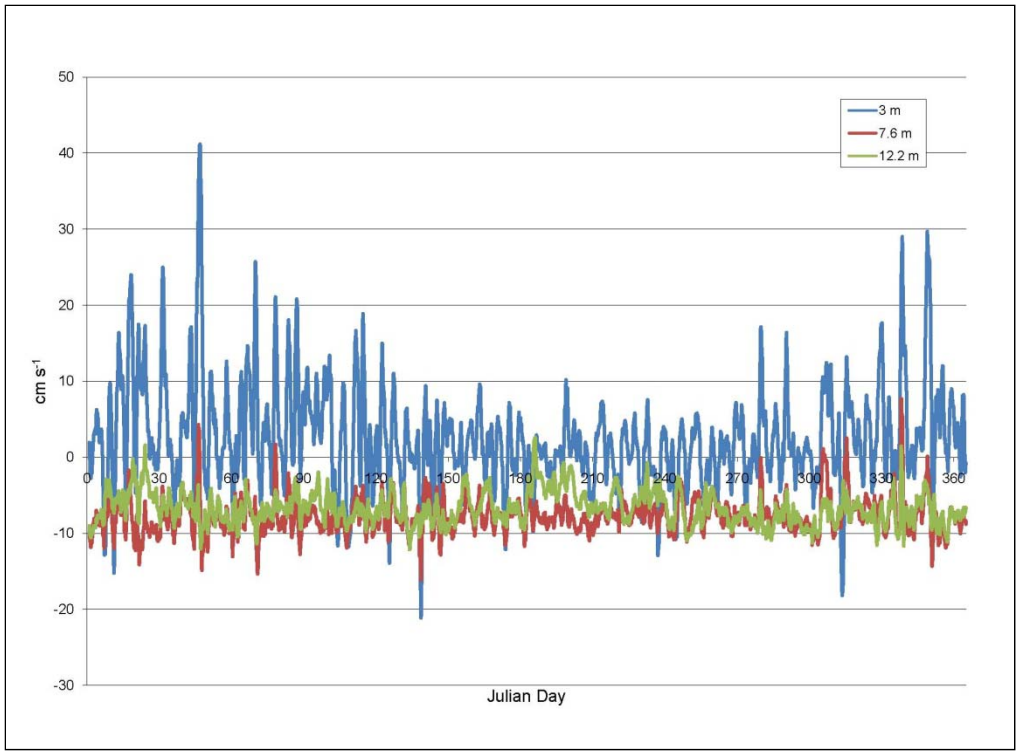

Figure 35. Model residual currents in the Potomac River corresponding to Elliott's (1978) measurements.

6 Basic Particle Simulation

Introduction

The base simulation extends from November 1, 1993 through May 31, 1994. The duration is selected to encompass the spring bloom period. The year 1994 corresponds to an average hydrologic year selected for analysis of Chesapeake Bay model results, although flows in the Potomac during the interval are above average. Two flood events in quick succession occur 30 days into the model run (Figure 36). Another succession of flood events, spaced two to three weeks apart, commences ≈ 90 days into the run and continues through the termination. Peak flows of 4,000 $m^3 s^{-1}$ occur circa Day 152.

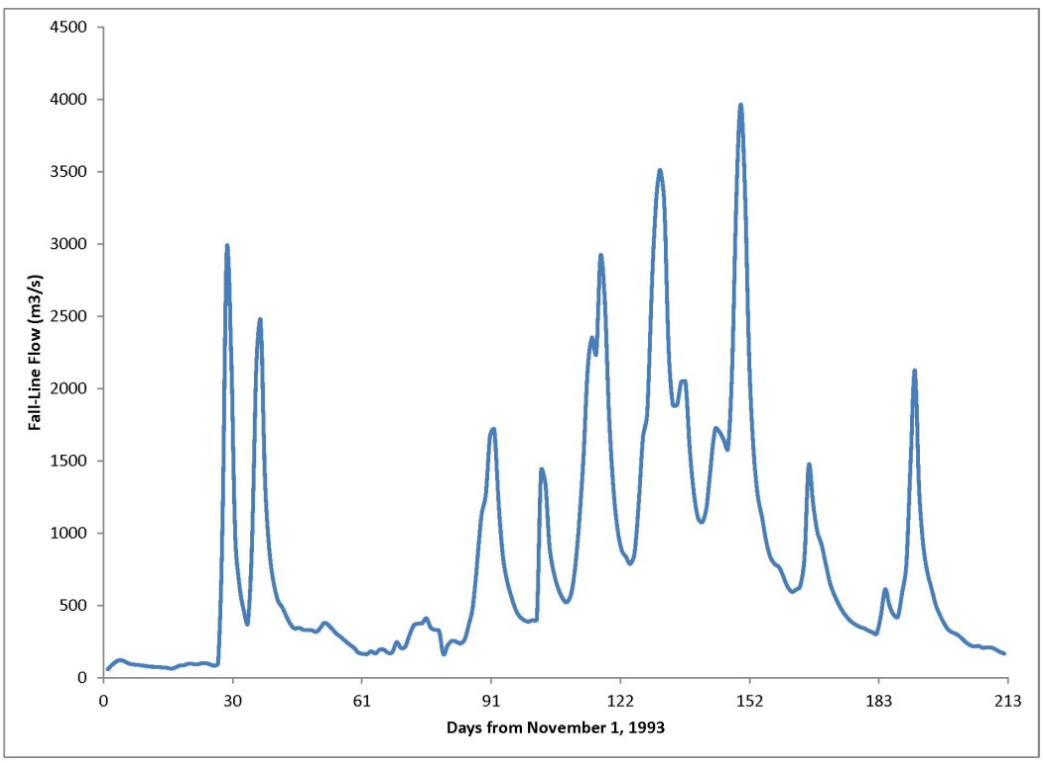

Figure 36. Fall-line flow in the Potomac River November 1, 1993, to May 31, 1994.

Ten thousand particles are released 45 days into the run and are spaced uniformly from top to bottom in the channel of the river between km 30 and 80. Particles are distributed in model grid cells with the number in each cell specified to yield 4 x 10^{-6} particles m^{-3}. The release timing and region correspond to the typical appearance date and expanse of bloom algae.

Presentation Formats

Elevation Plots

Elevation plots extend along a mid-channel transect from the mouth of the river (km 0) to the head of tide (km 160). Particles are shown only when they are within the one-cell wide transect and are colored according to the mass of algae each represents. (The algal simulations are described in a subsequent chapter). The elevation plots are originally rendered as animations from which extractions are included in this report. Figure 37 shows computed particle distributions at four intervals ranging from the release to the end of the simulation. In this simulation, particles that leave the model domain through open boundaries are not replaced. Consequently, the number of particles in the system decreases from the initial release.

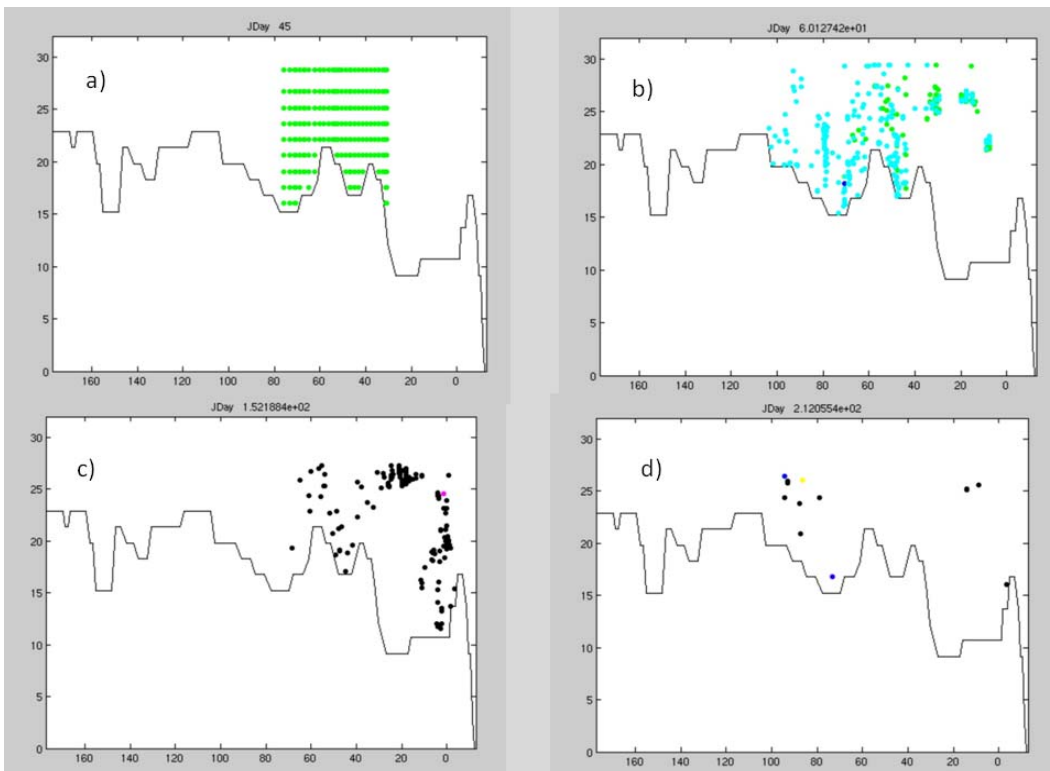

Figure 37. Elevation view of particle distribution at four time intervals: a) Day 45 (particle release); b) Day 60; c) Day 152; d) Day 212 (end of simulation). The number of particles in the system declines as particles exit across open boundaries.

Plan Views

Plan views illustrate the entire domain with particles superimposed upon the computational grid. Particles are shown at all depths from surface to bottom and are colored, according to depth, to increase contrast. Figure 38 presents a plan view corresponding to the elevation plots in Figure 37.

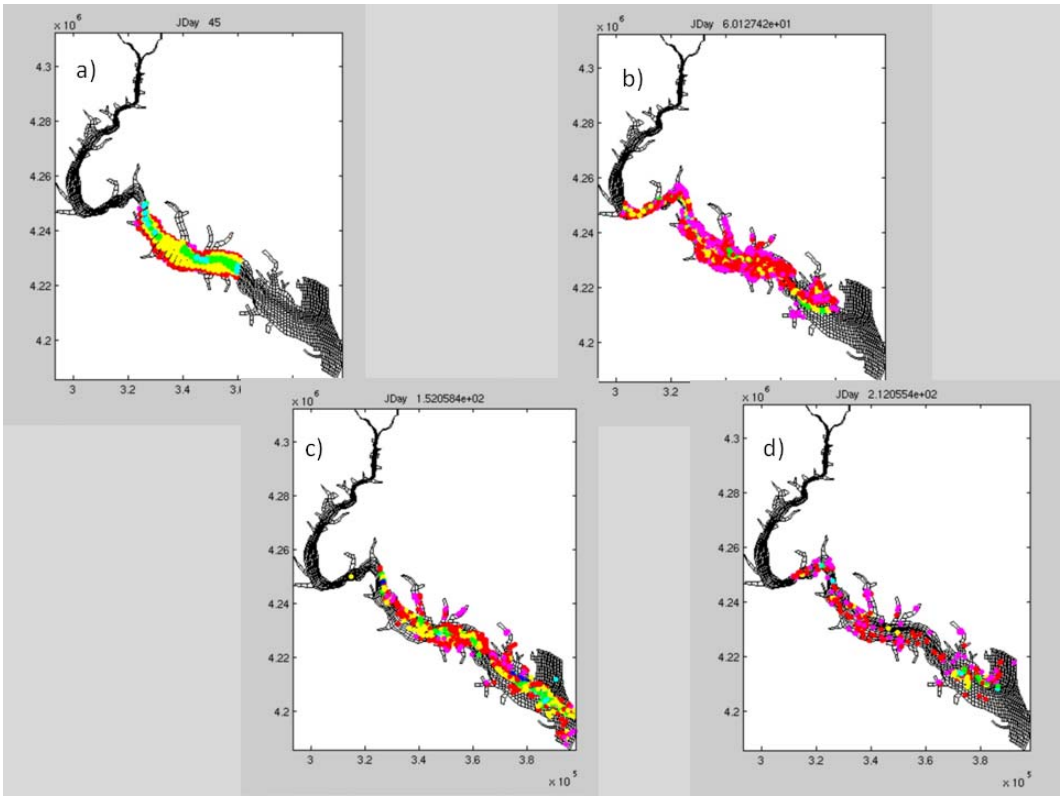

Figure 38. Plan view of particle distribution at four time intervals: a) Day 45 (particle release); b) Day 60; c) Day 152; d) Day 212 (end of simulation).

Tracker Statistics

The tracker statistics provide a format for summarizing the particle distribution and number. The number of particles is summarized, by level, within 10-km reaches of the river. Levels are derived from conventions derived for the mainstem of Chesapeake Bay and are:

- surface (Level I), 0 to 6.7 m from surface;
- mid-Depth (Level II), 6.7 to 12.8 m from surface; and
- bottom (Level III), more than 12.8 m from surface.

The figures show particle counts, not concentrations. At the initiation of the simulation, the preponderance of particles is in the surface (Figure 39), even though the concentration is uniform from surface to bottom. The vertical particle distribution reflects the greater volume of water contained between 0 and 6.7 m depth. For this simulation, corresponding to the results shown in Figures 37 and 38, the number of particles within the model domain declines from 10,000, at release, to 3,764 at the end of the simulation.

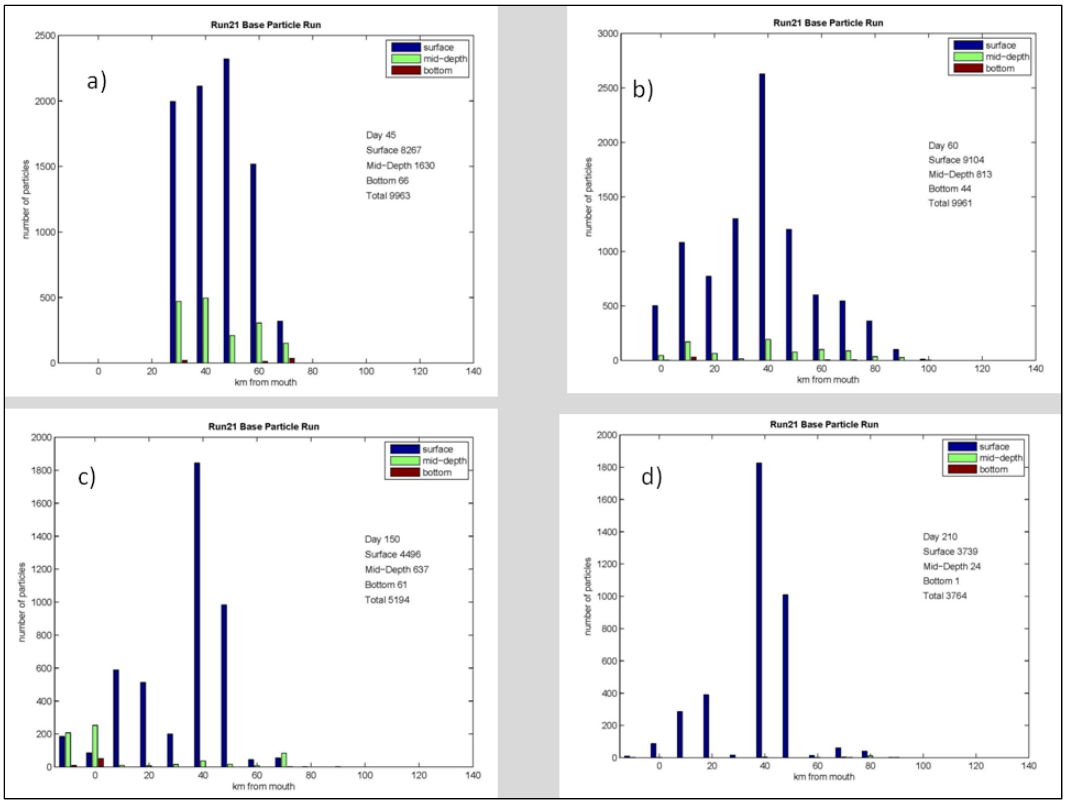

Figure 39. Tracker statistics at four time intervals: a) Day 45 (particle release); b) Day 60; c) Day 150; d) Day 210 (end of simulation). The plots indicate the number of particles at 10-km intervals and three depth levels. The Potomac River mouth is at km 0. The bars at this location indicate the number of particles between km 0 and km 10. Subsequent graphics are placed at the lower end of 10 km intervals. The number of particles outside the river mouth but inside the model domain is plotted at -10 km.

Comparison to Dissolved Substance

The transport of particles versus a dissolved substance was examined by initiating a tracer release (salt) simultaneous with the particle release. As with the particles, the tracer was distributed uniformly from top-to-bottom between km 30 and 80. Results (Figure 40) indicated that less than one percent of the tracer remained in the model domain 90 days after the release (Day 135 of the simulation). In contrast, 65% of the particles remained in the system after 90 days and nearly 40% remained at the end of the simulation, 167 days after the particle release.

Elevation (Figure 41) and plan views (Figure 42) of salinity illustrate the rapid dissipation of the dissolved substance. For comparison with these results, particle distribution was converted to concentration through summing the number of particles in each grid cell and dividing by cell volume (Figures 43, 44). Aside from the residence time, the dramatic

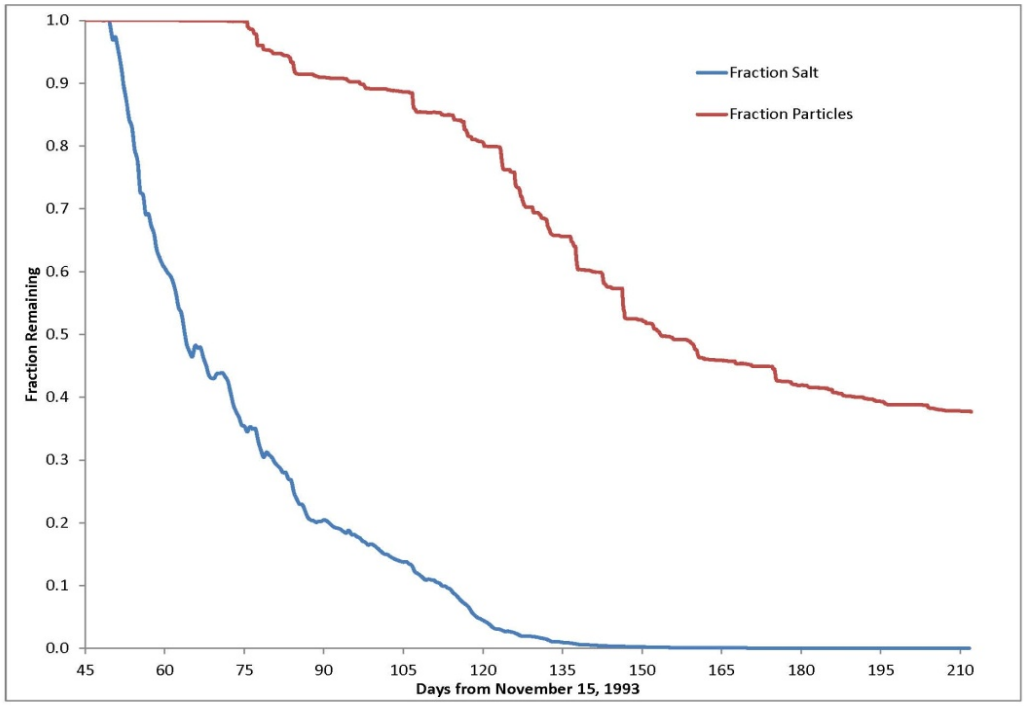

Figure 40. The fraction of initial mass remaining following simultaneous releases of particles and dissolved substance. Less than 1% of the dissolved substance remains 90 days after release versus 65% of the particles.

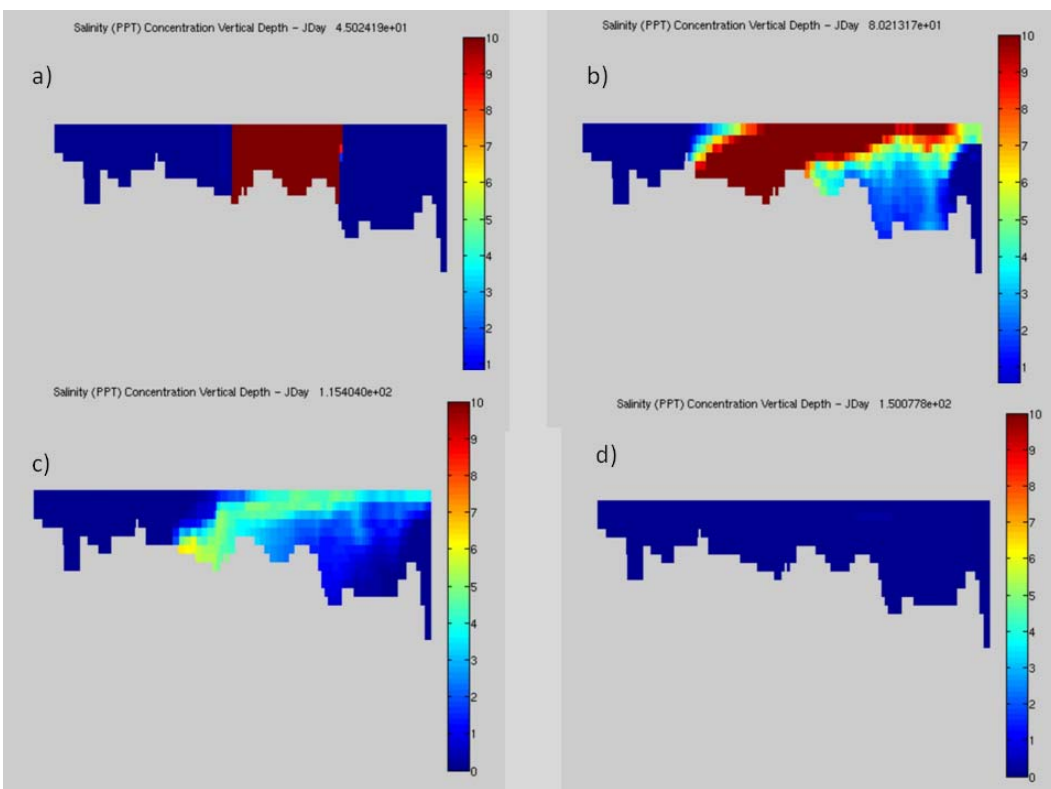

Figure 41. Elevation view of dissolved substance concentration at four time intervals: a) Day 45 (release); b) Day 80; c) Day 115; d) Day 150. The substance has disappeared by Day 150.

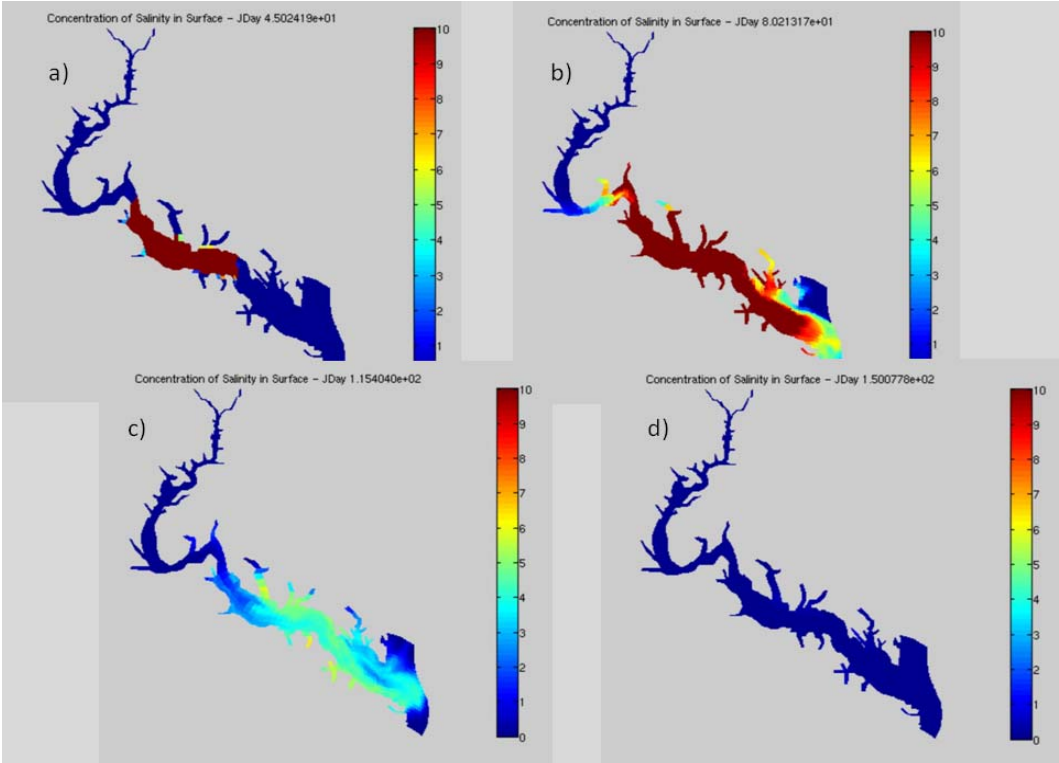

Figure 42. Surface view of dissolved substance concentration at four time intervals: a) Day 45 (release); b) Day 80; c) Day 115; d) Day 150.

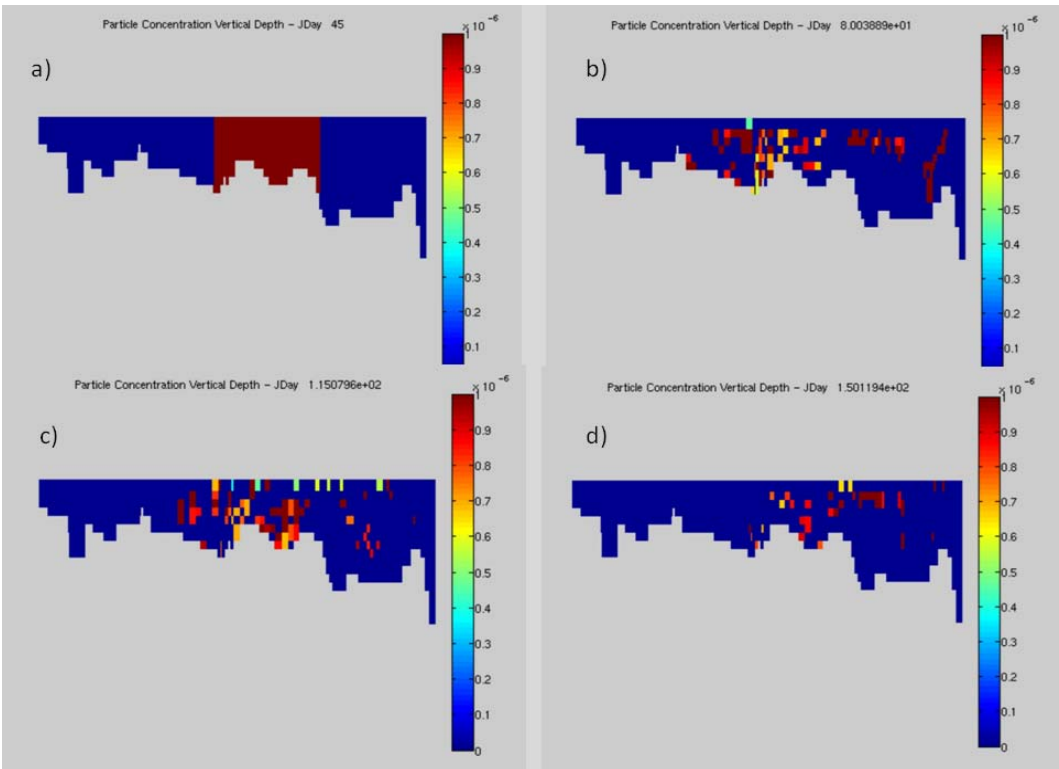

Figure 43. Elevation view of particle concentration at four time intervals: a) Day 45 (release); b) Day 80; c) Day 115; d) Day 150. Note the "patchy" distribution of particles compared to dissolved substance.

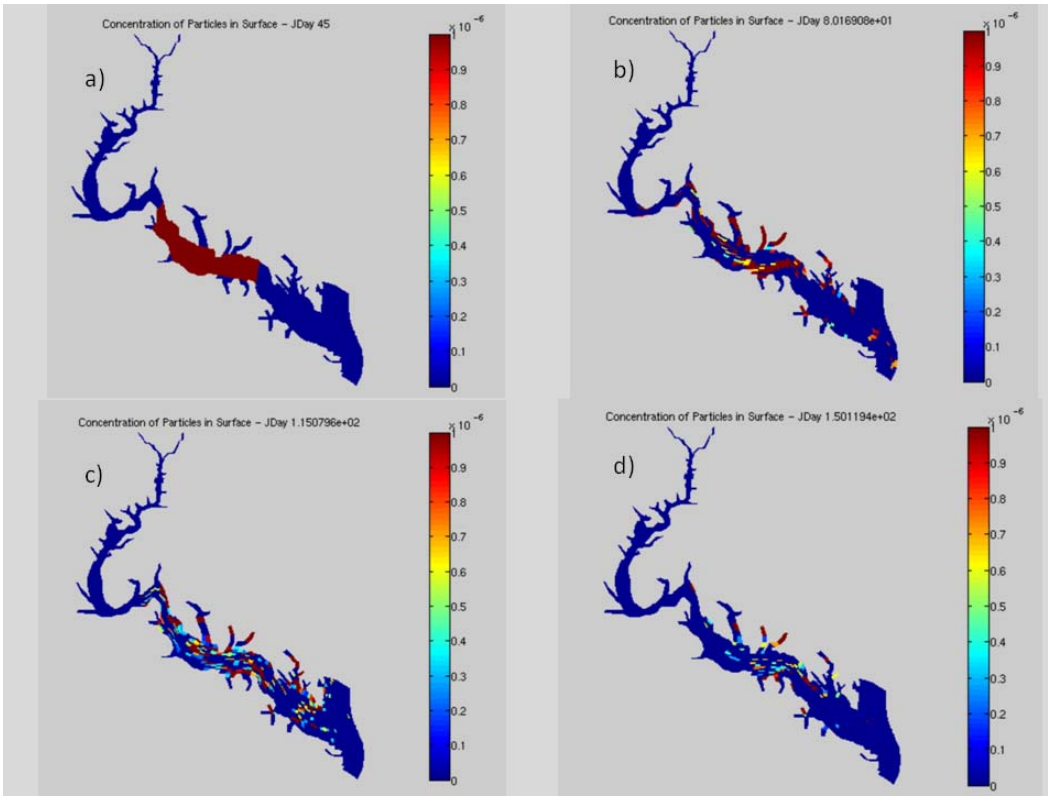

Figure 44. Surface view of particle concentration at four time intervals: a) Day 45 (release); b) Day 80; c) Day 115; d) Day 150.

contrast between particles and dissolved substance is in the "patchy" distribution of the particles. The patchiness develops despite the uniform initial distribution of the particles.

Sensitivity to Number of Particles Released

The sensitivity of results to the number of particles was examined by doubling the initial release from 10,000 to 20,000 particles and then by doubling it again to 40,000 particles. The proportion of particles retained and the spatial distribution of particles were similar for all runs, as evidenced by the tracker statistics at Day 210 (Figure 45). Increasing the number of particles over the initial 10,000 placed a slightly larger fraction in the lower two layers, but the fraction of the total was negligible in any event. Particle retention was ≈ 38% of the initial release regardless of the number released. Based on these findings, initial release of 10,000 particles was retained in all subsequent runs.

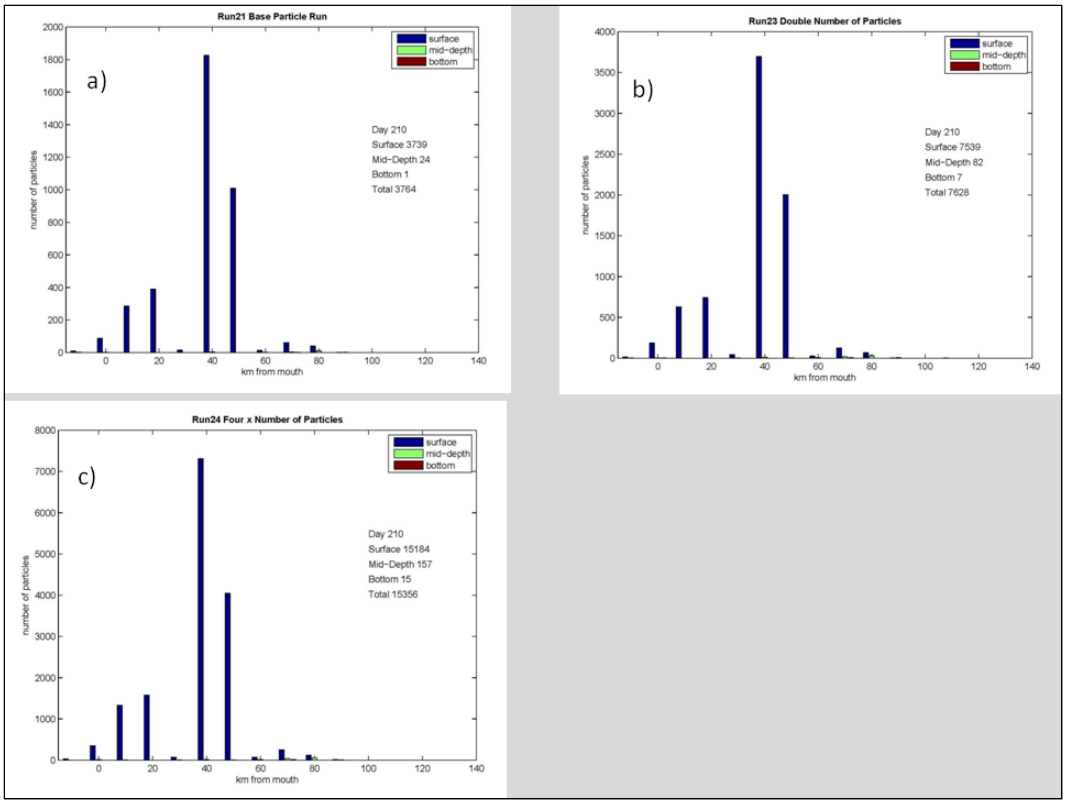

Figure 45. Sensitivity to number of particles released. Tracker statistics are shown at the end of the simulation for release of: a) 10,000 particles; b) 20,000 particles; c) 40,000 particles. The fraction particles remaining at the end of the simulation and their distribution are nearly identical for all initial release numbers.

Sensitivity to Rules

A set of kinetics rules for particles is described in Chapter 3. These rules are intended to keep the number of particles in the system constant and to ensure that each particle is associated with viable algal biomass. The rule with the greatest effect on particle distribution is the replacement of particles, which leave through open boundaries (Figure 46). Under this rule, the number of particles in the system remains constant at the initial value. The rules governing the replacement of particles that adhere to the bottom or that no longer represent viable algae diminish the number of particles in the system. With no rules in force, ≈ 38% of the particles released are present at the end of the simulation. When particles adhering to the bottom or containing no algae are replaced, particle retention declines to ≈ 5%. This rule replaces an inert particle by splitting the particle with the greatest algal biomass. The algorithm effectively relocates particles from sluggish regions at the bottom into the surface where they are subject to flushing from the system by runoff events. Enforcement of all rules retains the initial number of particles in the system, as does

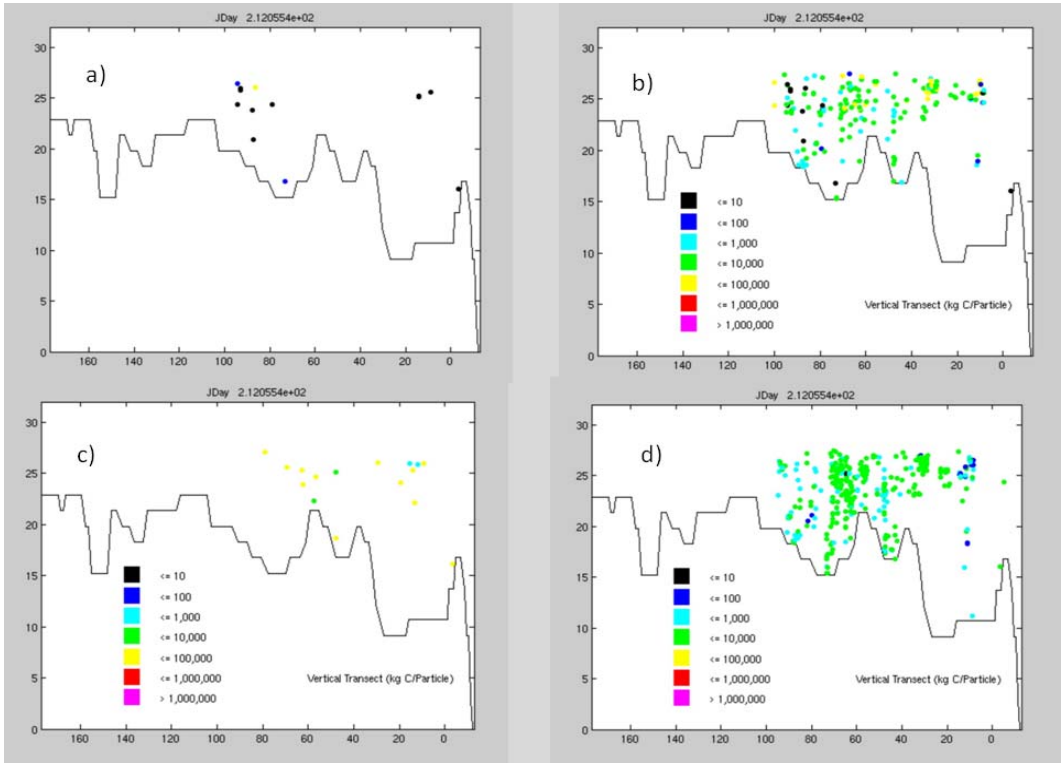

Figure 46. Sensitivity to Kinetics Rules for Particles (Elevation views). Results are presented for particle distributions at the completion of simulations for four rule sets: a) No rules; b) Particles which leave the system are replaced; c) Particles which adhere to the bottom or contain no viable algae are replaced; d) Combination of b) and c).

simply replacing particles that leave the system. With all rules in place, however, the axial particle distribution is more uniform and a greater fraction of the particles are below the surface, relative to the run with replacement only (Figure 47).

Base Run for Phytoplankton Simulation

The experiments with particle tracking indicate that particle transport is fundamentally different than transport of a dissolved substance. In particular, the residence time of particles released in the center of the Potomac Estuary is longer than the residence time of a comparable release of dissolved substance (Figure 40). Ninety days after the release, 65% of the particles remain in the model domain while the dissolved substance has disappeared. A second distinction is in the “patchy” distribution of particles compared to the continuous distribution of dissolved substance. The particle experiments, supplemented by initial experiments with phytoplankton, help determine a base particle simulation (Figures 48, 49) for subsequent development of the phytoplankton model. The run has the following characteristics:

- Release 10,000 particles at Day 45 of a 212-day simulation.
- Enforce kinetics rules that govern the replacement of particles leaving the system, adhering to the bottom, or representing no viable algae.
- Incorporate particle dispersion based on modeled axial dispersion and characteristic vertical turbulent diffusion.

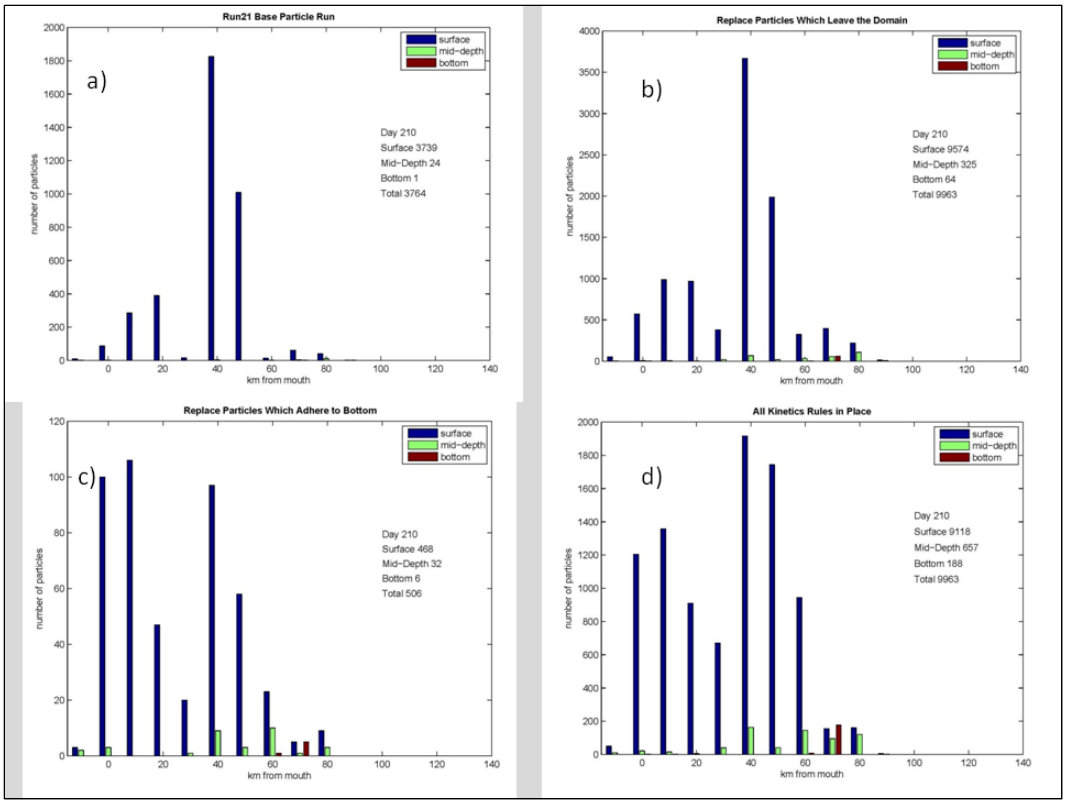

Figure 47. Sensitivity to Kinetics Rules for Particles (Tracker Statistics). Results are presented for particle distributions at the completion of simulations for four rule sets: a) No rules; b) Particles which leave the system are replaced; c) Particles which adhere to the bottom or contain no viable algae are replaced; d) Combination of b) and c).

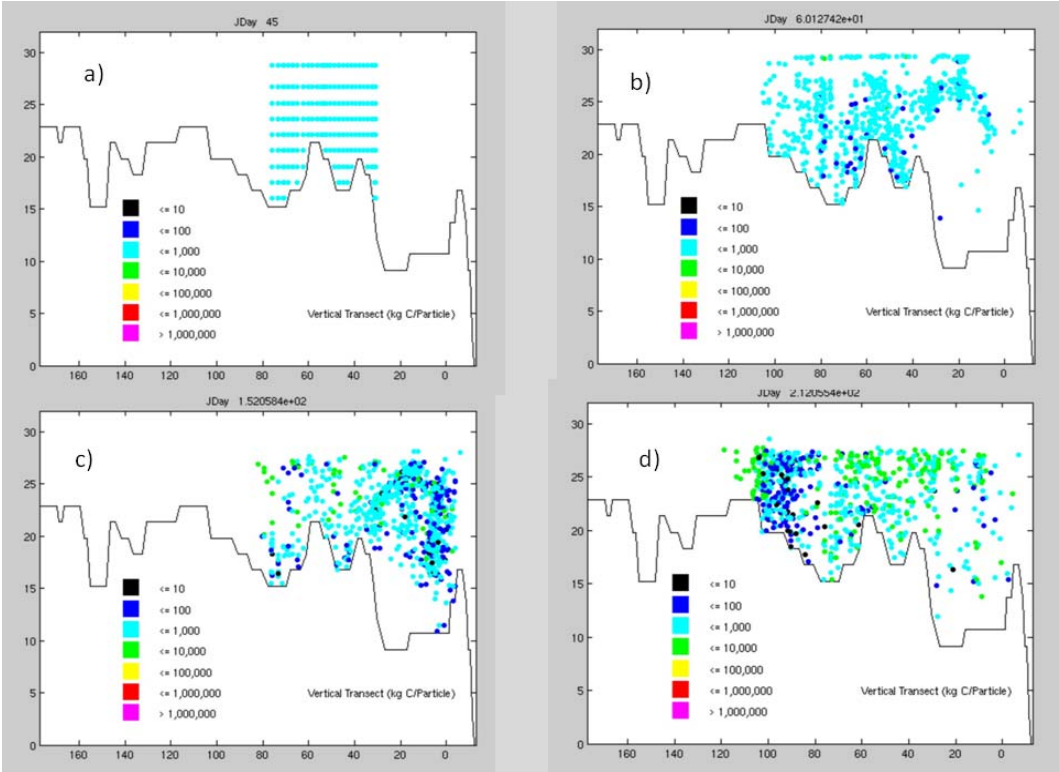

Figure 48. Elevation view of particle distribution for base phytoplankton run. This run incorporates the kinetics rules set and particle dispersion. Results are presented at four time intervals: a) Day 45 (particle release); b) Day 60; c) Day 152; d) Day 212 (end of simulation).

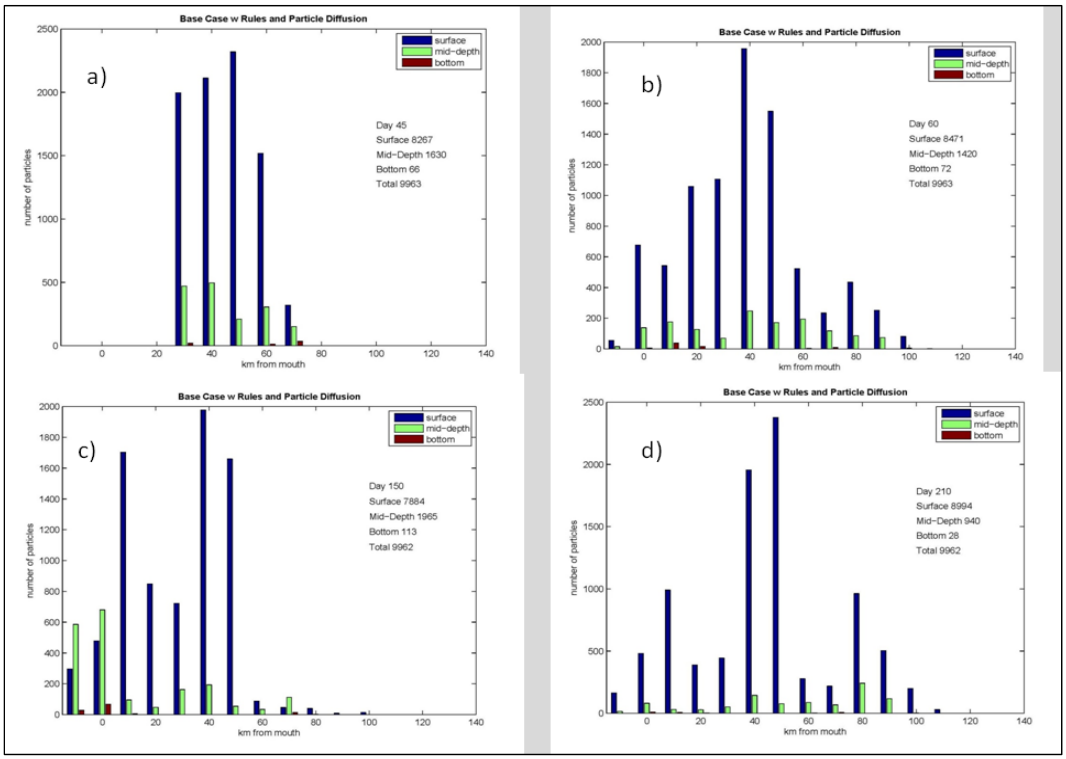

Figure 49. Tracker statistics for base phytoplankton run. Results are presented at four time intervals: a) Day 45 (particle release); b) Day 60; c) Day 150; d) Day 210 (end of simulation).

7 Algae as Particles – Spatial and Temporal Distribution

Introduction

The base model run with algae as particles accompanies the basic particle simulation described in the previous chapter. Ten thousand particles are released in the central portion of the Potomac River 45 days after commencement of a model run, which extends from November 1, 1993, through May 31, 1994. Each particle is initiated with 2.5 x 10^5 g algal carbon, yielding 1.0 g C m^{-3} at initiation of the simulation. Parameters for the algal kinetics (Table 2) are drawn from the spring diatom group of the Chesapeake Bay Model (Cerco et al. 2010). These values are employed to provide comparison to algae as simulated in conventional models. No attempt is made, at this stage of development, to optimize the performance of the model with algae as particles.

Table 2. Algal Kinetics Parameters

Symbol	Definition	Value	Units
ANC	algal nitrogen-to-carbon ratio	0.167	g N g^{-1} C
APC	algal phosphorus-to-carbon ratio	0.0125	g P g^{-1} C
ASC	algal silica-to-carbon ratio	0.3	g Si g^{-1} C
BM	basal metabolic rate of algae at reference temperature Tr	0.01	d^{-1}
CChl	algal carbon-to-chlorophyll ratio	75	g C g^{-1} Chl
KHn	half-saturation concentration for nitrogen uptake by algae	0.025	g N m^{-3}
KHp	half-saturation concentration for phosphorus uptake by algae	0.0025	g P m^{-3}
KHs	half-saturation concentration for silica uptake by algae	0.03	g Si m^{-3}
KTb	effect of temperature on basal metabolism of algae	0.032	$^oC^{-1}$
KTg1	effect of temperature below Tm on growth of algae	0.0018	$^oC^{-2}$
KTg2	effect of temperature above Tm on growth of algae	0.006	$^oC^{-2}$
Phtl	predation rate on algae	0.01	m^3 g^{-1} C d^{-1}
Pm^B	maximum photosynthetic rate	300	g C g^{-1} Chl d^{-1}
Presp	photo-respiration fraction	0.25	$0 \leq Presp \leq 1$
Topt	optimal temperature for growth of algae	16	^oC
Tr	reference temperature for metabolism	20	^oC
Trpr	reference temperature for predation	20	^oC
Wa	algal settling rate (conventional model only)	0.5	m d^{-1}
α	initial slope of production vs. irradiance relationship	8.0 (spring	g C g^{-1} Chl $(E\ m^{-2})^{-1}$

Two conventional model runs were completed to provide comparisons with the particle approach. The first is a "Duplicate" run. Algae are initiated at a concentration of 1.0 g C m^{-3} at the same time and in the same extent of the Potomac River as the particle release. Concentration boundary conditions at the open ends of the model domain are specified as zero. Kinetics parameters are identical to the particle simulation with one exception. The Duplicate run employs an algal settling velocity, as in the Chesapeake Bay model. Settling is omitted from the base particle simulation. The Duplicate run is employed in the majority of comparisons with the particle simulation. A run referred to as "Original" was also completed. The original run simulates spring diatoms exactly as in the Chesapeake Bay model. The foremost characteristic of this run is that diatoms are initiated at the open boundaries rather than in the mid-river. Advection and dispersion transport diatoms to regions that are favorable to growth.

Plan and Elevation Views

Elevation views of algae as particles along the axial transect are provided in Figure 48. The distribution of attached algae is heterogeneous and demonstrates no apparent pattern. Particles with varying amounts of attached algae are distributed along the transect and in the vertical direction. Particles with widely different amounts of attached algae are found immediately adjacent to each other. At Days 152 and 212, individual particles with high amounts of attached algae occur at depths greater than 20 m. The amount of algae attached to particles at great depths can exceed the amount of attached algae above, in the photic zone. In this regard, the simulation resembles the observations (e.g., Figures 18, 19) in which chlorophyll concentration near the bottom exceeds chlorophyll concentration at the surface.

Views of algae as particles in the model surface layer (Figure 50) reflect the properties apparent in the elevation views. The spatial distribution is heterogeneous and lacks apparent pattern. Circulation carries algae into the smallest tributaries where they remain when the mainstem of the river is largely cleared by the flood event (Figure 36) circa day 152. At the completion of the simulation, the amount of algae attached to individual particles varies through multiple orders of magnitude in the range > 10^4 g C $particle^{-1}$ but < 10^7 g C $particle^{-1}$. The lower limit is affected by the rule which eliminates particles with no viable attached algae; particles are eliminated when attached algae falls below 2,500 g C $particle^{-1}$. Particles with more than 2.5 x 10^5 g attached algae demonstrate growth above the initial concentration.

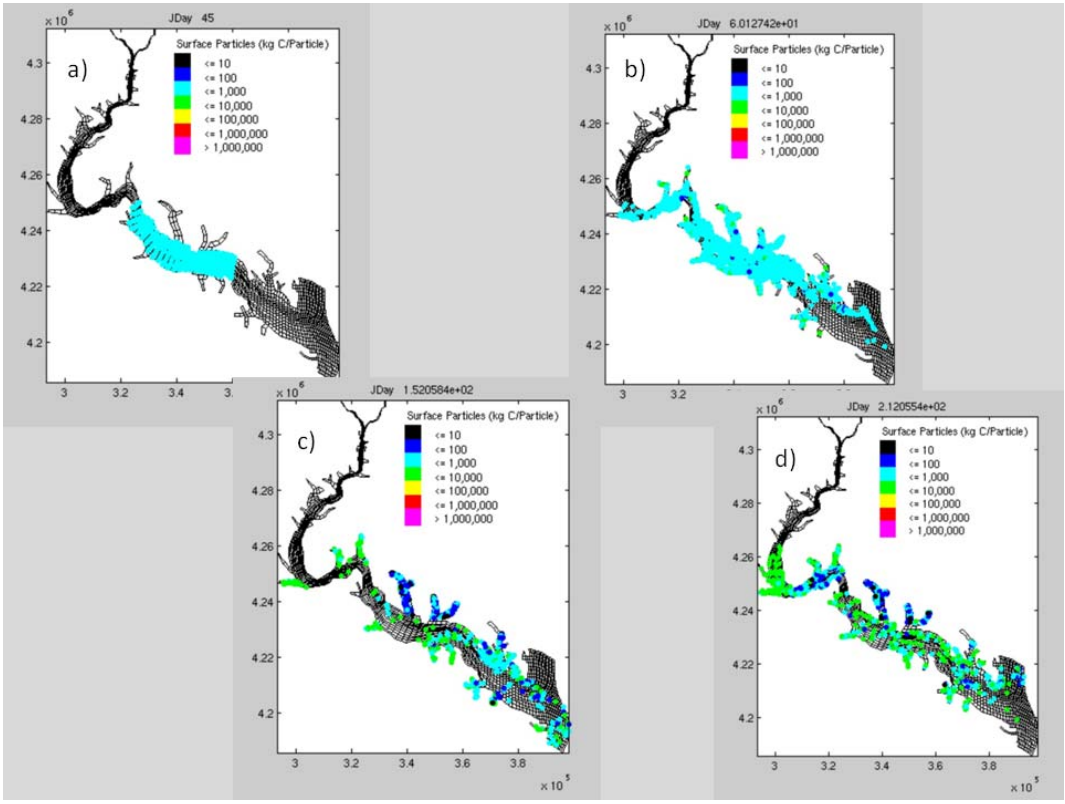

Figure 50. Surface view of particle distribution and attached algal biomass for base phytoplankton run. Results are presented at four time intervals: a) Day 45 (particle release); b) Day 60; c) Day 152; d) Day 212 (end of simulation).

The upper limit is also influenced by the rules since the particle with the highest algal concentration is split to compensate for particles which leave the system or are eliminated.

Comparison with Conventional Model

Two conversions were conducted to enable comparison of algae computed in the particle model with algae computed in the conventional model. The two conversions were also conducted to facilitate comparisons of both models with observations. First, attached algal carbon was converted to volumetric concentration. Carbonaceous biomass in each grid cell was summed over all the particles in the cell and then divided by cell volume. In the second conversion, carbon concentration in both models was converted to chlorophyll concentration through division by the model carbon-to-chlorophyll ratio. Comparisons were completed along the mid-channel transect and in the surface plane.

The elevation views of the particle model (Figure 51) demonstrate a heterogeneous spatial distribution which manifests immediately upon release of the particles. Chlorophyll concentrations near the bottom commonly exceed concentrations at lesser depths above. The surface layer, which receives the greatest illumination, is at times devoid of algae. Chlorophyll concentrations computed in the conventional, Duplicate, model are much more smoothly distributed (Figure 52). On Day 60, soon after bloom initiation, there is an indication of a subsurface chlorophyll maximum caused by upstream advection of the initial uniform chlorophyll distribution. Otherwise, the vertical chlorophyll distribution declines monotonically from the illuminated surface waters to the bottom. No surface cells within the bloom region are devoid of algae.

Surface chlorophyll concentrations computed by the particle model follow the heterogeneous pattern previously observed in the computed particle distribution (Figure 53). As noted in the particle distributions, chlorophyll penetrates into the smallest tributaries and, by the end of the simulation, the highest concentrations are in the tributaries rather than in the surface waters of the mainstem Potomac. The conventional model provides more uniform surface chlorophyll distributions (Figure 54). At the end of the simulation, chlorophyll concentrations in the mainstem are as high, or higher, than in the tributaries. The contrast between the uniform surface distribution in the conventional model and the patchy distribution in the particle model is striking.

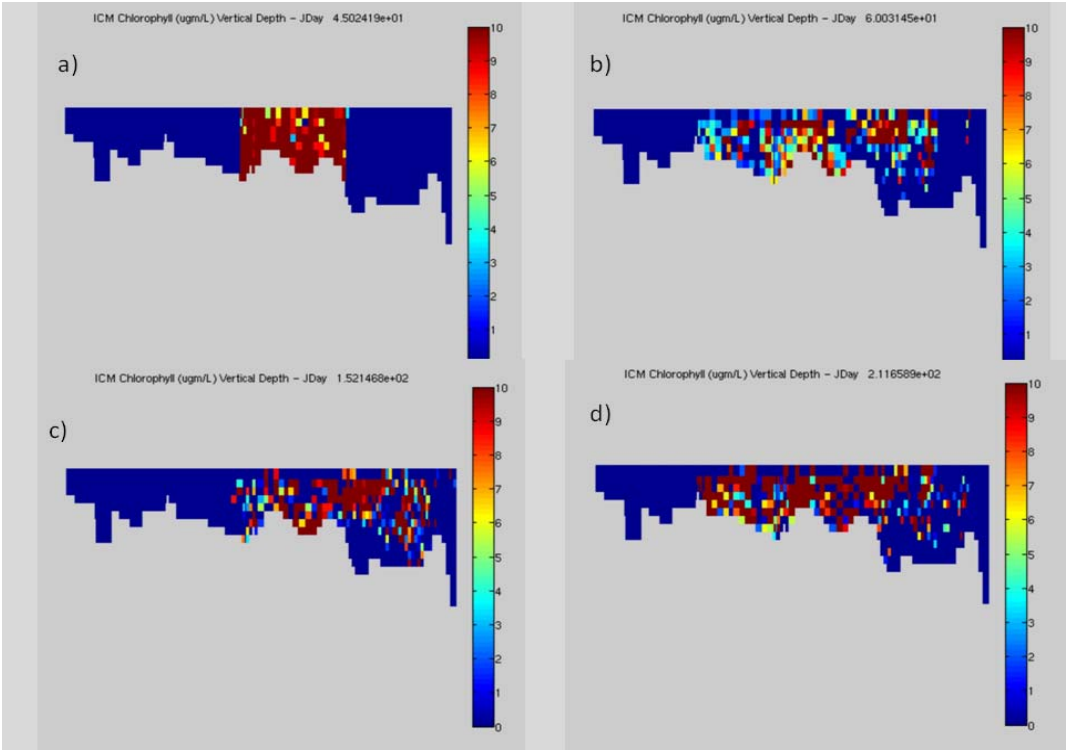

Figure 51. Elevation view of chlorophyll concentration derived from the model of algae as particles. Results are shown at four time intervals: a) Day 45 (release); b) Day 60; c) Day 152; d) Day 212 (end of simulation). Note the "patchy" distribution of chlorophyll and the occurrence of high concentrations near the bottom of the river.

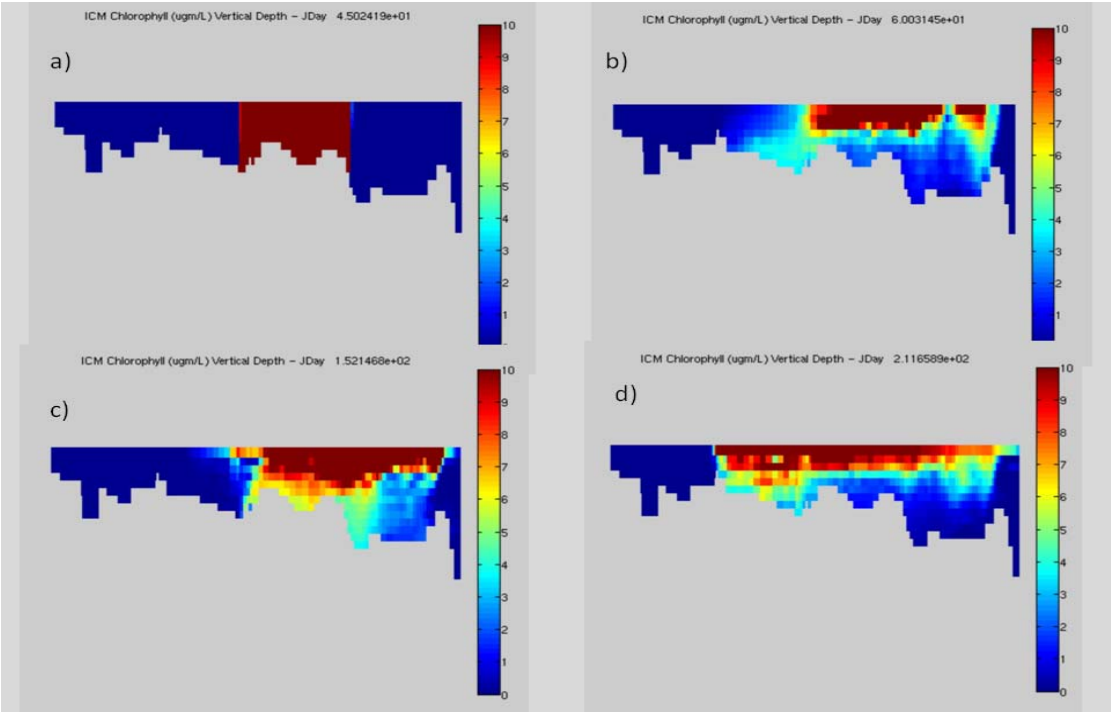

Figure 52. Elevation view of chlorophyll concentration computed by the conventional algal model. Results are shown at four time intervals: a) Day 45 (release); b) Day 60; c) Day 152; d) Day 212 (end of simulation). Note the monotonic decline of chlorophyll from surface to bottom.

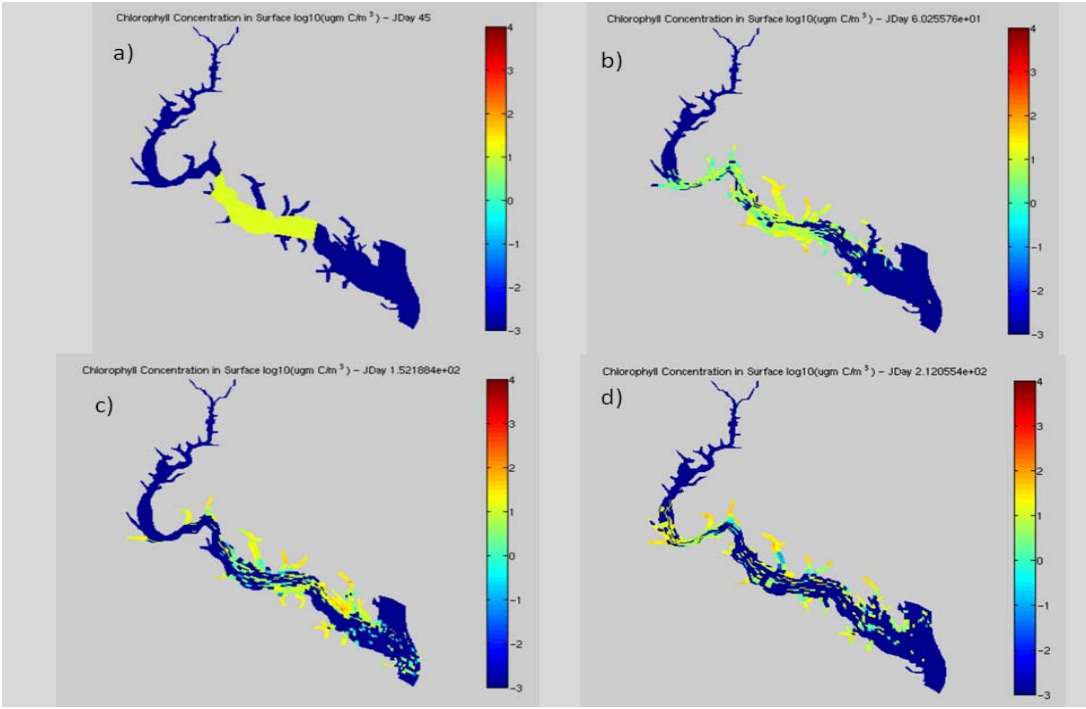

Figure 53. Surface view of chlorophyll concentration derived from the model of algae as particles (Note the use of a log scale). Results are shown at four time intervals: a) Day 45 (release); b) Day 60; c) Day 152; d) Day 212 (end of simulation). At the end of the simulation, the highest chlorophyll concentrations are in small tributaries.

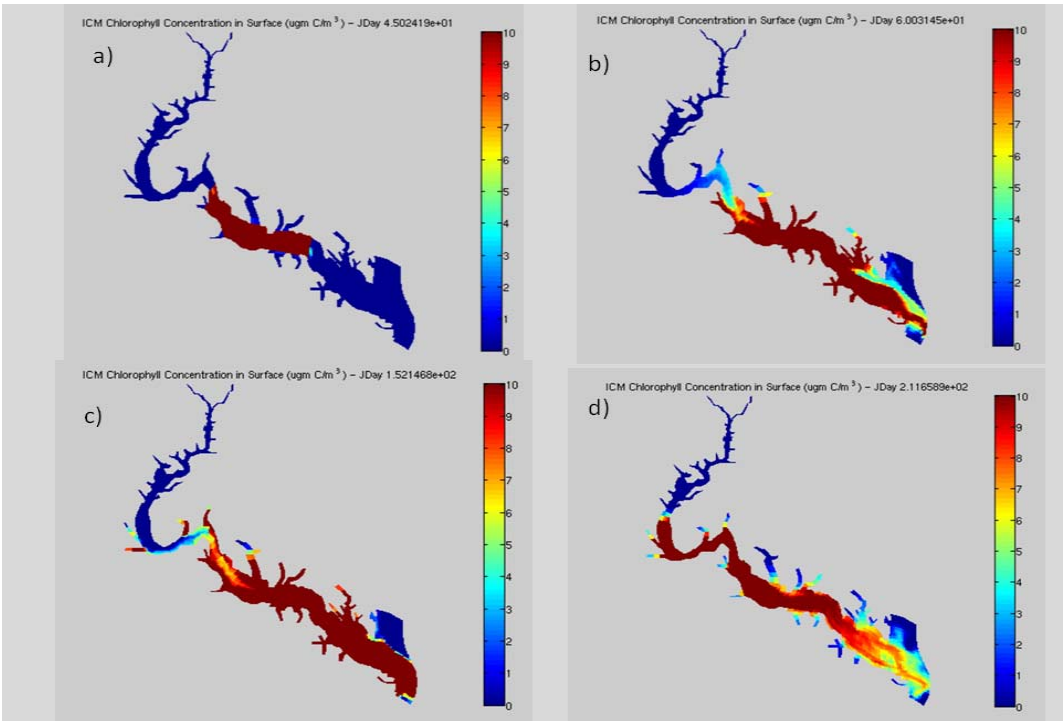

Figure 54. Surface view of chlorophyll concentration computed by the conventional model. Results are shown at four time intervals: a) Day 45 (release); b) Day 60; c) Day 152; d) Day 212 (end of simulation). At the end of the simulation, the highest chlorophyll concentrations are in mainstem.

8 Algae as Particles – Comparisons with Observations

Introduction

Chlorophyll concentrations derived from the model of algae as particles are compared to observations in three formats: time series, seasonal spatial distribution, and cumulative distribution. Concentrations from the conventional model with algae as a dissolved substance are presented in the same formats for comparison with the alternate model and with the observations.

Time series comparisons are presented at four stations: RET2.2, RET2.4, LE2.2, and LE2.3 (Figure 8). These stations encompass the spatial extent of the spring algal bloom. Chlorophyll observations were collected 1 m below the surface and 1 m above the bottom at each station, once or twice monthly. Samples were also collected 1 m above and 1 m below the pycnocline at the LE stations. These samples were linearly interpolated to create a mid-depth observation. The observations are compared to daily-average model outputs at station locations and sample depths. The temporal origin of the plots (Year 0) is the commencement of the model run (November 1, 1993) and the temporal extent is one year, although the run extends through only May 31.

Seasonal spatial distributions are presented for two seasons: winter (December – February) and spring (March – May). The mean and range of surface and bottom observations were computed for each season and compared with the mean and range of the daily model outputs. The spatial origin of the plots (km 0) is the mouth of the Potomac Estuary and the spatial extent is from the eastern edge of the computational grid (km -10) to the Potomac River fall line (km 180). The preponderance of the diatom bloom occurs below km 120.

The cumulative distribution plots summarize and compare observations at the time series stations with model results at the same locations and depths. The observations and computations are sorted from smallest to largest values. The sorted arrays are divided into quantiles and plotted as cumulative distributions. A point on the line in x-y space indicates the percentage

of observations or computations (x-axis) less than the indicated concentration (y-axis). The 50th percentile indicates the median value. Perfect correspondence in the range of computed and observed variables is indicated when the cumulative distribution of modeled values exactly overlays the cumulative distribution of observed values.

Time Series Comparisons

The temporal characteristics of results from the two models and of comparisons with the observations vary with station locations. Some salient characteristics and trends can be discerned, however. The particle model demonstrates high-frequency oscillations, with periods on the order of days, at all stations (Figures 55 – 58). The amplitude of the oscillations is large relative to the magnitude of the computations. The conventional model demonstrates comparable oscillations at the most downstream station, LE2.3 (Figure 55). The high-frequency oscillations are damped with distance upstream, however, and variations with longer periods, weeks to months, predominate (Figures 56 – 58). The lengthy intervals between the observations confound verification of the oscillatory behavior.

At the most downstream station, the magnitude of results from both models compares with the observations at the surface and mid-depth while both models underestimate the chlorophyll concentration at the bottom (Figure 55). Further upstream, the particle model computes lower surface chlorophyll concentrations than the conventional model (Figures 56 – 58). The magnitude of surface chlorophyll computed by the particle model reflects the magnitude of the observations better than the conventional model. Both models underestimate observed chlorophyll at the bottoms of the LE stations (Figures 55, 56), although correct magnitudes are computed by both models at the RET stations (Figures 57, 58).

Seasonal Spatial Distributions

The seasonal spatial distributions “average out” the high-frequency oscillations in the computations and produce more readily interpreted comparisons between the characteristic values provided by the models and the observations. During the winter months, the characteristics of the two models differ substantially, although neither is apparently superior with regard to the observations. The particle model computes highest surface concentrations at the mouth of the estuary; concentrations generally decrease in the upstream direction and are lower than the observations

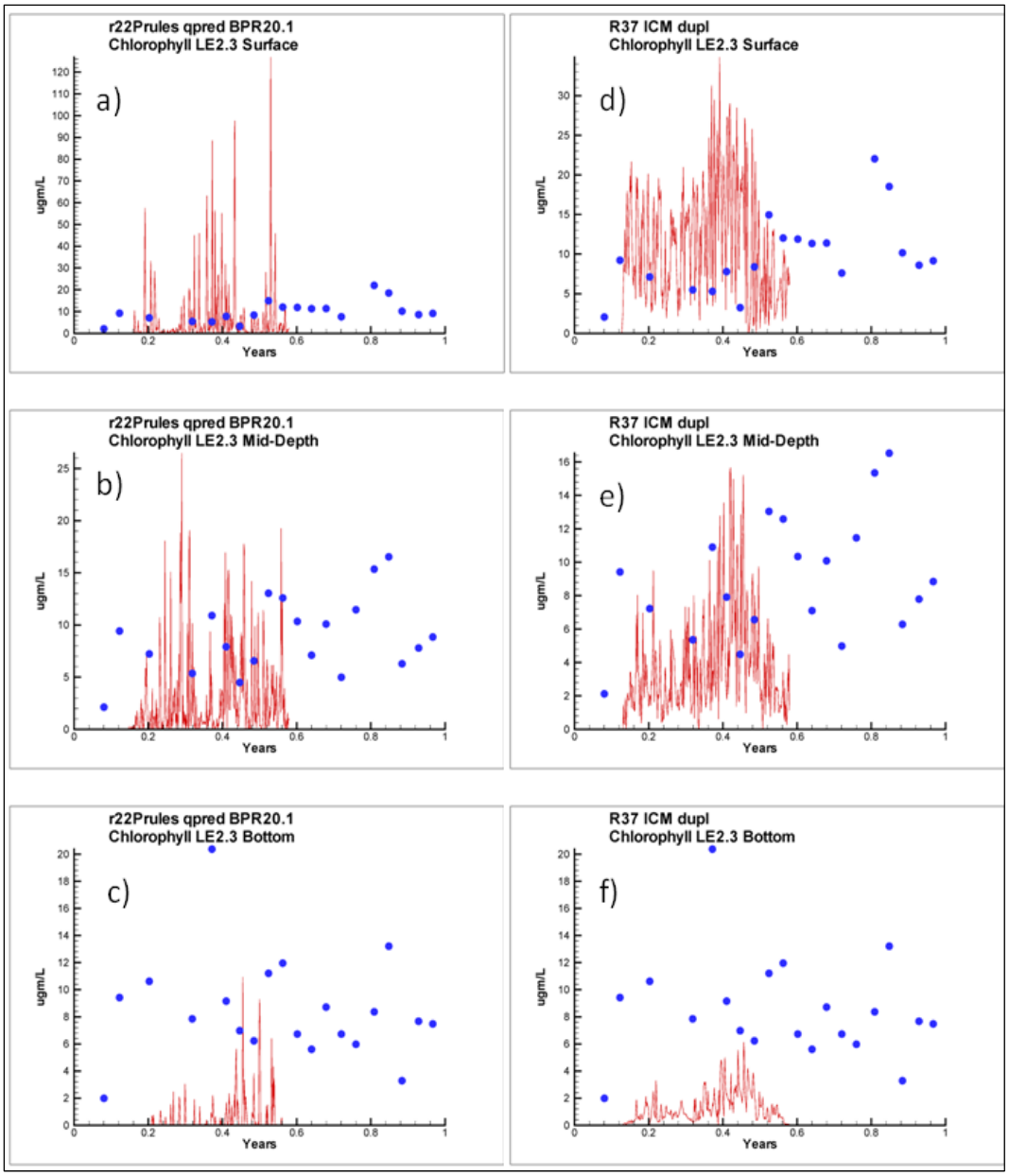

Figure 55. Observed and computed chlorophyll concentrations at station LE2.3. Results are shown from the model with algae as particles at (a) surface, (b) mid-depth, and (c) bottom and from a conventional model at (d) surface, (e) mid-depth, and (f) bottom.

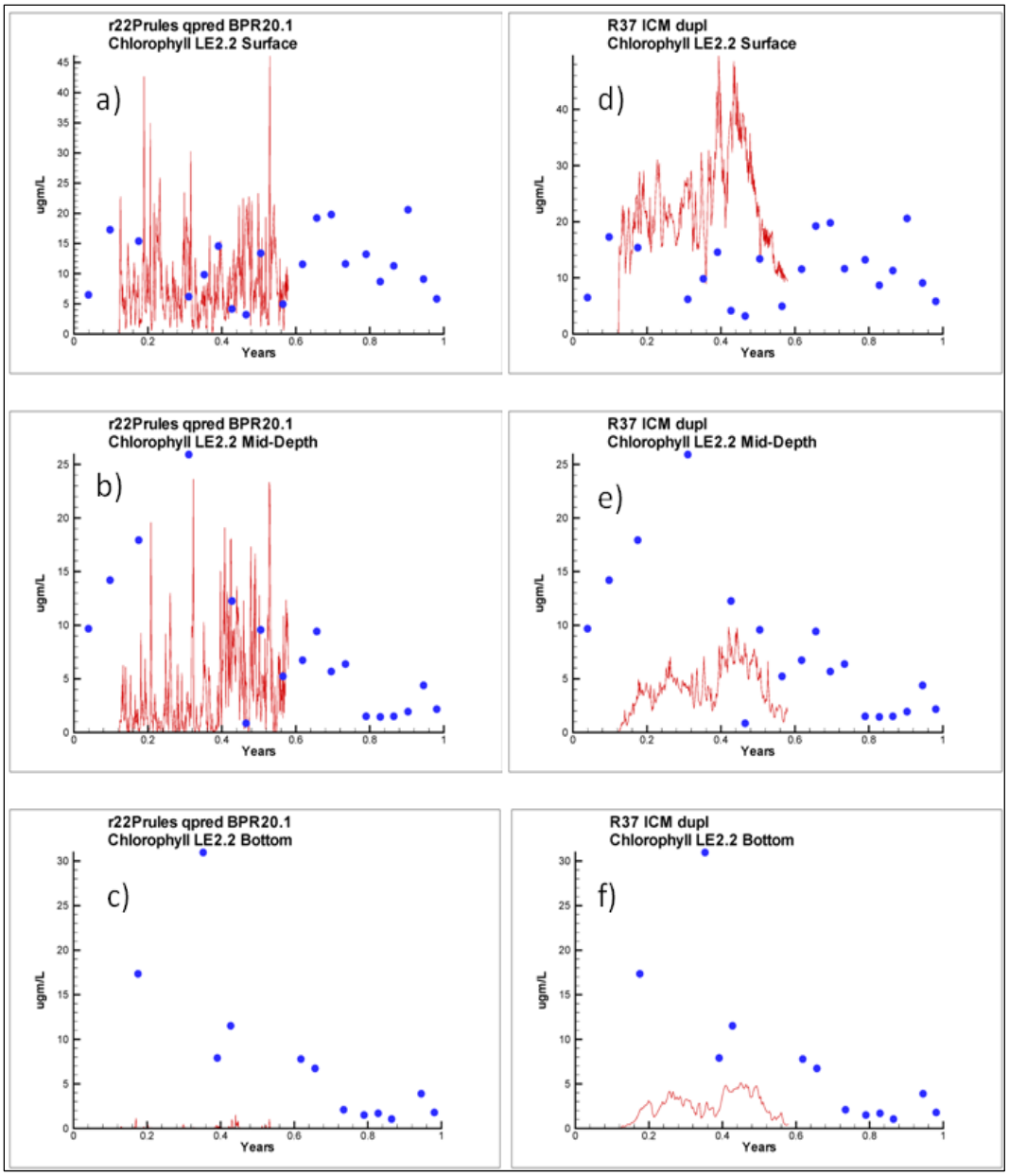

Figure 56. Observed and computed chlorophyll concentrations at station LE2.2. Results are shown from the model with algae as particles at (a) surface, (b) mid-depth, and (c) bottom and from a conventional model at (d) surface, (e) mid-depth, and (f) bottom.

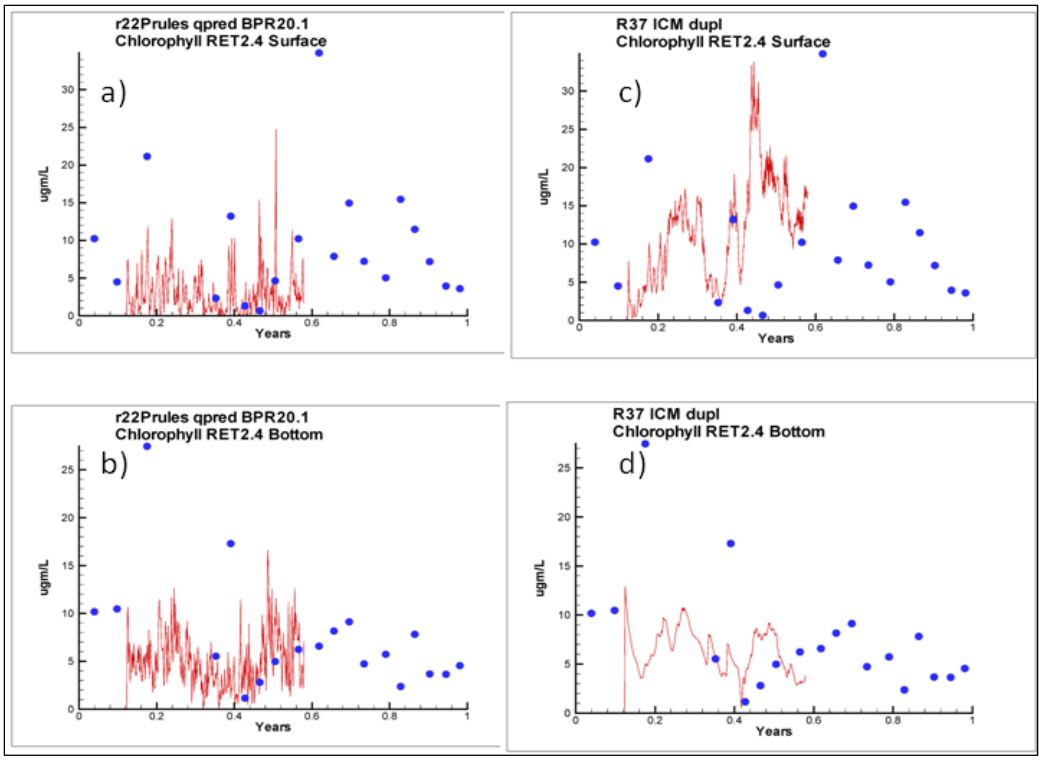

Figure 57. Observed and computed chlorophyll concentrations at station RET2.4. Results are shown from the model with algae as particles at (a) surface and (b) bottom and from a conventional model at (c) surface and (d) bottom.

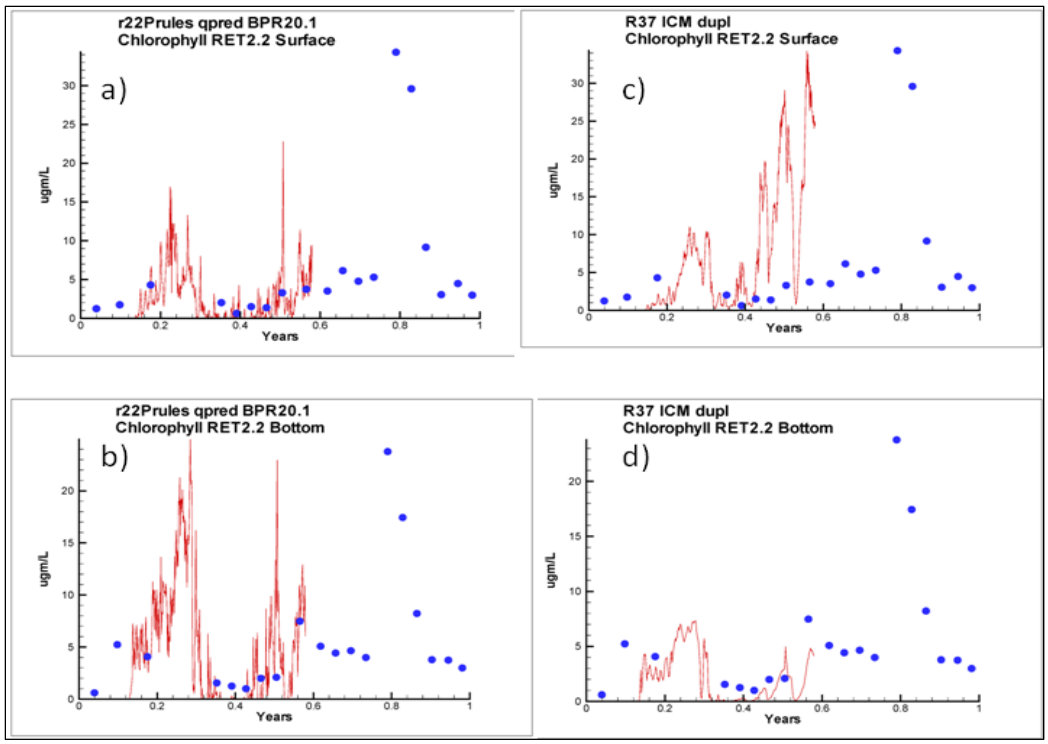

Figure 58. Observed and computed chlorophyll concentrations at station RET2.2. Results are shown from the model with algae as particles at (a) surface and (b) bottom and from a conventional model at (c) surface and (d) bottom.

between km 30 and 80 (Figure 59). The conventional model computes highest surface computations from km 30 to 50 and overestimates the observations in this reach (Figure 59). Peak subsurface computations in both models occur upstream of peak surface concentrations and are substantially less than observations in both cases (Figure 59). The particle model does compute a subsurface chlorophyll maximum, however, circa km 40 to 60. Mean computed bottom concentrations exceed 10 mg m^{-3} while mean computed surface concentrations in this reach never exceed 6 mg m^{-3}.

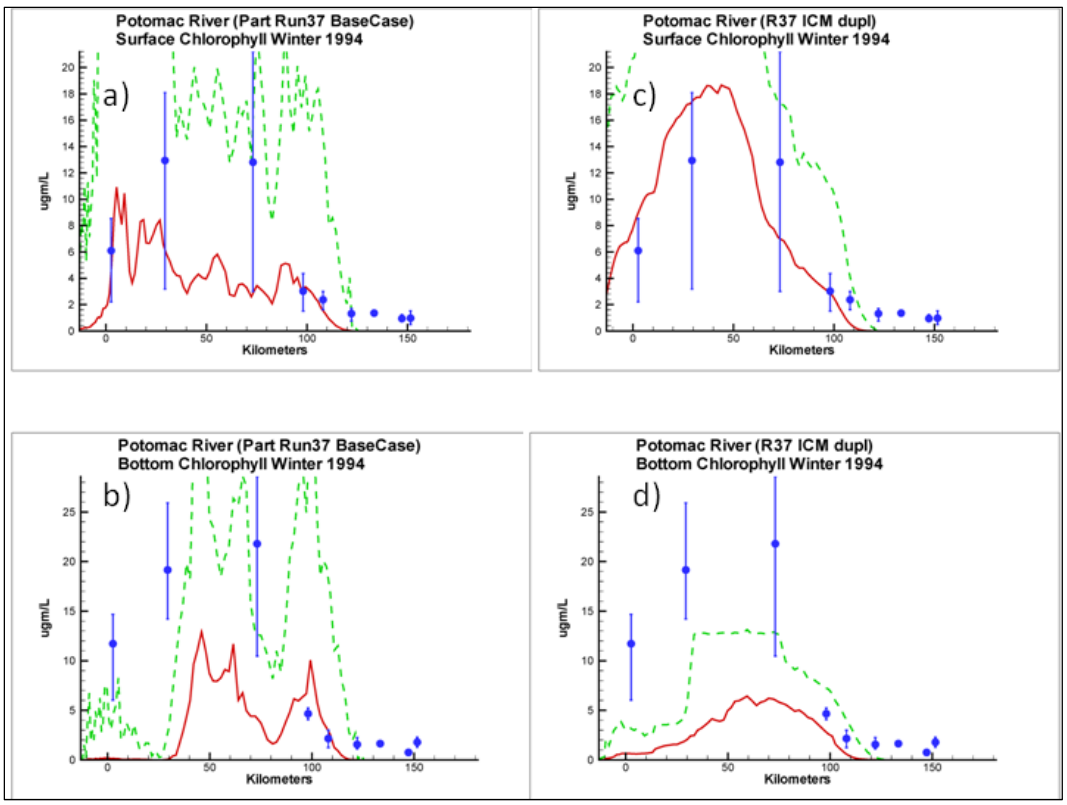

Figure 59. Observed and computed chlorophyll concentrations for the winter season (December – February). Km zero is at the mouth of the estuary. Results are shown from the model with algae as particles at (a) surface and (b) bottom and from a conventional model at (c) surface and (d) bottom.

The shapes of the spatial distributions from both models are preserved from winter to spring. The particle model computes maximum surface concentrations at the mouth of the estuary, while the conventional model computes maximum concentrations between km 30 and 50 (Figure 60). The particle model provides excellent agreement with the observations, however, while the conventional model overestimates surface concentrations at all stations (Figure 60). Both models persist in locating the greatest subsurface chlorophyll concentrations upstream of the greatest surface concentrations.

Only the particle model, however, computes a true subsurface maximum in which the mean chlorophyll concentration at the bottom, ≈ 18 mg m^{-3} circa km 50, exceeds the mean surface concentration, ≈ 8 mg m^{-3}, at the same location (Figure 60).

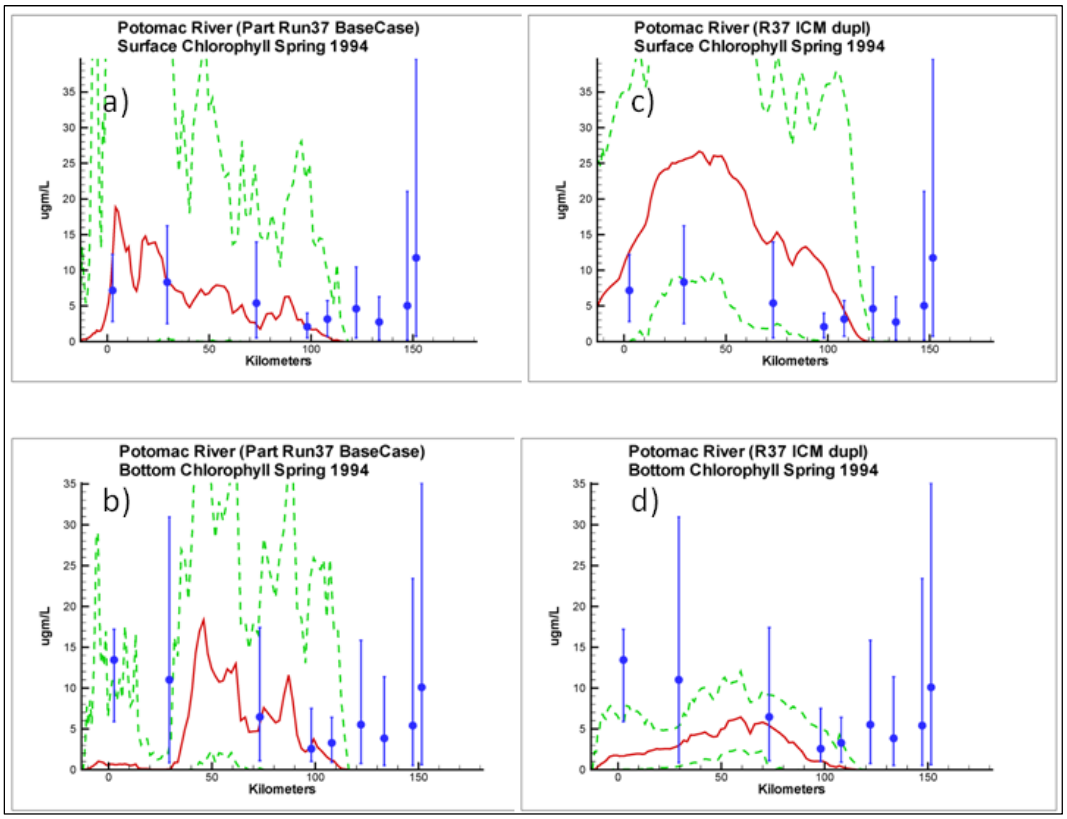

Figure 60. Observed and computed chlorophyll concentrations for the spring season (March - May). Km zero is at the mouth of the estuary. Results are shown from the model with algae as particles (a) at surface and (b) bottom and from a (c) conventional model at surface and (d) bottom.

Cumulative Distribution Plots

Cumulative distribution plots were prepared for the surface observations and corresponding model computations (Figure 61), for the bottom observations and corresponding model computations (Figure 62), and for all observations, including mid-depth, and corresponding model computations (Figure 63). The plot at the surface indicates the distribution of algae computed as particles more closely represents the observed distribution. The preponderance of the particle distribution is below the observed, while the distribution of algae as dissolved substance exceeds the observations throughout. Both model approaches underestimate the distribution of chlorophyll observed at the bottom. A noticeable distinction between the

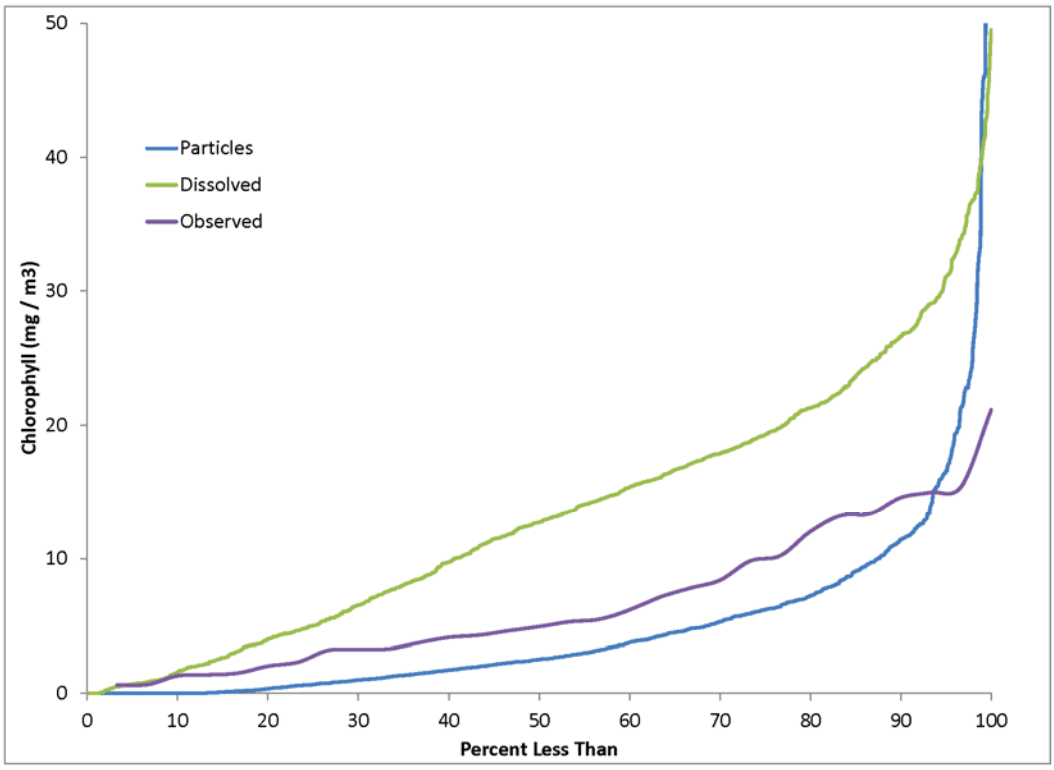

Figure 61. Cumulative distribution plot of observed and modeled surface chlorophyll concentration.

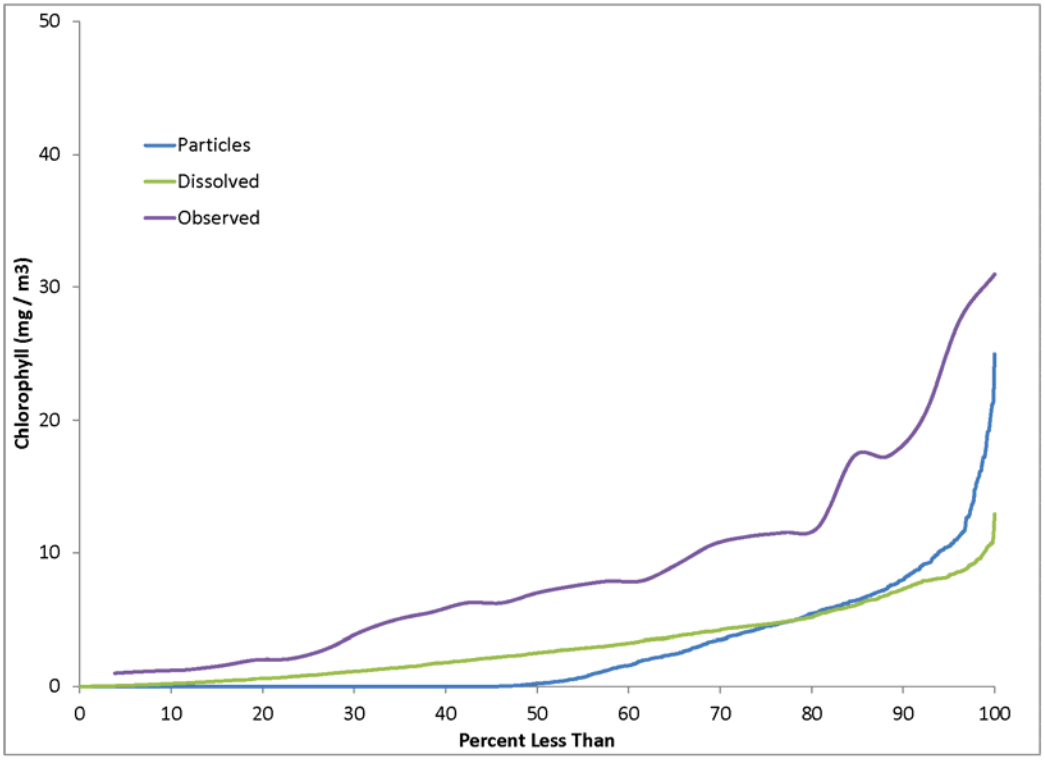

Figure 62. Cumulative distribution plot of observed and modeled bottom chlorophyll concentration.

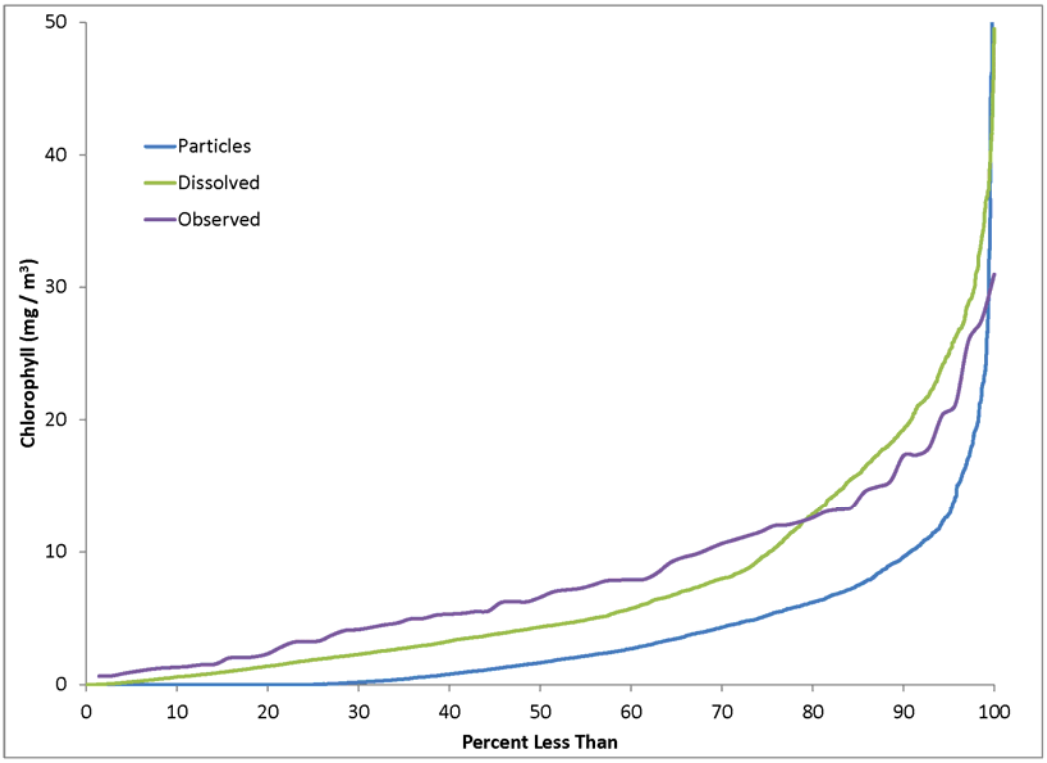

Figure 63. Cumulative distribution plot of observed and modeled chlorophyll concentration at all depths.

two approaches is that half the particle computations are exactly zero, while less than 5% of the dissolved computations are zero. The cumulative distribution plot, which considers observations and comparable computations at all stations and depths, indicates two overarching conclusions. First, chlorophyll computations from the conventional model exceed chlorophyll computations from the particle model. The median concentration from the conventional model is 4.3 mg m^{-3} versus 1.7 mg m^{-3} from the particle model. Second, the preponderance of observations exceeds both models. The median observed concentration is 6.6 mg m^{-3}. Both models compute extreme concentrations, which exceed the maximum observation, however. This effect is especially noticeable in the conventional model for which the upper 20% of the chlorophyll computations exceeds the upper 20% of the observations.

Time Series Analysis

The results from the two models demonstrate periodic behavior. The amplitudes and dominant periods vary between the two models, as described earlier in this chapter. The periodic behaviors cannot be validated with the conventional monitoring data due to the lengthy and

irregular gaps between observations. More recent data from alternate monitoring programs provides insight into the periodic behavior of in-situ chlorophyll and allows comparisons with the model patterns.

Continuous Monitoring Data

The Chesapeake Bay Program and its partner agencies commenced a Shallow Water Monitoring Program circa 2005. The program incorporates continuous remote sensors in locations throughout the bay system. One station was operated at Nomini Bay, on the south shore of the Potomac adjacent to monitoring station LE2.2 (Figure 64), from 2007 through 2009. Surface chlorophyll measures (1.5 m below mean low water) were recorded at 15-minute intervals from April through October of each year. Observations for time series analysis were retrieved from an on-line database (VIMS 2012) for the period April – June 2008. Although the observations were not concurrent with the model application, analyses were conducted based on the assumption that characteristic periodic behaviors are consistent from year to year.

A second station was operated at St. George's Island, on the northern shore of the Potomac (Figure 64), from 2006 through 2012. Surface chlorophyll measures (1.3 m below mean low water) were recorded at 10 to 15 minute intervals from April through October of these years. Inspection of the data (MD DNR 2012) indicated the record from mid-April through June 2012 provided the best opportunity for time series analysis due to regular sampling intervals and limited data gaps. Model results for comparison with these observations were retrieved from the surface cell at Station LE2.2 for the period January 1 through May 31, 1994.

The observations (Figure 65, 66) demonstrate three properties: regular oscillations with a period on the order of days, longer-term variations with periods of tens of days, and irregular large-amplitude spikes. Qualitatively, the observations resemble the results from the model with algae as a dissolved substance (Figure 67), except the model lacks the spikes. The spikes and regular oscillations are present in the particle model (Figure 68), but the longer-term variations are difficult to perceive. The particle model is distinctive in that it computes concentrations of zero, which are not present in either the observations or the dissolved model.

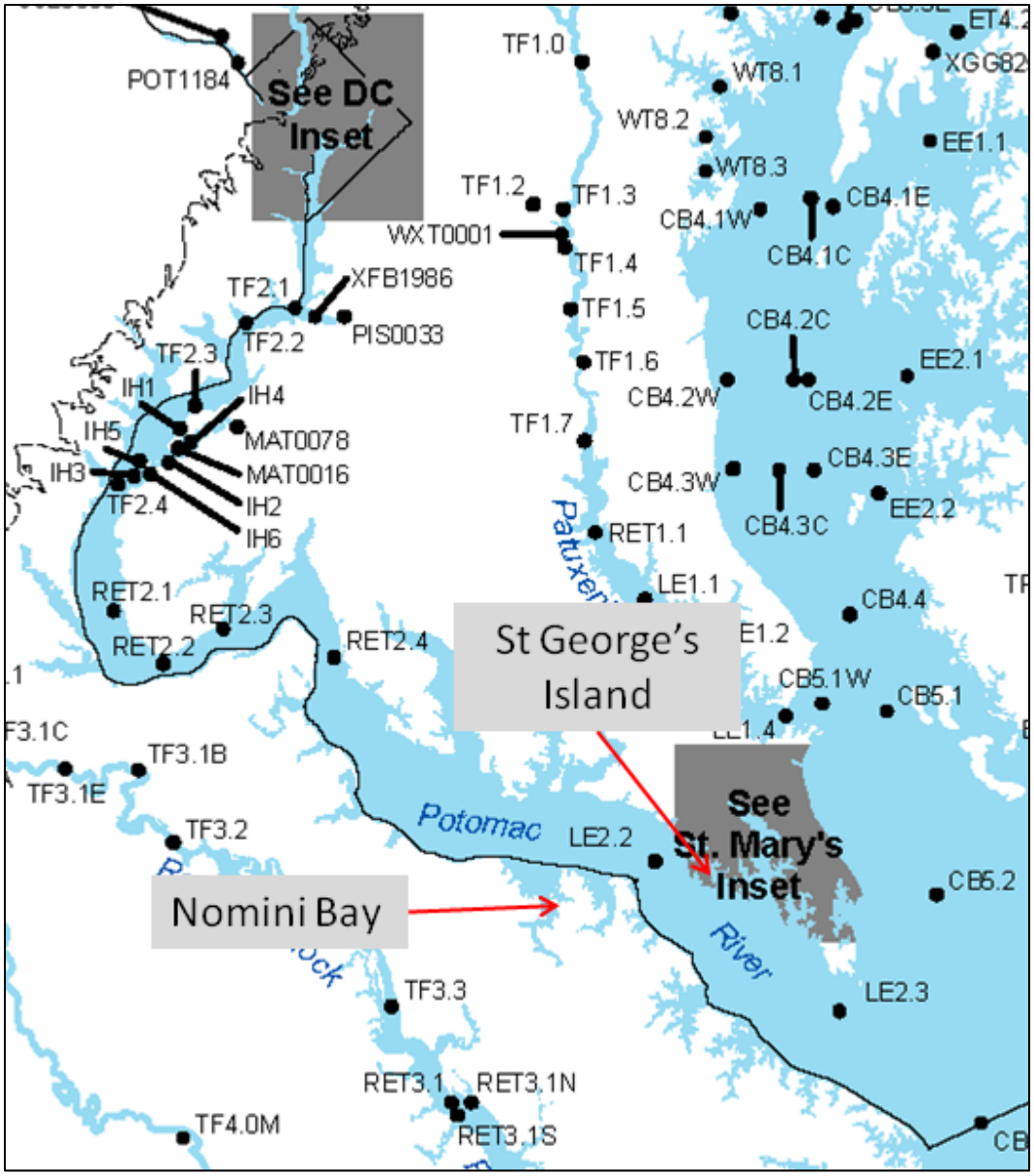

Figure 64. Location of Nomini Bay and St. George's Island continuous monitoring stations.

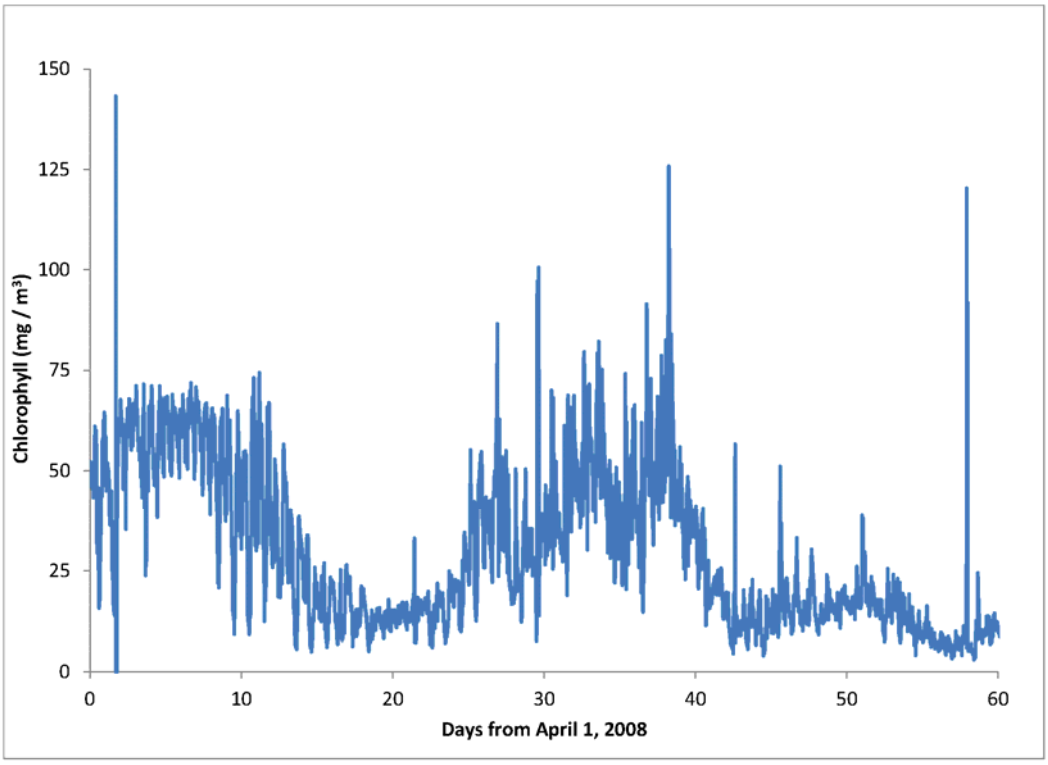

Figure 65. Observed chlorophyll at Nomini Bay, April – May 2008.

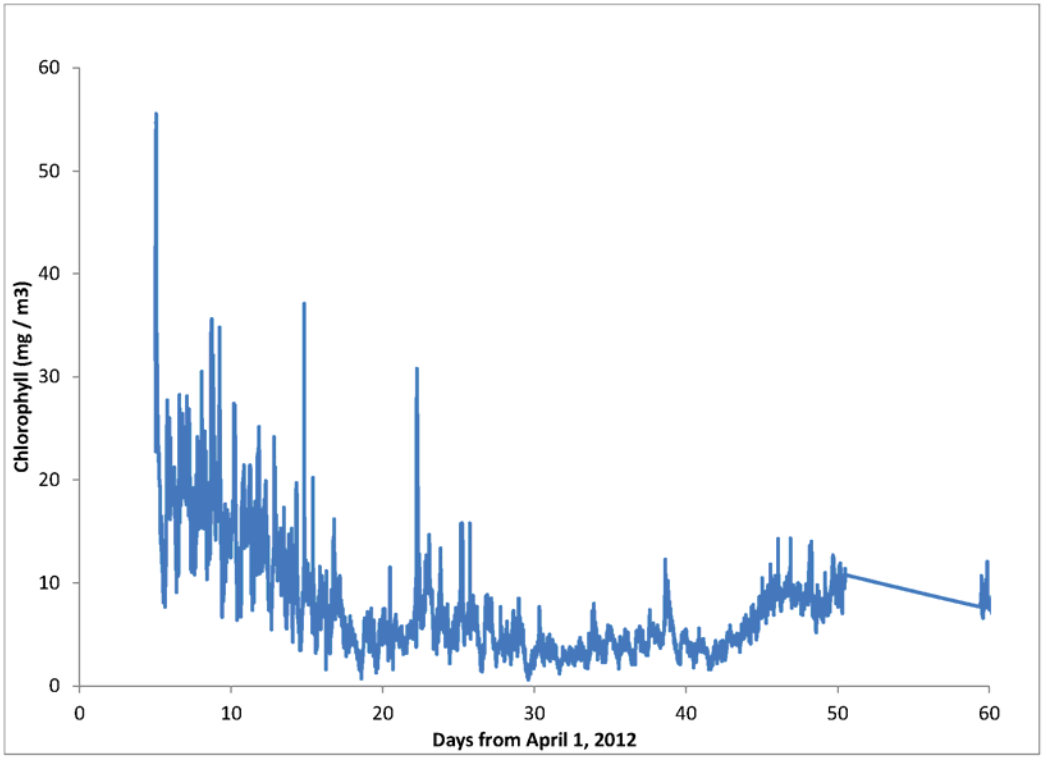

Figure 66. Observed chlorophyll at St. George's Island, April – May 2012.

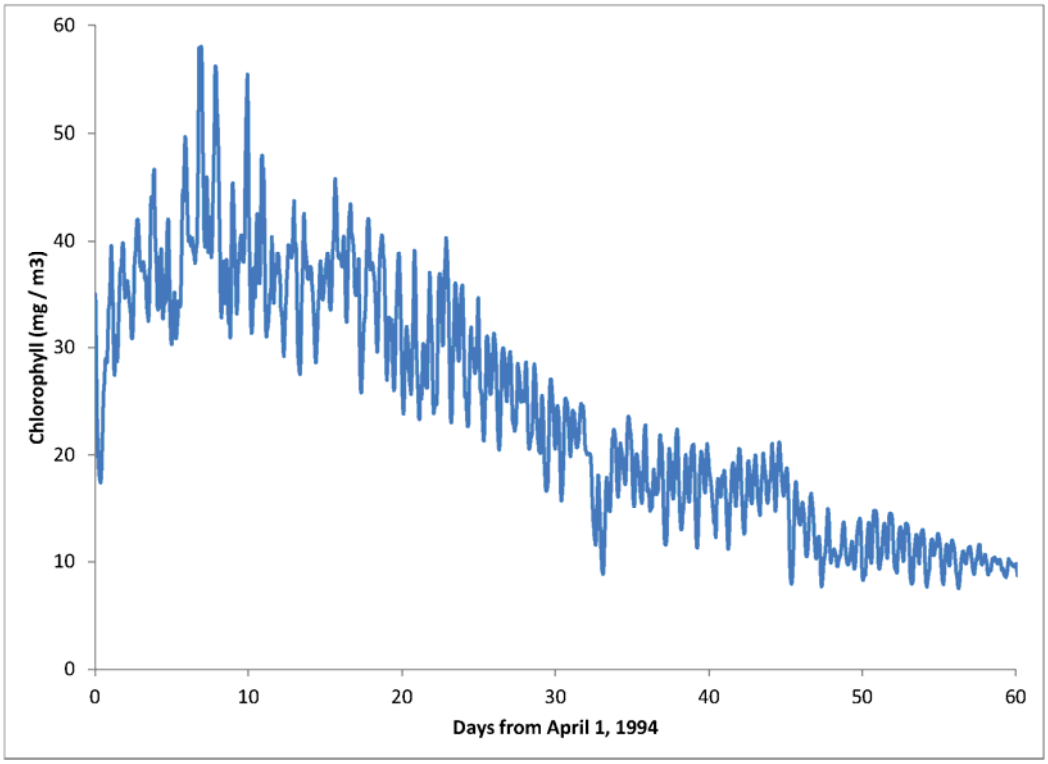

Figure 67. Surface chlorophyll computed at Station LE2.2 using a conventional model of algae as a dissolved substance.

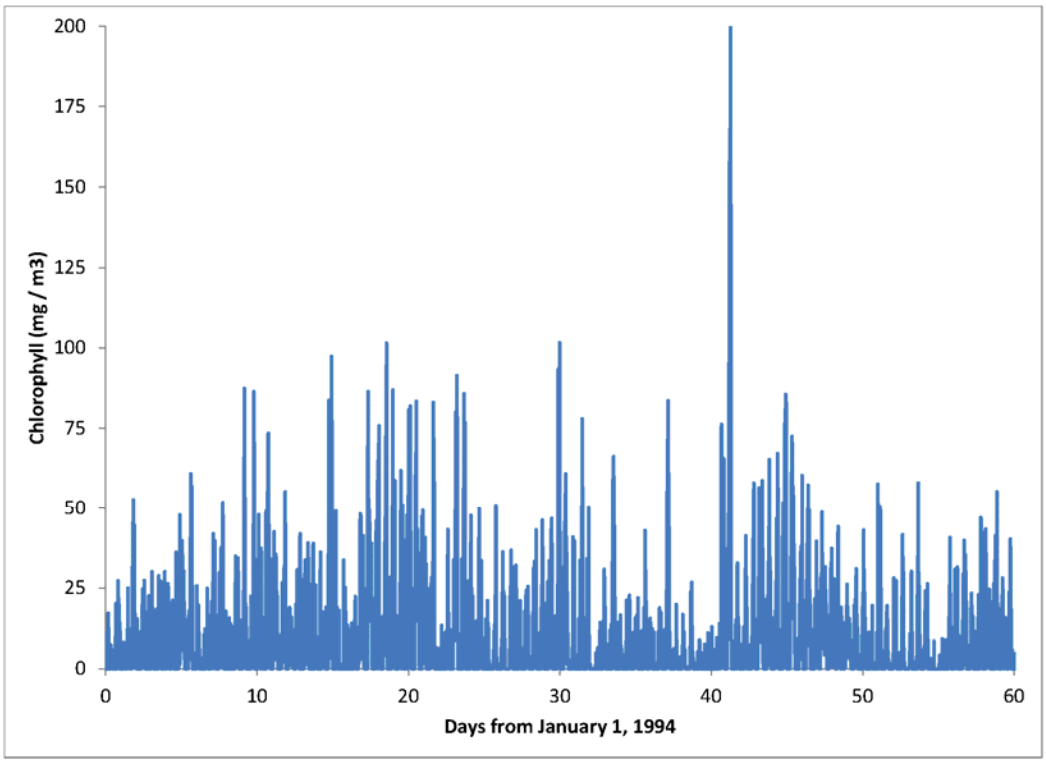

Figure 68. Surface chlorophyll computed at Station LE2.2 using a model of algae as particles.

Harmonic Analysis

A linear model was proposed to describe the observed record and the predicted time series at LE2.2:

$$chl = a + b1 \bullet t + b2 \bullet sin\left[\frac{2\pi t}{12.4}\right] + b3 \bullet cos\left[\frac{2\pi t}{12.4}\right] + b4 \bullet sin\left[\frac{2\pi t}{24}\right] + b5 \bullet cos\left[\frac{2\pi t}{24}\right] \quad (9)$$

in which:

chl = Chlorophyll concentration (mg m^{-3})
t = Time
a, b1 ... b5 = Model parameters

The b2 and b3 parameters represent the amplitudes of harmonics with the period of the lunar semi-diurnal tide, 12.4 hours. The b4 and b5 parameters represent harmonics with a daily period. The amplitudes of the sin and cos can be combined using the identity:

$$A\sin(\alpha) + B\cos(\alpha) = \sqrt{A^2 + B^2}\ \sin\left(\alpha + \tan^{-1}\left(B/A\right)\right) \quad (10)$$

Parameters for the observations and the predicted time series were determined via linear regression. The fraction of variation explained by the models was typically small ($R^2 \approx 0.1$) but highly significant ($p < 0.001$). The amplitudes of the semi-diurnal and diurnal harmonics were roughly equal for the observations and for the model of algae as dissolved substance (Figure 69). The influences of tides and of diurnal irradiance were equivalent. The semi-diurnal amplitude for the particle model was several times larger than any other amplitude, while the diurnal amplitude was the least of all. The particle model exhibited a strong influence from tides but almost no influence from diurnal irradiance.

Power Spectra

Power spectra for the observed and computed time series were obtained using the Fast Fourier Transform feature of MATLAB (MathWorks 2012). Power spectra of the observed time series indicate substantial peaks at the semi-diurnal and diurnal periods. The Nomini Bay spectrum (Figure 70) indicates more power in the semi-diurnal period. The St. Georges's spectrum (Figure 71) indicates more power in the diurnal period. The

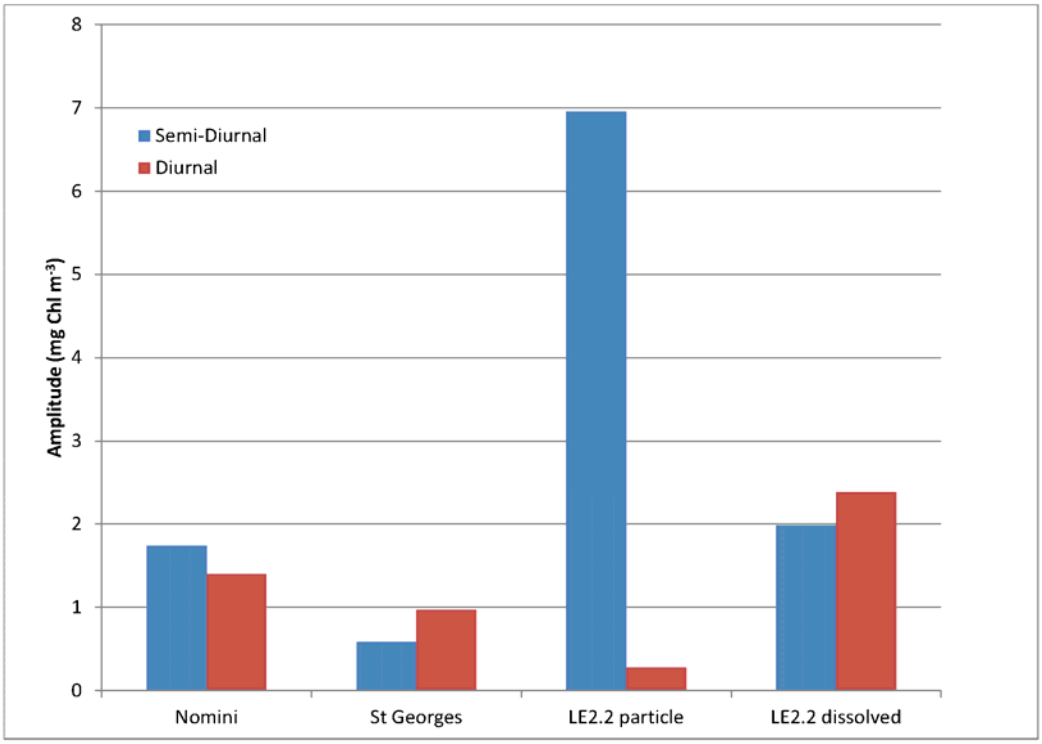

Figure 69. Amplitudes of lunar semi-diurnal and diurnal harmonics of observed and computed chlorophyll time series. Observations from Nomini Bay and St. George's island. Model results at LE2.2 using algae as particles and as dissolved substance.

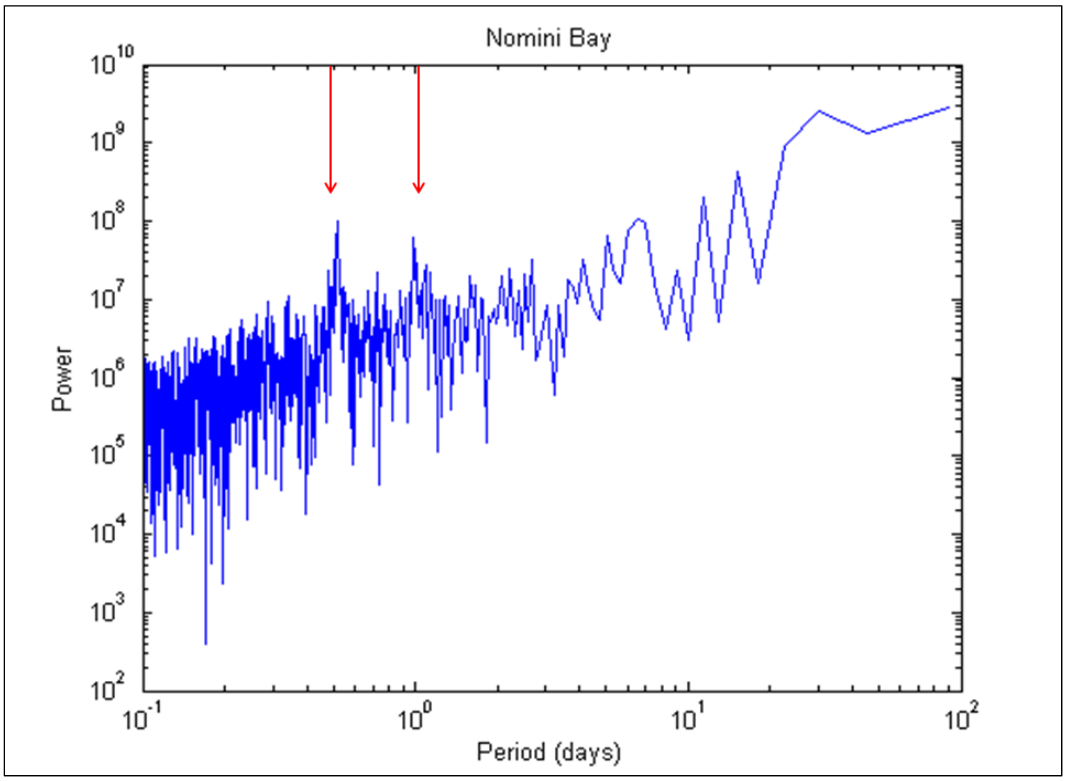

Figure 70. Power spectrum of chlorophyll observations at Nomini Bay. The red arrows indicate the semi-diurnal and diurnal periods.

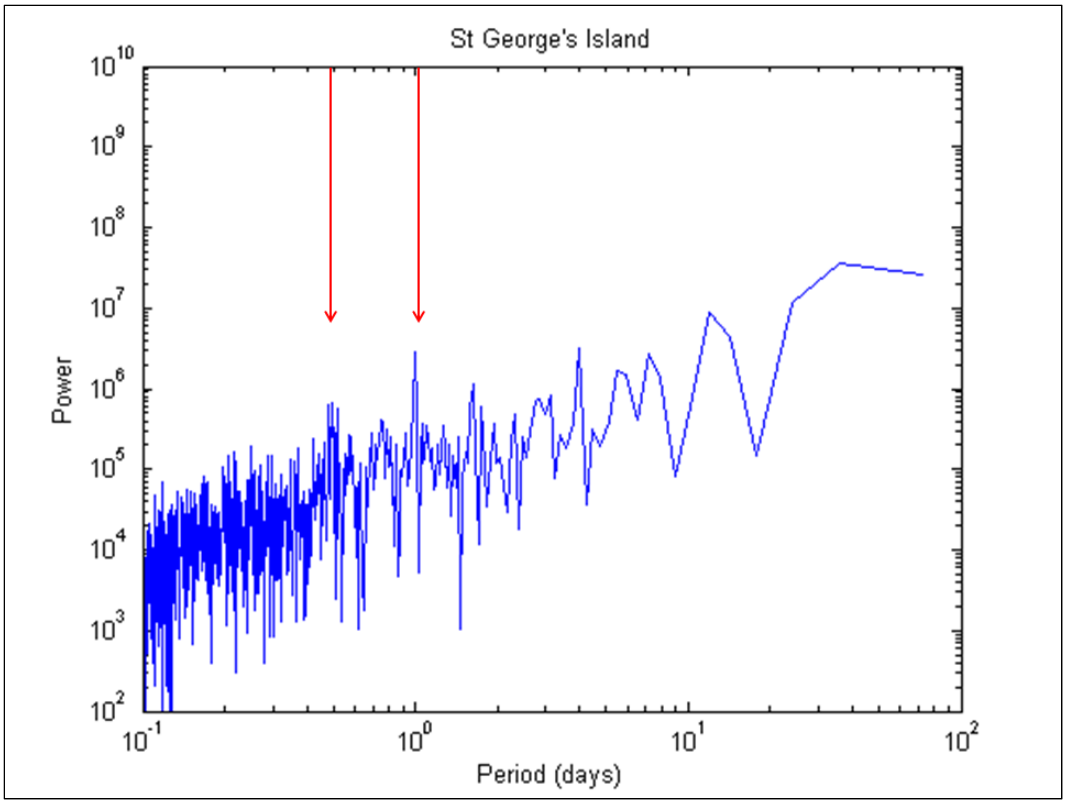

Figure 71. Power spectrum of chlorophyll observations at St. George's Island. The red arrows indicate the semi-diurnal and diurnal periods.

relative magnitude of these two peaks corresponds to the relative magnitude of the amplitudes in the harmonic analysis (Figure 69). Both observed spectra exhibit power roughly equivalent to the semi-diurnal and diurnal periods at periods of seven days or more.

The spectrum from the dissolved model (Figure 72) resembles the observations by demonstrating peaks with nearly equivalent power at the semi-diurnal and diurnal periods. As with the observations, power nearly equivalent to the semi-diurnal and diurnal periods occurs at periods greater than 10 days. The particle model (Figure 73) demonstrates its greatest power at the semi-diurnal period. Diurnal fluctuations are virtually absent. The power in both models at periods greater than 10 days is equivalent. The particle model has orders of magnitude more power than the dissolved model at high frequencies, less than 0.5 days. These high-frequency fluctuations are also present at Nomini Bay but not St. George's.

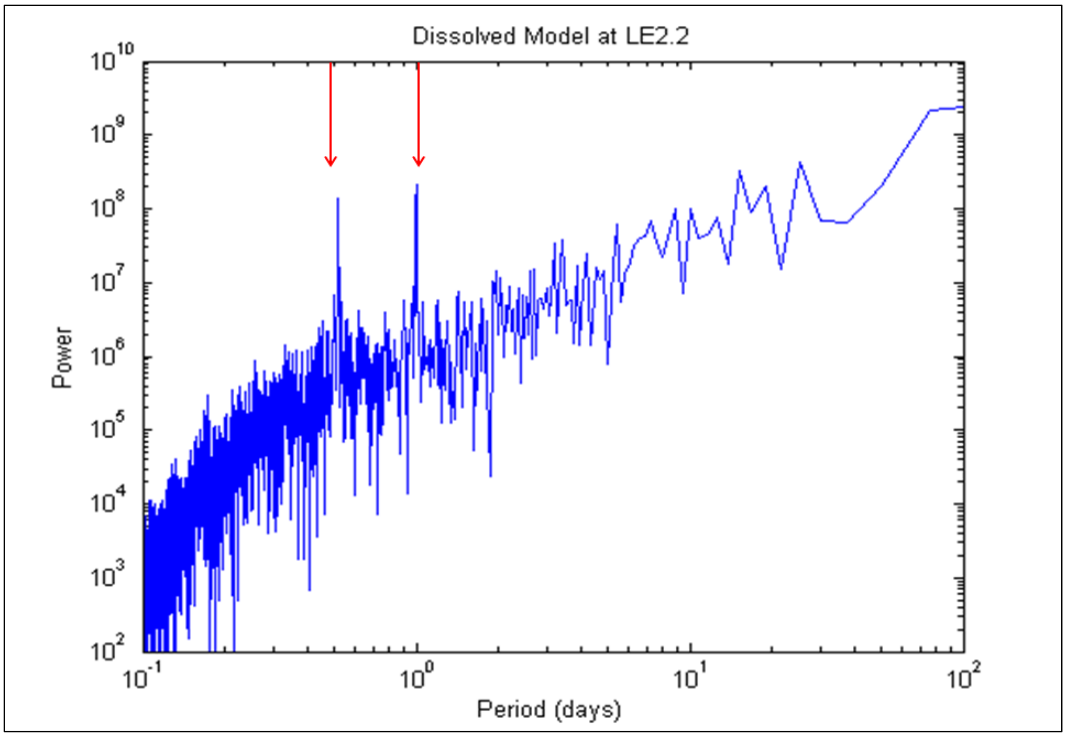

Figure 72. Power spectrum of surface chlorophyll computed at Station LE2.2 using a conventional model of algae as a dissolved substance. The red arrows indicate the semi-diurnal and diurnal periods. Note the equivalent power at these two periods.

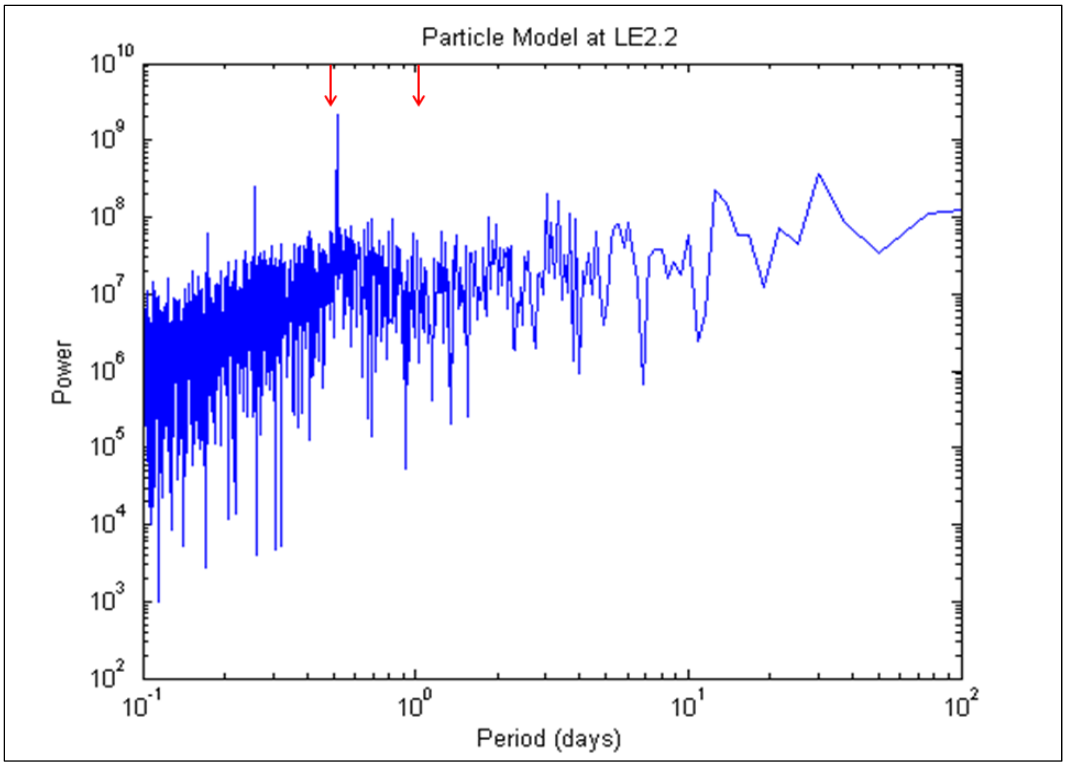

Figure 73. Power spectrum of surface chlorophyll computed at Station LE2.2 using the model of algae as particles. The red arrows indicate the semi-diurnal and diurnal periods. Note the predominance of the semi-diurnal period and the absence of power at the diurnal period.

Summary

Results from the model with algae treated as particles were compared to observations and to results from a conventional model, with algae as dissolved substance, in a variety of formats. Salient results are:

- The model with algae as particles is superior to the conventional model in two regards. The particle model computes high chlorophyll concentrations at great depths and the particle model produces a true subsurface chlorophyll maximum.
- The spatial distributions of chlorophyll computed by the two models differ. The particle model computes maximum chlorophyll at the mouth of the estuary. The conventional model computes maximum chlorophyll further upstream. Surface chlorophyll concentrations computed by the conventional model are greater than the particle model. Neither model is clearly superior with regard to reproducing the observations.
- Both models underestimate the cumulative distribution of the observations. The distribution from the conventional model is closer to the distribution from the observations, since the excess chlorophyll computed at the surface partially compensates for the absence of computed chlorophyll in deep water near the mouth of the estuary.
- The particle model exhibits high-frequency (period < 1 day) oscillations and spikes that are absent from the model with algae as dissolved substance. The oscillations and spikes are present in observations from at least one station with a database sufficient for analysis. Power spectra of observations and of computations from the dissolved model indicate significant peaks at the semi-diurnal (tidal) and diurnal (daily) periods. The power spectrum of the particle model shows its greatest power at the semi-diurnal period, indicating strong influence from tidal transport. Diurnal fluctuations, produced by the daily cycle of solar irradiance, are completely absent, however.
- Results from the particle model are “patchy” in time and space. Nearly 40% of the computations corresponding to observations are zero. The large fraction of null concentrations does not correspond to observations.
- Results from the conventional model reflect intense effort to tune the model to observations. For comparison purposes, the particle model used an identical parameter set. Improved results may be attainable with the particle model following development of a specific parameter set.

9 Algae as Particles – Sensitivity Analyses

The basic characteristics of particle transport and of algae modeled as particles have been established in preceding chapters. The present chapter examines sensitivity of particles and algae to basic particle behaviors and then investigates the potential effects of different hydrology on the previous conclusions.

Sensitivity to Particle Behavior

Chapter 1 describes a conceptual model of the Potomac River spring diatom bloom. The model proposes that algae regulate their buoyancy to maintain their residence in the central portion of the estuary. The authors perform three experiments here that initiate the investigation into the potential effects of buoyancy regulation on particle residence time and location and on chlorophyll concentration:

1. Particles rise at the rate of 1 m d^{-1}.
2. Particles sink at the rate of 1 m d^{-1}.
3. Particles sink at the rate of 1 m d^{-1} in the LE portion of the estuary and rise at the rate 1 m d^{-1} in the RET portion of the estuary.

For the examination of particle residence time and location, the kinetics rules that keep the number of particles in the system constant are disabled. Particles are free to exit the system or to adhere to the bottom. The kinetics rules remain in place for the examination of chlorophyll. The three sensitivity runs are compared to the base particle simulation and to the base run of algae as particles.

Particle residence time and location

The tracker statistics provide quantitative measures of the particle residence time and location. The initial distribution of particles (Figure 74a – 74d) is the same in all runs and as described in Chapter 6: 10,000 particles are released between km 30 and 80 on Day 45 of the model run. By Day 60, 15 days after the particle release, the run with buoyant particles indicates that particles move into the surface layer and downstream relative to the base condition with neutrally-buoyant particles (Figure 75a, 75b). The run in which particles sink (Figure 75c) and the run in which particles rise and

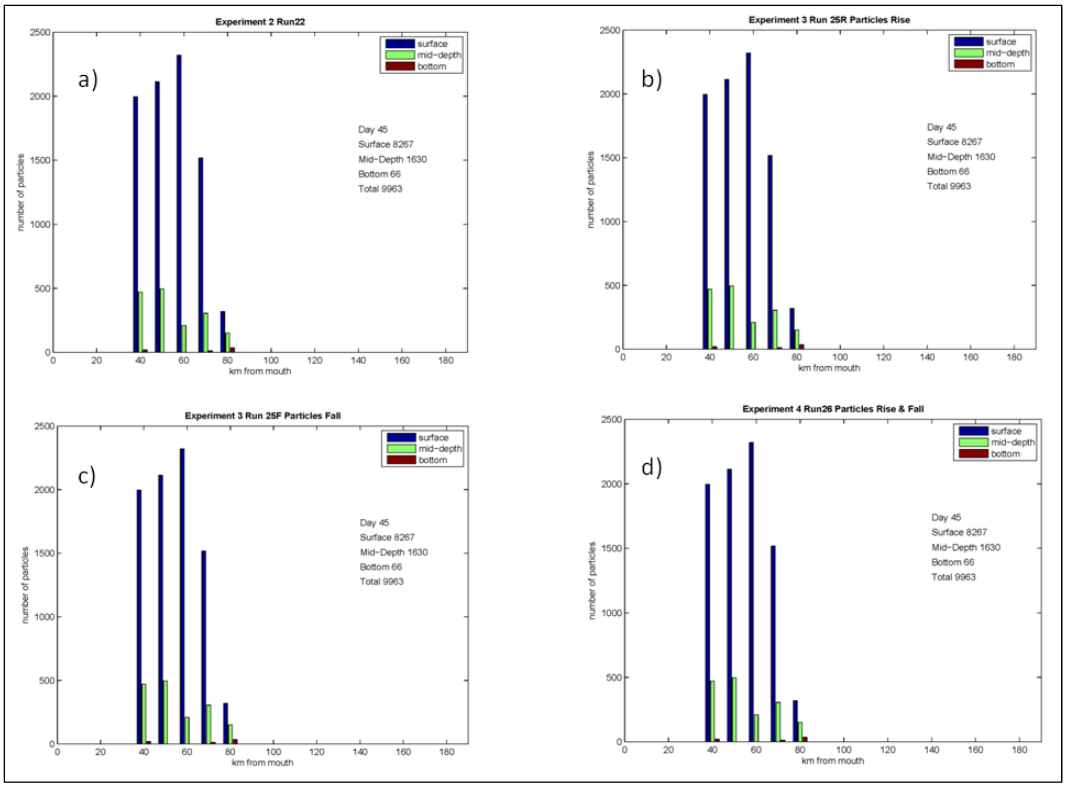

Figure 74. Initial particle distribution (Day 45) for four model runs: a) base case; b) particles rise at 1 m d^{-1}; c) particles sink at 1 m d^{-1}; and d) particles rise in RET and sink in LE.

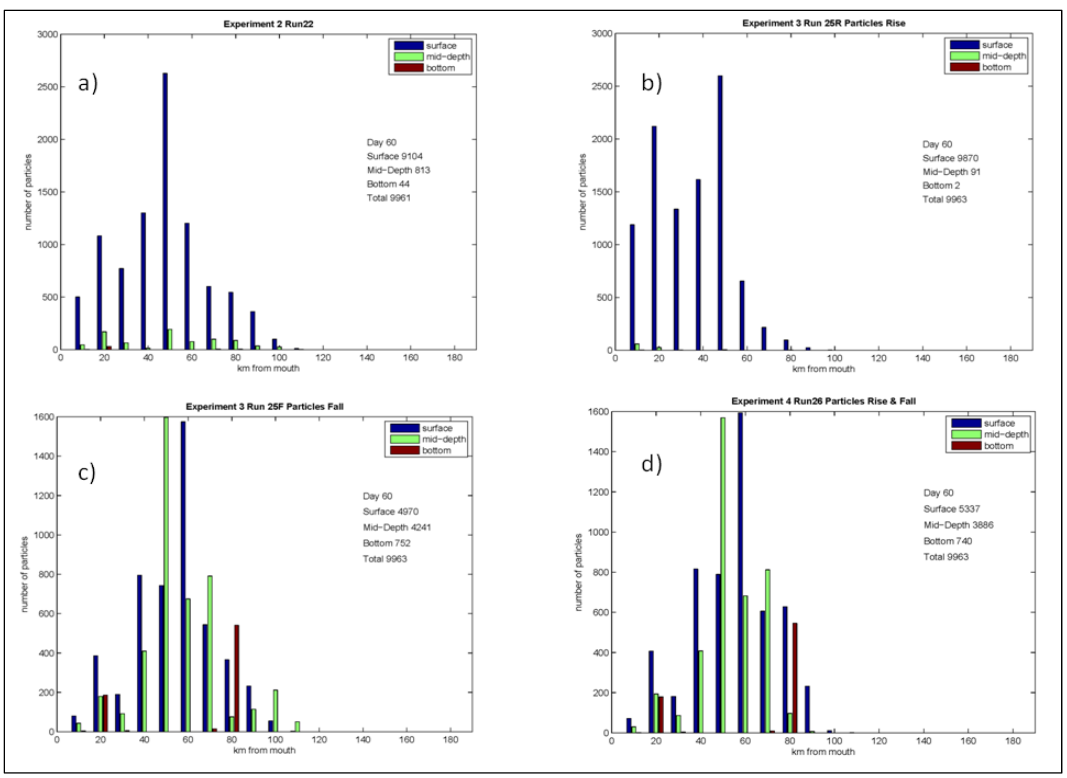

Figure 75. Particle distribution at Day 60 for four model runs: a) base case; b) particles rise at 1 m d^{-1}; c) particles sink at 1 m d^{-1}; and d) particles rise in RET and sink in LE.

sink (Figure 75d) are similar to each other. Particle concentration diminishes in the surface layer of the LE region and increases in the subsurface layers of the RET reach. The presence of particles in the subsurface layers of RET while particles are rising indicates transport upstream from the lower estuary, in keeping with the conceptual model.

By Day 150, most of the buoyant particles have left the system (Figure 76b). The remaining fraction is substantially lower than the remaining fraction of neutrally-buoyant particles, indicating a characteristic of particle buoyancy. Particles which rise tend to leave the system on the net outflowing surface currents. Few particles have left the system in the runs in which particles sink (Figure 76c) and in which particles rise and sink (Figure 76d). Instead, particles accumulate in the mid-depth and bottom of the RET reach. These runs indicate that sinking tends to increase the residence time of particles in the system.

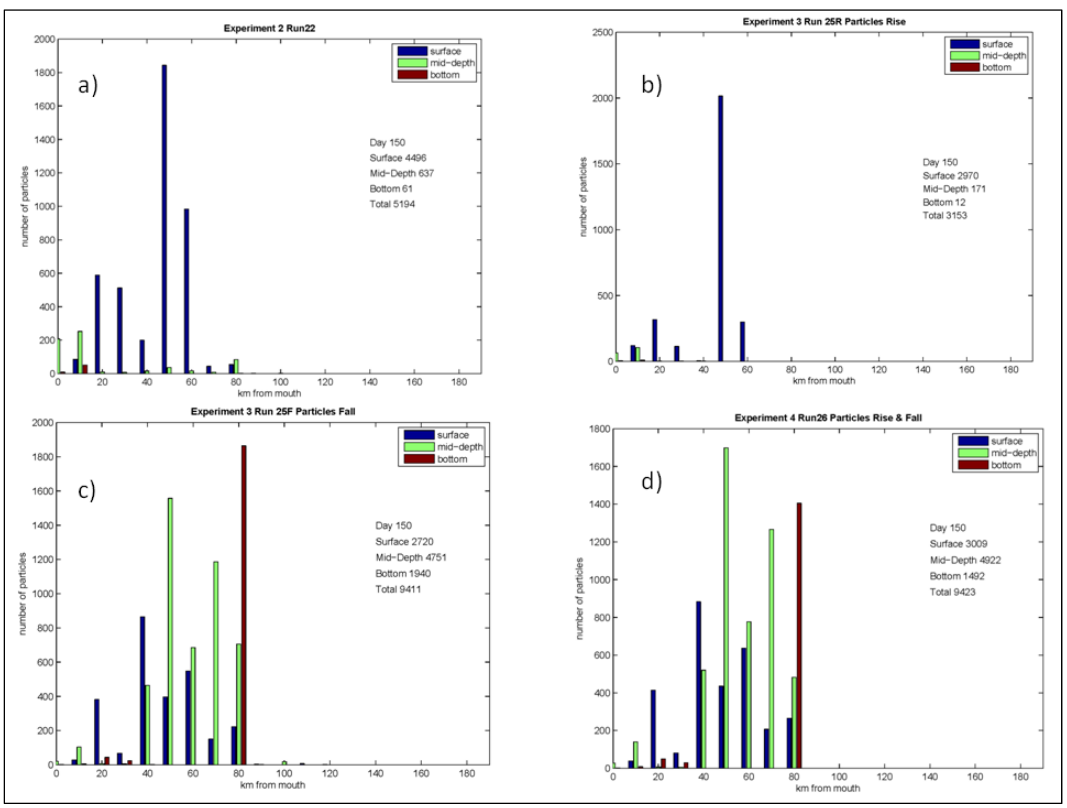

Figure 76. Particle distribution at Day 150 for four model runs: a) base case; b) particles rise at 1 m d^{-1}; c) particles sink at 1 m d^{-1}; and d) particles rise in RET and sink in LE.

The characteristics noted at Day 150 persist at the completion of the runs (Figure 77). The run with buoyant particles retains fewer particles than the run with neutrally buoyant particles. The runs in which particles sink

accumulate particles in the subsurface layers of the RET reach. The run in which particles rise and sink (Figure 76d) is not materially different from the run in which particles sink exclusively (Figure 76c). Apparently, the buoyancy is not sufficient to raise particles to the surface. The particles are effectively trapped at the bottom.

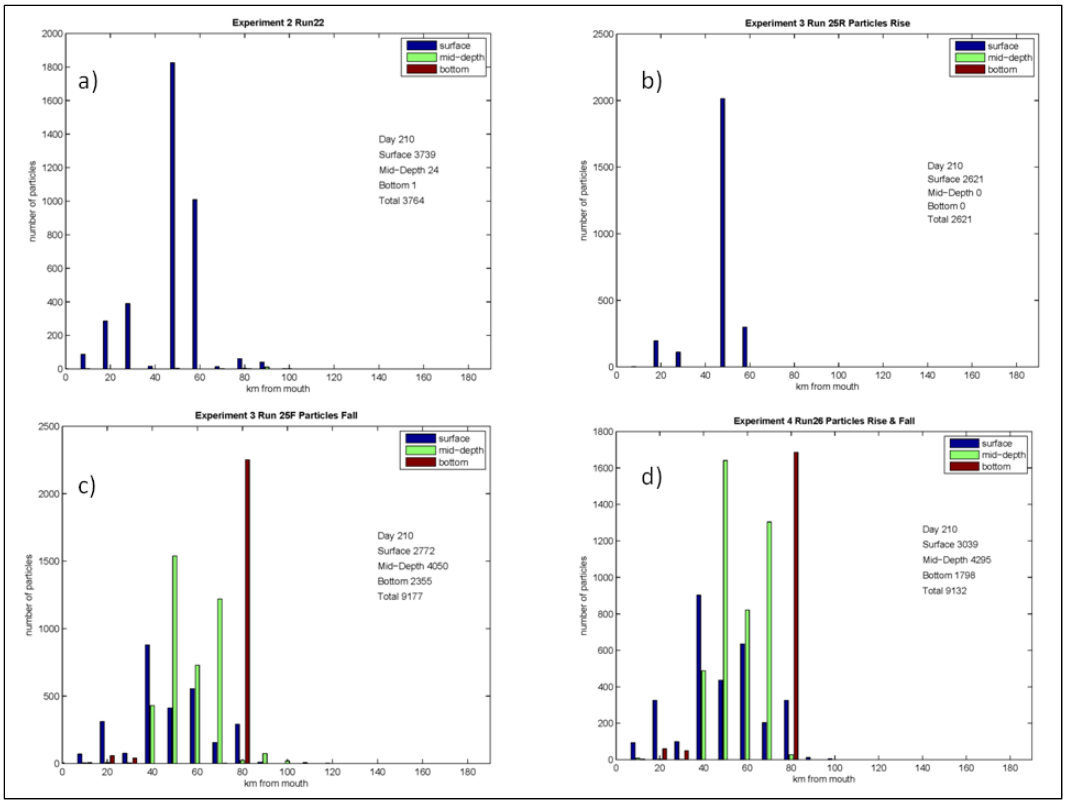

Figure 77. Particle distribution at run completion (Day 210) for four model runs: a) base case; b) particles rise at 1 m d^{-1}; c) particles sink at 1 m d^{-1}; and d) particles rise in RET and sink in LE.

Chlorophyll Concentration

Chlorophyll concentrations are examined using the seasonal-average longitudinal plots. As expected, particle buoyancy diminishes the chlorophyll concentration along the bottom in both winter (Figure 78b) and spring (Figure 80b) relative to the run with neutrally buoyant particles. Particle sinking increases the amount of chlorophyll at the bottom upstream of km 50 (Figure78 c and d, Figure 80 c and d). The run in which particles sink exclusively increases bottom chlorophyll concentration upstream as far as km 100. The run with rising and sinking demonstrates the influence of buoyancy at the head of the algal bloom, circa km 80 to 100. Algae in this reach apparently rise to the surface. No run matches the elevated observed chlorophyll concentrations in the lower 40 km of the estuary.

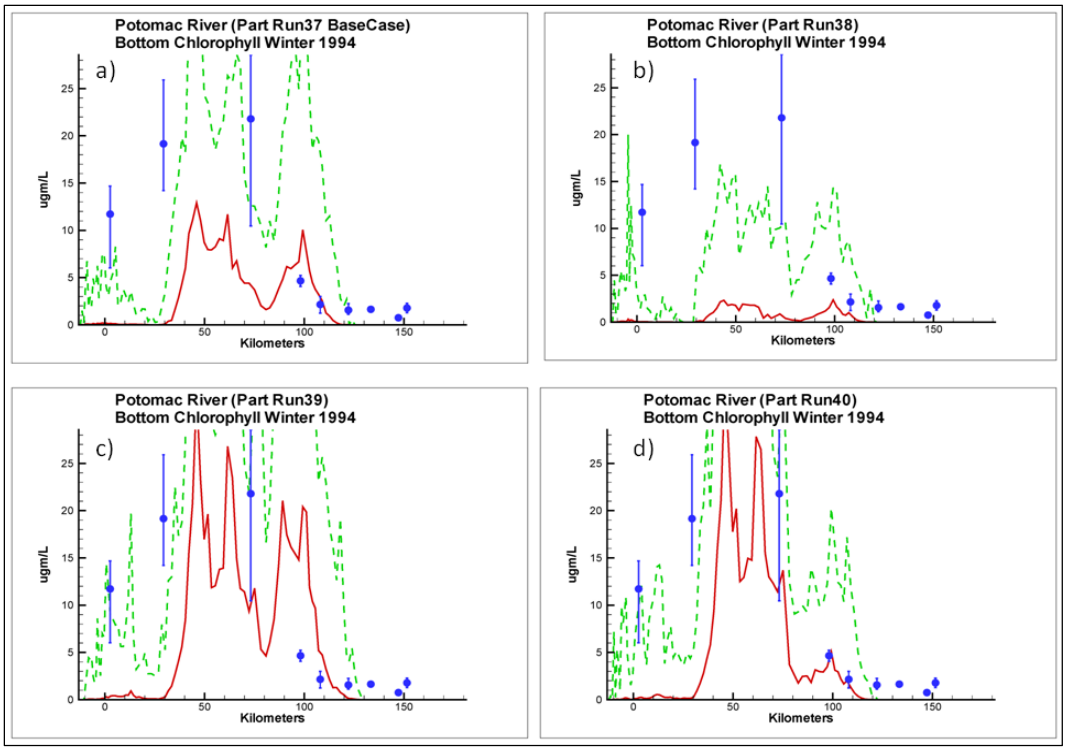

Figure 78. Observed and computed winter, bottom, chlorophyll concentrations for four model runs: a) base case; b) particles rise at 1 m d^{-1}; c) particles sink at 1 m d^{-1}; and d) particles rise in RET and sink in LE.

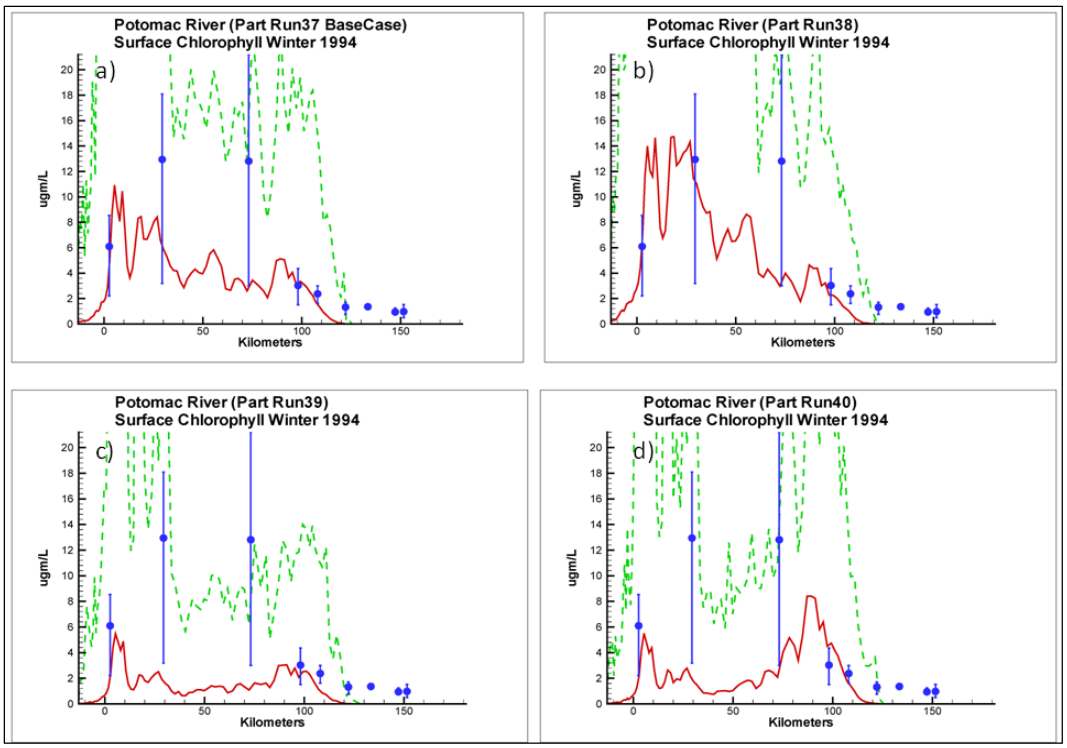

Figure 79. Observed and computed winter, surface, chlorophyll concentrations for four model runs: a) base case; b) particles rise at 1 m d^{-1}; c) particles sink at 1 m d^{-1}; and d) particles rise in RET and sink in LE.

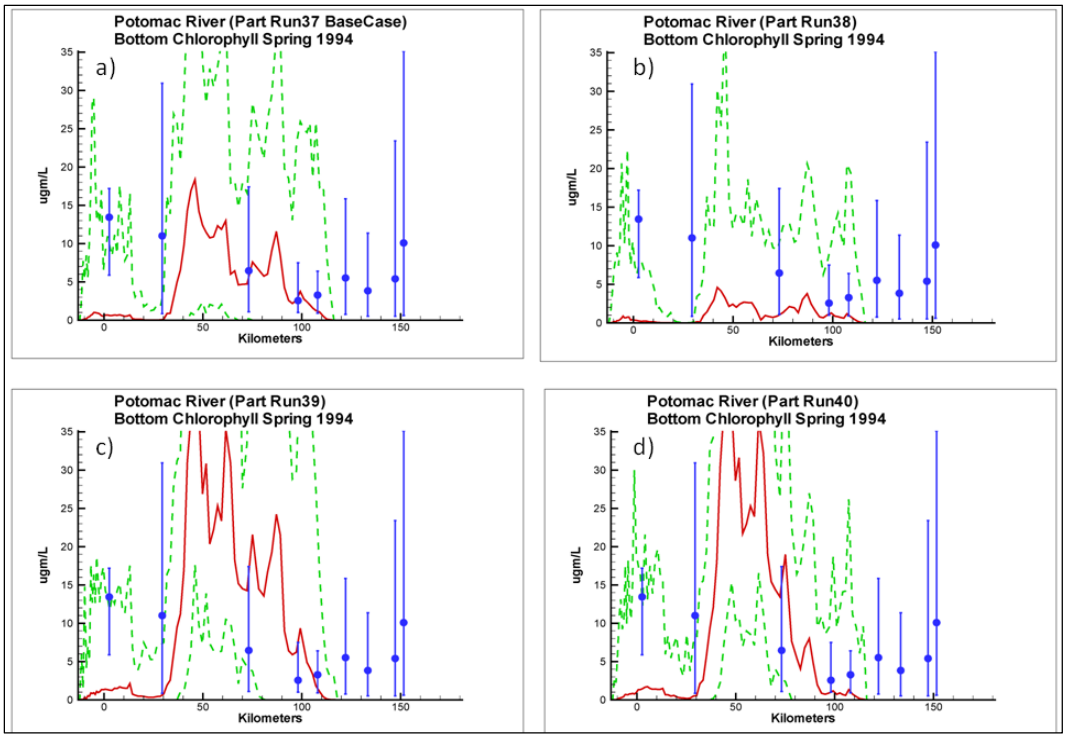

Figure 80. Observed and computed spring, bottom, chlorophyll concentrations for four model runs: a) base case; b) particles rise at 1 m d^{-1}; c) particles sink at 1 m d^{-1}; and d) particles rise in RET and sink in LE.

The run with buoyant particles provides superior surface chlorophyll computations in winter (Figure 79b) and computations equivalent to the neutrally buoyant run in spring (Figure 81b). At the surface, the run in which particles sink exclusively provides the least satisfactory observations (Figures 79c, 81c). The run in which particles rise and sink provides a surface chlorophyll peak circa km 90 and partially validates the conceptual model, especially during winter (Figure 79d), although elsewhere this model shares the unsatisfactory properties of the run in which particles sink exclusively.

Chlorophyll Distribution Plot

The distributions of chlorophyll computed by the base model, the model in which particles sink, and the model in which particles rise and sink are virtually congruent through 75% of their distributions (Figure 82). The chlorophyll distribution in the run with buoyant particles is lower than the others through 90% of its distribution. The differences in the distributions are primarily in the extreme values. The run in which particles sink exclusively provides the larger portion of extreme values, indicating the effects of particle accumulation in a few patches. The chlorophyll distributions from all runs are characteristically less than the observations.

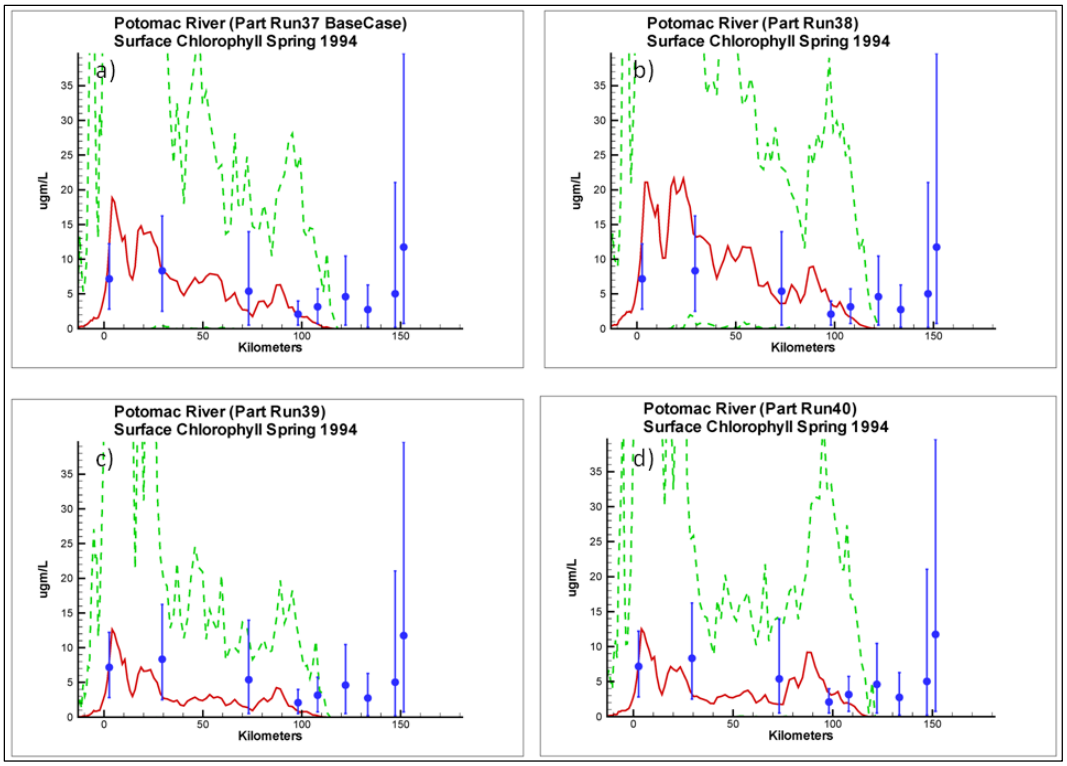

Figure 81. Observed and computed spring, surface, chlorophyll concentrations for four model runs: a) base case; b) particles rise at 1 m d^{-1}; c) particles sink at 1 m d^{-1}; and d) particles rise in RET and sink in LE.

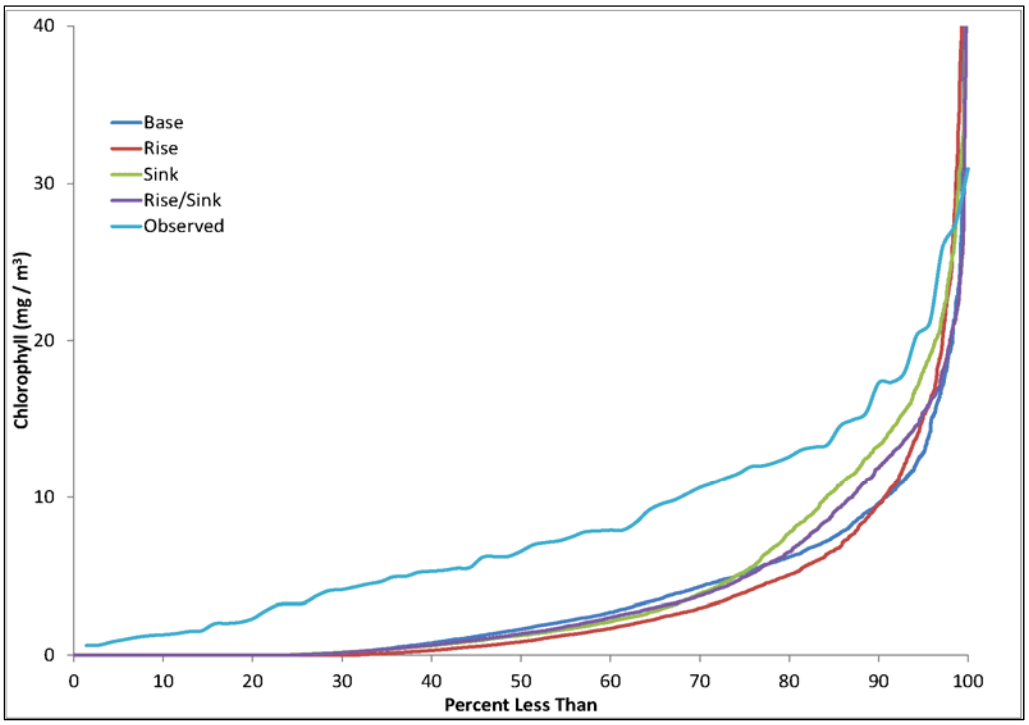

Figure 82. Cumulative distribution plot of observed and computed chlorophyll concentration at all depths and stations. Computed results from four model runs: base case; particles rise at 1 m d^{-1}; particles sink at 1 m d^{-1}; and particles rise in RET and sink in LE.

Sensitivity to Hydrology

The year 1994 selected for the base runs is a year of average hydrology in the Chesapeake Bay system and of above-average runoff in the Potomac River. The year 1999 is, by contrast, a dry year in both the Chesapeake Bay system and in the Potomac. Average flow at the Potomac fall line for the period November 1998 through May 1999 is 208 $m^3 s^{-1}$, compared to 802 $m^3 s^{-1}$ for the period November 1993 through May 1994. The 1999 period lacks the number of flood events and the peak flows present in 1994 (Figure 83). To test the sensitivity of model results to hydrology, the model of algae as particles was run for the period November 1998 through May 1999, using the same initial conditions and parameter set as the base run. The tracker statistics indicate the effects of the dry hydrology as early as 15 days after the particle release (Figure 84b, f). More particles penetrate further upstream in 1999 than in 1994. This characteristic persists through the remainder of the run. The dry year shows more particles upstream of km 60 than the wet year. Since the number of particles is constant, the wet year has more particles in the downstream portion of the estuary than the dry year. The change in spatial distribution of particles is entirely consistent with the relative magnitudes of the net flows in the two years.

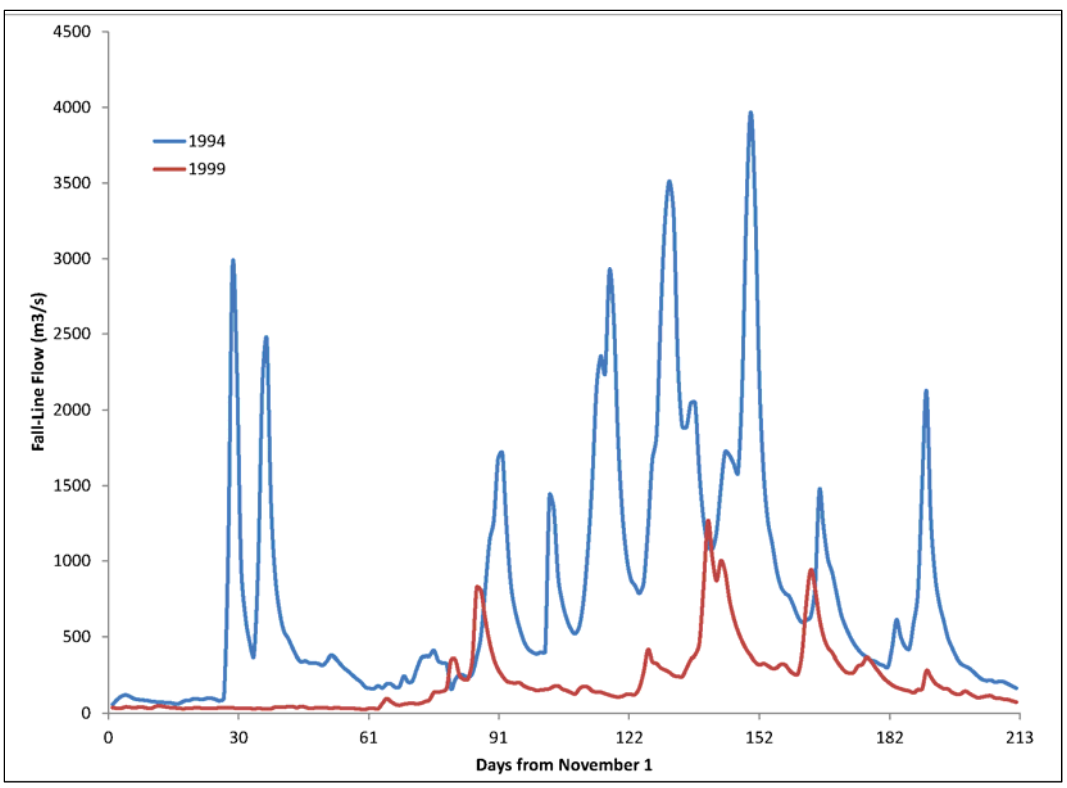

Figure 83. Fall-line flow in the Potomac River for dry (1999) versus wet (1994) hydrologic conditions.

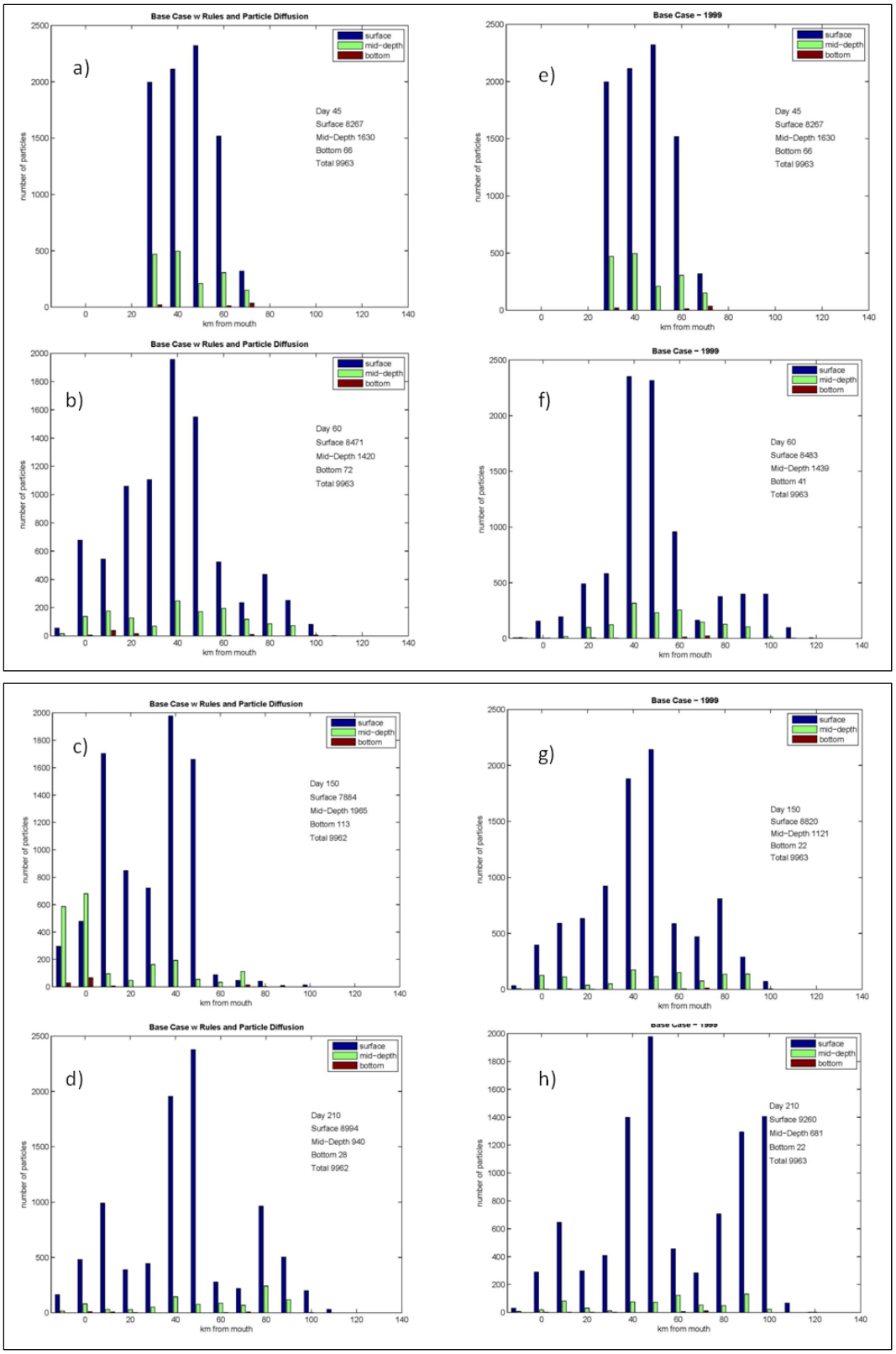

Figure 84. Particle distribution computed for dry hydrology (1999) versus base (1994) conditions. Base conditions are in the left column (panels a - d). The dry conditions are in the right column (panels e - h).

The periodic behavior and the vertical distributions of computed chlorophyll are similar in the two years (Figure 85). Both runs demonstrate high-frequency oscillations and both runs reflect the magnitude of observed surface chlorophyll while underestimating the observed chlorophyll in the deep waters of the lower estuary. A large algal bloom occurred in April 1999 (0.5 years from model commencement) that is not represented in the simulation.

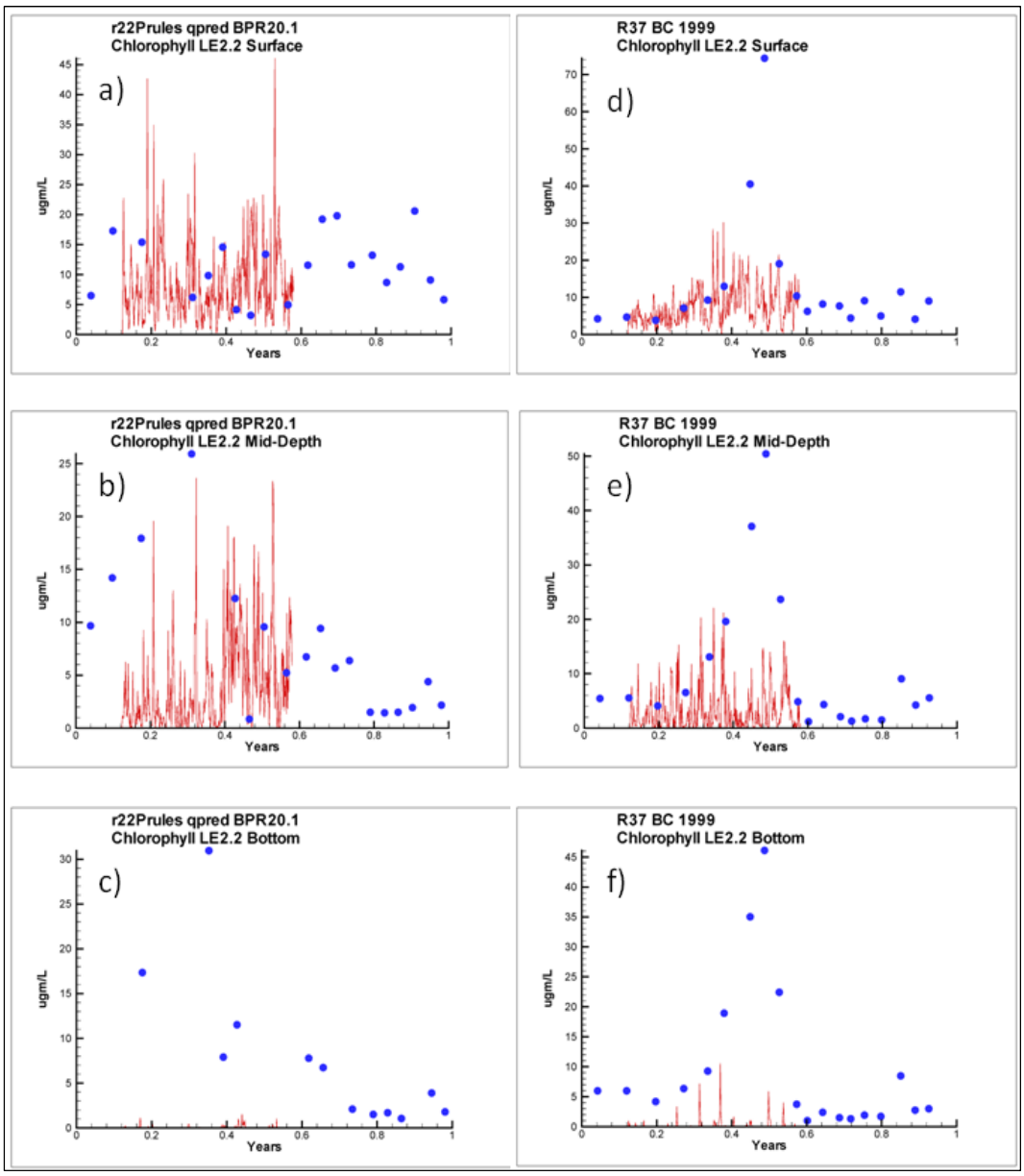

Figure 85. Observed and computed chlorophyll at LE2.2 for three depths (surface, mid-depth, bottom) and two hydrologic conditions: 1994, wet (panels a - c) and 1999, dry (panels d - f).

Despite the difference in hydrology, the computed spatial chlorophyll distributions are similar in the two years (Figure 86). Computed chlorophyll in the bottom is restricted to the reach between km 30 and km 110. No bottom chlorophyll is computed in the lower 30 km of the estuary despite the high concentrations observed. The computed surface chlorophyll is shifted farther downstream in spring 1994 compared to 1999, perhaps driven by the higher runoff. Magnitudes of computed surface chlorophyll are similar in the two years, however. Model results in both years match the surface observations with the exception of the bloom event centered at km 30 during 1999.

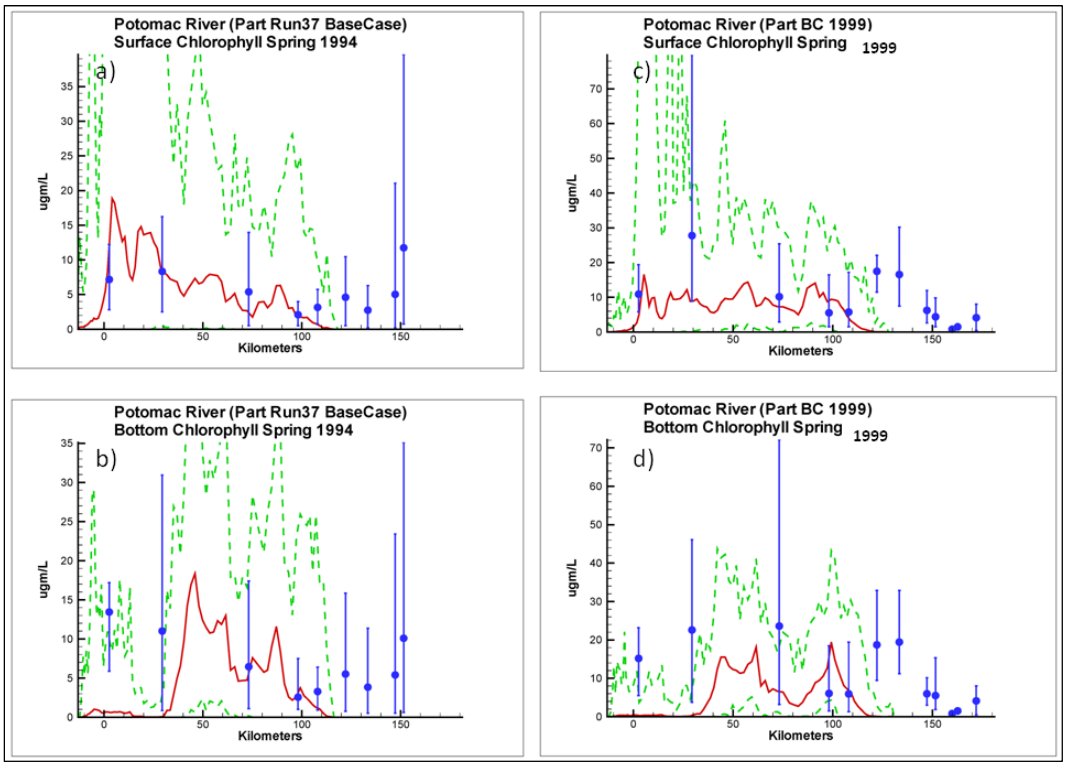

Figure 86. Observed and computed spring chlorophyll concentrations for two hydrologic conditions: 1994, wet (panels a, b) and 1999, dry (panels c, d).

Comparisons of observed and computed chlorophyll distributions in 1999 (Figure 87) resemble the comparisons from 1994 (Figure 63). The computed distribution is less than observed and demonstrates a substantial fraction of zero values which are not present in the observations. The chlorophyll results from 1999 indicate the model characteristics demonstrated in the base run can be generalized across varying hydrologic conditions. The large alteration in hydrology from 1994 to 1999 induced no aberrant behavior in the model and the model is suitable for further investigation and application.

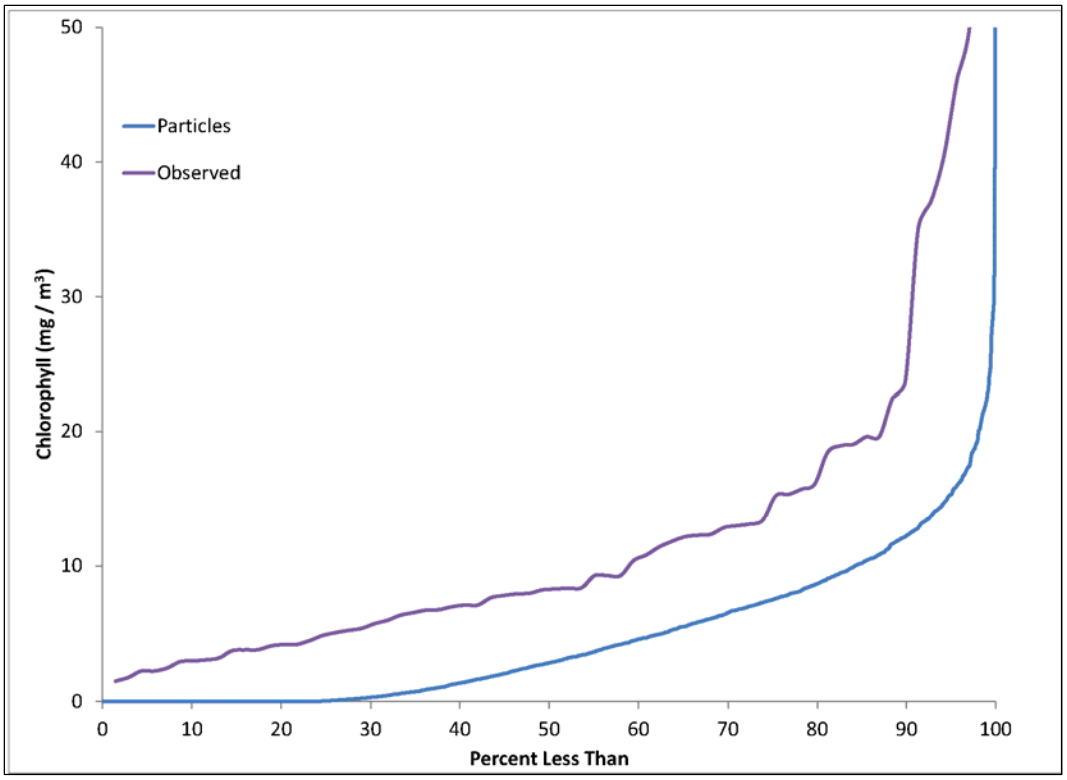

Figure 87. Cumulative distribution plot of observed and computed chlorophyll concentration at all depths and stations for 1999.

10 Summary and Conclusions

Introduction

Reliable prediction of phytoplankton transport and production is central to the understanding and remediation of a host of environmental problems, including eutrophication and the occurrence of harmful algal blooms. Quantitative phytoplankton models have existed for decades, yet virtually all examples are based on the original framework wherein phytoplankton are a dissolved substance transported passively and exclusively by hydrodynamic processes. Herein, the authors test the hypothesis that phytoplankton dynamics (particularly the occurrence of blooms) can be more accurately predicted by treating phytoplankton as discrete particles capable of self-induced transport via buoyancy regulation or other behaviors.

ICM Particle Tracking

The transport of discrete particles is accommodated through development of a particle-tracking algorithm which works within the CE-QUAL-ICM eutrophication model. Incorporation of the algorithm into ICM is necessary in order for particles to respond to environmental cues computed by the eutrophication model. The calculations are performed within the physical plane through the application of general algebra, geometry, and physics. The effects of turbulent diffusion and dispersion are translated into random displacement in the particle model. The random displacement is added to the deterministic location derived from advection. As a first approach, spatially uniform diffusion and dispersion are considered.

Phytoplankton Kinetics

Algae are quantified as biomass (carbon) per particle. The number of particles in the system is constant. Changes in algal biomass are represented by altering the biomass attached to a particle rather than by changing the number of particles. The particle-based kinetics are derived from phytoplankton kinetics in the CE-QUAL-ICM eutrophication model.

The rate of change in biomass attached to a particle is determined by the environment surrounding the particle; e.g., light and temperature. The rate of change also influences the environment; e.g., ambient nutrient

concentration. A means is necessary to translate from the particle-based system to the continuum. The approach employed here takes advantage of the discrete computational grid employed by the ICM eutrophication model. The particles are arrayed in a computational structure that labels each particle with its current grid cell. The structure and labeling allow the computer code to loop over all particles or over all cells. The code can query particles "What cell am I in?" or it can query cells "What particles do I contain?" The revised ICM code with particle-based kinetics employs the algal subroutine from the conventional ICM code to provide the particle environment, compute growth and loss rates, and to provide interactions with quantities computed in the continuum such as nutrient concentration.

Particle-tracking models conventionally incorporate rules for particle behavior. Rules are especially common for determining particle behavior when the trajectory takes a particle outside the model domain. Three rules are enforced that keep the number of particles in the system constant and ensure that each particle is associated with viable algal biomass. Particles that exit through an open boundary, that adhere to the bottom, or that contain no viable algae are eliminated and replaced by splitting the particle containing the largest algal biomass in two.

The Potomac River Estuary

The Potomac River Estuary is a major sub-estuary of the larger Chesapeake Bay system. The estuary extends 190 km from the junction with Chesapeake Bay to the head of tide at Washington DC. Mean tide range near the mouth is 0.38 m and is 0.84 m at Washington DC. The estuary is a drowned river valley and the saline portion is weakly stratified. The primary freshwater source is from the 29,940 km^2 upland watershed and enters at the head of tide. Lesser volumes enter the estuary from the adjacent watershed below the head of tide. Long-term mean runoff at Washington DC is 339 $m^3 s^{-1}$. This long-term mean is subject to regular seasonal fluctuations as well as extremes due to flood and drought.

The particle-tracking model is inserted into the Chesapeake Bay Environmental Model Package (CBEMP). The CBEMP consists of three independent models: a watershed model (WSM), a hydrodynamic model (HM), and a eutrophication model (WQM). The WSM provides distributed flows to the HM and nutrient and solids loads to the WQM. The HM computes three-dimensional intra-tidal transport and supplies transport parameters to the WQM on an hourly basis. The WQM computes algal

biomass, nutrient cycling, and dissolved oxygen, as well as numerous additional constituents and processes.

Both the HM and WQM operate on a three-dimensional grid which encompasses the entire Chesapeake Bay system. For this study, the Potomac River portion of the grid was extracted along with the associated hydrodynamics. An adjacent portion of Chesapeake Bay was included so that downstream boundary conditions could be specified at a distance sufficient to minimize influence on the upstream portions of the system. The resulting grid extended the 190 km length of the Potomac River estuary and incorporated numerous embayments and tributaries. The extracted model was checked against the original model and against data to ensure that the extraction was performed correctly. This model version was used as a starting point for the particle-tracking algorithms and associated algal kinetics.

Basic Particle Simulation

The basic particle simulation was determined following a variety of numerical experiments and sensitivity runs. The base simulation extends from November 1, 1993 through May 31, 1994. The duration is selected to encompass the spring algal bloom period. The year 1994 corresponds to an average hydrologic year selected for analysis of Chesapeake Bay model results, although flows in the Potomac during the interval are above-average. Ten-thousand particles are released 45 days into the run and are spaced uniformly from top-to-bottom in the channel of the river between km 30 and 80. Particles are distributed in model grid cells with the number in each cell specified to yield 4×10^{-6} particles m^{-3}. The release timing and region correspond to the typical appearance date and expanse of bloom algae.

The experiments with particle tracking indicate that particle transport is fundamentally different than transport of a dissolved substance. In particular, the residence time of particles released in the center of the Potomac Estuary is longer than the residence time of a comparable release of dissolved substance. Ninety days after the release, 65% of the particles remain in the model domain while the dissolved substance has disappeared. A second distinction is in the “patchy” distribution of particles compared to the continuous distribution of dissolved substance.

Algae as Particles – Spatial and Temporal Distribution

The base model run with algae as particles accompanies the basic particle simulation. Each particle is initiated with 2.5 x 10^5 g algal carbon, yielding 1.0 g C m^{-3} at initiation of the simulation. Parameters for the algal kinetics are drawn from the spring diatom group of the CBEMP. These values are employed to provide comparison to algae as simulated in conventional models. No attempt is made, at this stage of development, to optimize the performance of the model with algae as particles.

A conventional model run was completed to provide comparison with the particle approach. Algae were initiated at a concentration of 1.0 g C m^{-3} at the same time and in the same extent of the Potomac River as the particle release. Concentration boundary conditions at the open ends of the model domain were specified as zero. Kinetics parameters were identical to the particle simulation with one exception. The conventional run employed an algal settling velocity, as in the Chesapeake Bay model. Settling was omitted from the base particle simulation.

Particle model results rendered as elevation views along the river transect demonstrate a heterogeneous spatial distribution, which manifests immediately upon release of the particles. Chlorophyll concentrations near the bottom commonly exceed concentrations at lesser depths above. The surface layer, which receives the greatest illumination, is at times devoid of algae. Chlorophyll concentrations computed in the conventional model are much more smoothly distributed. Soon after bloom initiation, there is an indication of a subsurface chlorophyll maximum caused by upstream advection of the initial uniform chlorophyll distribution. Otherwise, the vertical chlorophyll distribution declines monotonically from the illuminated surface waters to the bottom. No surface cells within the bloom region are devoid of algae.

Surface chlorophyll concentrations computed by the particle model follow the heterogeneous pattern observed in the elevation views. Chlorophyll penetrates into the smallest tributaries and, by the end of the simulation, the highest concentrations are in the tributaries rather than in the surface waters of the mainstem Potomac. The conventional model provides more uniform surface chlorophyll distributions. At the end of the simulation, chlorophyll concentrations in the mainstem are as high, or higher, than in the tributaries. The contrast between the uniform surface distribution in

the conventional model and the patchy distribution in the particle model is striking.

Algae as Particles – Comparisons with Observations

Results from the model with algae treated as particles were compared to observations and to results from a conventional model, with algae as dissolved substance, in a variety of formats. Salient results are the following:

- The model with algae as particles is superior to the conventional model in two regards. The particle model computes high chlorophyll concentrations at great depths and the particle model produces a true subsurface chlorophyll maximum.
- The spatial distributions of chlorophyll computed by the two models differ. Neither model is clearly superior with regard to reproducing the observations.
- The particle model exhibits high-frequency (period < 1 day) oscillations and spikes that are absent from the model with algae as dissolved substance. The oscillations and spikes are present in observations from at least one station with a database sufficient for analysis. The power spectrum of the particle model shows its greatest power at the semi-diurnal period, indicating strong influence from tidal transport. Diurnal fluctuations, produced by the daily cycle of solar irradiance, are completely absent, however.
- Results from the particle model are "patchy" in time and space. Nearly 40% of the computations corresponding to observations are zero. The large fraction of null concentrations does not correspond to observations.

Algae as Particles – Sensitivity Analyses

Two sensitivity analyses were performed. The first examined the sensitivity of particle location and computed chlorophyll to basic particle behaviors. The second examined sensitivity of particle location and computed chlorophyll to hydrology.

The authors performed three experiments that initiated the investigation into the potential effects of buoyancy regulation on particle residence time and location and on chlorophyll concentration:

1. Particles rise at the rate of 1 m d^{-1}.

2. Particles sink at the rate of 1 m d^{-1}.
3. Particles sink at the rate of 1 m d^{-1} in the LE portion of the estuary and rise at the rate 1 m d^{-1} in the RET portion of the estuary.

Buoyant (rising) particles were rapidly carried out of the estuary by surface currents. Few particles left the system in the runs in which particles sink and in which particles rise and sink. Instead particles accumulated in the mid-depth and bottom of the RET reach. These runs indicated that sinking tends to increase the residence time of particles in the system.

Chlorophyll concentrations were examined by seasonally averaging computations along the longitudinal axis of the river. Particle buoyancy diminished the chlorophyll concentration along the bottom in both winter and spring relative to the base run with neutrally buoyant particles. The run with buoyant particles provided superior surface chlorophyll computations in winter and computations equivalent to the neutrallybuoyant run in spring. The run in which particles rise and sink provided a surface chlorophyll peak 90 upstream from the river mouth and partially validated the conceptual model of algal blooms that prompted this study. Elsewhere, however, results from the run in which algae rise and sink were unsatisfactory.

The year 1994, which was selected for the base runs, is a year of average hydrology in the Chesapeake Bay system and of above-average runoff in the Potomac River. The year 1999 is, by contrast, a dry year in the Chesapeake Bay system. Average flow at the Potomac fall line for the period November 1998 through May 1999 is 208 m^3 s^{-1}, compared to 802 m^3 s^{-1} for the period November 1993 through May 1994. To test the sensitivity of model results to hydrology, the model of algae as particles was run for the period November 1998 through May 1999, using the same initial conditions and parameter set as the base run.

Results from the dry year showed more particles upstream of km 60 than the wet year, while the wet year had more particles in the downstream portion of the estuary than the dry year. The change in spatial distribution of particles was entirely consistent with the relative magnitudes of the net flows in the two years. Chlorophyll results from the two years were similar. Both runs demonstrated similar periodic behavior, similar spatial distributions, and similar comparisons to observations. The large alteration in hydrology, from 1994 to 1999, induced no aberrant behavior in the model

and confirmed that the model is suitable for further investigation and application.

Conclusions

The characteristics and applicability of the particle approach to modeling algal blooms are now established. The particle approach yields results that differ distinctly from a conventional model of algae as a dissolved substance. Several aspects of the particle approach are superior to the conventional approach. In particular, the particle approach reproduces elevated chlorophyll concentrations observed at great depths in the Potomac River. The particle approach is not clearly superior to the conventional approach in reproducing the population of chlorophyll observations. Results from the conventional model reflect intense effort to tune the model to observations. For comparison purposes, the particle model used an identical parameter set. Improved results may be expected from the particle model following development of a specific parameter set. Now that the particle model has been formulated, explored, and documented, dedicated applications to blooms in the Potomac River and elsewhere are recommended.

References

Cerco, C., and T. Cole. 1993. Three-dimensional eutrophication model of Chesapeake Bay. *Journal of Environmental Engineering* 119(6): 1006-1025.

Cerco, C. 2000. Phytoplankton kinetics in the Chesapeake Bay model. *Water Quality and Ecosystem Modeling* 1:5-49.

Cerco, C., and M. Noel. 2004. Process-based primary production modeling in Chesapeake Bay. *Marine Ecology Progress Series* 282: 45-58.

Cerco, C., S-C Kim, and M. Noel, 2010. *The 2010 Chesapeake Bay eutrophication model.* A Report to the US Environmental Protection Agency Chesapeake Bay Program and to the US Army Engineer Baltimore District. http://www.chesapeakebay.net/publication.aspx?publicationid=55318

Cerco, C., and M. Noel. 2012. Twenty-one year simulation of Chesapeake Bay water quality using the CE-QUAL-ICM eutrophication model. *Journal of the American Water Resources Association*. In press.

Chapman, R., T. Gerald, and M. Dortch. 1994. *New York Bight study report 3: Three-dimensional particle tracking model for floatables and dissolved and suspended materials*. Technical Report CERC-94-4. Vicksburg MS: US Army Corps of Engineers Waterways Experiment Station.

Chesapeake Bay Program. 2012a. CBP Water Quality Database (1984 to present). http://www.chesapeakebay.net/data/downloads/cbp_water_quality_database_1984_present

Chesapeake Bay Program. 2012b. Baywide CBP Plankton Database. http://www.chesapeakebay.net/data/downloads/baywide_cbp_plankton_database

DiToro, D., D. O'Connor, and R. Thomann. 1971. A dynamic model of the phytoplankton population in the Sacramento-San Joaquin Delta. *Advances in Chemistry Series 106*, Washington DC: American Chemical Society 131-180.

Elliott, A. 1978. Observations of the meteorologically induced circulation in the Potomac River estuary. *Estuarine and Coastal Marine Science* 6:285-299.

Fennel, K., and T. Neumann. 1996. The mesoscale variability of nutrients and plankton as seen in a coupled model. *German Journal of Hydrography* 48:55-62.

Grieco, L., L.-B. Tremblay, and E. Zambianchi. 2005. A hybrid approach to transport processes in the Gulf of Naples: An application to phytoplankton and zooplankton population dynamics. *Continental Shelf Research* 25:711-728.

Hellweger, F., E. Kravchuk, V. Novotny, and M. Gladyshev. 2008. Agent-based modeling of the complex life cycle of a cyanobacterium (*Anabena*) in a shallow reservoir. *Limnology and Oceanography* 53(4):1227-1241.

Hellweger, F, and V. Bucci. 2009. A bunch of tiny individuals – Individual-based modeling for microbes. *Ecological Modeling* 220:8-22.

Johnson, B., K. Kim, R. Heath, B. Hsieh, and L. Butler. 1993. Validation of a three-dimensional hydrodynamic model of Chesapeake Bay. *Journal of Hydraulic Engineering* 199(1):2-10.

Kim, S-C. 2012. Evaluation of a three-dimensional hydrodynamic model applied to Chesapeake Bay through long-term simulation of transport processes. *Journal of the American Water Resources Association*. In review.

Kremer, J., and S. Nixon. 1978. *A coastal marine ecosystem*. Berlin-Heidelberg: Springer-Verlag.

Lanerolle, L., M. Tomlinson, T. Gross, F. Aikman, R. Stumpf, G. Kirkpatrick, and B. Pederson. 2006. Numerical investigation of the effects of upwelling on harmful algal blooms off the west coast of Florida. *Estuarine Coastal and Shelf Science* 70:599-612.

Maryland Department of Natural Resources. 2012. Eyes on the Bay. http://mddnr.chesapeakebay.net/eyesonthebay/index.cfm

Mathworks Inc., 2012. Fourier Analysis and Filtering. http://www.mathworks.com/help/matlab/fourier-analysis-and-filtering.html

Moll, A., and G. Radach. 2003. Review of three-dimensional ecological modeling related to the North Sea shelf system, Part I: Models and their results. *Progress in Oceanography* 57:175-217.

Pritchard, D. W. 1955. Estuarine circulation patterns. *Proceedings of the American Society of Civil Engineers* 81(717):1 – 11

Riley, G. 1946. Factors controlling phytoplankton populations on Georges Bank. *Journal of Marine Research* 6:54-73.

Ross, O., and J. Sharples. 2004. Recipe for 1-D Lagrangian particle tracking models in space-varying diffusivity. *Limnology and Oceanography: Methods* 2:289-302.

Shenk, G., and L. Linker. 2012. Development and application of the 2010 Chesapeake TMDL watershed model. *Journal of the American Water Resources Association*. In review.

Steele, J. 1974. Simulation of a plankton ecosystem. *The structure of marine ecosystems*. Cambridge: Harvard University, 58-73.

Thomann, R., and J. Fitzpartick. 1982. *Calibration and verification of a mathematical model of the eutrophication of the Potomac River estuary*. Contract No. ES-80-6. Mahwah NJ: HydroQual Inc.

Tyler, M., and H. Seliger. 1978. Annual subsurface transport of a red tide dinoflagellate to its bloom area: Water circulation patterns and organism distributions in Chesapeake Bay. *Limnology and Oceanography* 23(2):227-246.

Virginia Institute of Marine Science. 2012. VECOS: Virginia Estuarine and Coastal Observing System. http://www3.vims.edu/vecos/Default.aspx

Woods, J. 2005. The Lagrangian ensemble metamodel for simulating plankton ecosystems. *Progress in Oceanography* 67: 84-159.

Zheng, C., and G. Bennett. (2006a). Lecture 33, Particle Tracking Theory. http://jan.ucc.nau.edu/doetqp/courses/env303a/lec33/lec33.htm (last accessed June 2012).

Zheng, C., and G. Bennett. (2006b). Lecture 34, Particle Tracking Solutions. http://jan.ucc.nau.edu/doetqp/courses/env303a/lec34/lec34.htm (last accessed June 2012).

REPORT DOCUMENTATION PAGE

Form Approved
OMB No. 0704-0188

Public reporting burden for this collection of information is estimated to average 1 hour per response, including the time for reviewing instructions, searching existing data sources, gathering and maintaining the data needed, and completing and reviewing this collection of information. Send comments regarding this burden estimate or any other aspect of this collection of information, including suggestions for reducing this burden to Department of Defense, Washington Headquarters Services, Directorate for Information Operations and Reports (0704-0188), 1215 Jefferson Davis Highway, Suite 1204, Arlington, VA 22202-4302. Respondents should be aware that notwithstanding any other provision of law, no person shall be subject to any penalty for failing to comply with a collection of information if it does not display a currently valid OMB control number. **PLEASE DO NOT RETURN YOUR FORM TO THE ABOVE ADDRESS.**

1. REPORT DATE *(DD-MM-YYYY)*
July 2013

2. REPORT TYPE
Final report

3. DATES COVERED *(From - To)*

4. TITLE AND SUBTITLE

Phytoplankton as Particles – A New Approach to Modeling Algal Blooms

5a. CONTRACT NUMBER

5b. GRANT NUMBER

5c. PROGRAM ELEMENT NUMBER

6. AUTHOR(S)

Carl F. Cerco and Mark R. Noel

5d. PROJECT NUMBER

5e. TASK NUMBER

5f. WORK UNIT NUMBER

7. PERFORMING ORGANIZATION NAME(S) AND ADDRESS(ES)

U.S. Army Engineer Research and Development Center
Environmental Laboratory
3909 Halls Ferry Road, Vicksburg, MS 39180-6199

8. PERFORMING ORGANIZATION REPORT NUMBER

ERDC/EL TR-13-13

9. SPONSORING / MONITORING AGENCY NAME(S) AND ADDRESS(ES)

Headquarters, U.S. Army Corps of Engineers
Washington, DC 20314-1000

10. SPONSOR/MONITOR'S ACRONYM(S)

11. SPONSOR/MONITOR'S REPORT NUMBER(S)

12. DISTRIBUTION / AVAILABILITY STATEMENT

Approved for public release; distribution unlimited.

13. SUPPLEMENTARY NOTES

14. ABSTRACT

The authors investigate the hypothesis that phytoplankton blooms can be modeled by treating phytoplankton as discrete particles. A particle-tracking model is inserted into the CE-QUAL-ICM eutrophication model. Phytoplankton are quantified as carbonaceous biomass attached to the particles. Kinetics are adapted from CE-QUAL-ICM. The new model is operated along with existing hydrodynamic and watershed models of the Potomac River estuary. Initial application is to the winter-spring 1994 period. The new model is compared to observations and to a conventional model of the spring diatom bloom. The particle-based model successfully computes a subsurface chlorophyll maximum. The model characteristically displays heterogeneous spatial distribution of chlorophyll with high-amplitude oscillations at the semi-diurnal period. The characteristics and applicability of the particle approach are now established. The model requires optimization of parameter values to improve representation of the observed bloom in the Potomac.

15. SUBJECT TERMS

Algal Blooms
CE-QUAL-ICM model
Particle Tracking
Phytoplankton
Potomac River

16. SECURITY CLASSIFICATION OF:			**17. LIMITATION OF ABSTRACT**	**18. NUMBER OF PAGES**	**19a. NAME OF RESPONSIBLE PERSON**
a. REPORT	**b. ABSTRACT**	**c. THIS PAGE**			**19b. TELEPHONE NUMBER *(include area code)***
UNCLASSIFIED	UNCLASSIFIED	UNCLASSIFIED		105	

Standard Form 298 (Rev. 8-98)
Prescribed by ANSI Std. 239.18